GPU Implementation of Data-Aided Equalizers

Jeffrey T. Ravert

A thesis submitted to the faculty of
Brigham Young University
in partial fulfillment of the requirements for the degree of

Master of Science

Michael D. Rice, Chair
Brian D. Jeffs
Brian A. Mazzeo

Department of Electrical and Computer Engineering

Brigham Young University

April 2017

ABSTRACT

GPU Implementation of Data-Aided Equalizers

Jeffrey T. Ravert

Department of Electrical and Computer Engineering

Master of Science

Multipath is one of the dominant causes for link loss in aeronautical telemetry. Equalizers have been studied to combat multipath interference in aeronautical telemetry. Blind Constant Modulus Algorithm (CMA) equalizers are currently being used on SOQPSK-TG. The Preamble Assisted Equalization (PAQ) has been funded by the Air Force to study data-aided equalizers on SOQPSK-TG. PAQ compares side-by-side no equalization, data-aided zero forcing equalization, data-aided MMSE equalization, data-aided initialized CMA equalization, data-aided frequency domain equalization, and blind CMA equalization. An real-time experimental test setup has been assembled including an RF receiver for data acquisition, FPGA for hardware interfacing and buffering, GPUs for signal processing, spectrum analyzer for viewing multipath events, and an 8 channel bit error rate tester to compare equalization performance. Lab tests were performed with channel and noise emulators. The test setup achieved a 10 Mbps throughput with a 6 second delay. This thesis describes the GPU implementation of computing and application data-aided FIR equalizer filters.

Keywords: MISSING

ACKNOWLEDGMENTS

Students may use the acknowledgments page to express appreciation for the committee members, friends, or family who provided assistance in research, writing, or technical aspects of the dissertation, thesis, or selected project. Acknowledgments should be simple and in good taste.

Table of Contents

List of Tables **ix**

List of Figures **xi**

1 Introduction **1**

1.1 Multipath in Aeronautical Telemetry 1

1.2 Problem Statement 2

1.3 Organization 2

2 PAQ Project **3**

2.1 System Overview 3

2.2 Hardware Overview 5

2.3 Digital Signal Processing 7

2.3.1 Preamble Detection 9

2.3.2 Frequency Offset Compensation 10

2.3.3 Channel Estimation 11

2.3.4 Noise Variance Estimation 12

2.3.5 Equalizers 13

2.3.6 Symbol-by-Symbol Detector 17

3 Signal Processing in GPUs **21**

3.1 GPU and CUDA Introduction 22
3.1.1 An Example Comparing CPU and GPU 22
3.1.2 GPU kernel using threads and thread blocks 25
3.1.3 GPU Memory 26
3.1.4 Thread Optimization 27
3.1.5 CPU and GPU Pipelining 31
3.2 GPU Convolution 36
3.2.1 Floating Point Operation Comparison 37
3.2.2 CPU and GPU Single convolution using batch processing Comparison . . . 38
3.2.3 Convolution Using Batch Processing 45

4 Equalizer GPU Implementation **65**
4.1 Zero-Forcing and MMSE GPU Implementation 67
4.2 Constant Modulus Algorithm GPU Implementation 72
4.3 Frequency Domain Equalizer One and Two GPU Implementation 79
4.3.1 Frequency Domain Equalizer One 80
4.3.2 Frequency Domain Equalizer Two 81

5 Summary and Conclusions **85**
5.1 GPU Implementation 85
5.2 Contributions 85
5.3 Further Work 86

Bibliography **87**

List of Tables

3.1 The resources available with three NVIDIA GPUs used in this thesis (1x Tesla K40c 2x Tesla K20c). Note that CUDA configures the size of the L1 cache needed. 29

3.2 Defining start and stop lines for timing comparison in Listing 3.5. 41

3.3 Convolution computation times with signal length 12672 and filter length 186 on a Tesla K40c GPU. 43

3.4 Convolution computation times with signal length 12672 and filter length 23 on a Tesla K40c GPU. 44

3.5 Defining start and stop lines for execution time comparison in Listing 3.6. 46

3.6 Convolution using batch processing execution times with for a 12672 sample signal and 186 tap filter on a Tesla K40c GPU. 47

3.7 Convolution using batch processing execution times with for a 12672 sample signal and 23 tap filter on a Tesla K40c GPU. 47

3.8 Batched convolution execution times with for a 12672 sample signal and cascaded 23 and 186 tap filter on a Tesla K40c GPU. 49

4.1 Three different algorithms were explored to compute the ZF and MMSE equalizer filters. 73

4.2 CMA 77

4.3 Two different algorithms were explored to compute the cost function gradient ∇J. 78

4.4 Execution times for calculating and applying Frequency Domain Equalizer One and Two. 83

List of Figures

1.1 Multipath can occur when a signal is received multiple paths like line-of-sight or ground bounce or reflections. 1

2.1 The Received signal has multipath interference, frequency offset, phase offset and additive white Gaussian noise. The received signal is down-converted, filtered, sampled, and resampled to produce the sample sequence $r(n)$. 4

2.2 A diagram showing PAQ packetized sample structure. 4

2.3 A block diagram of the physical PAQ hardware. The components inside the rack mounted server are in the dashed box. All the components in the dashed and dotted box are housed in a rack mounted case. 5

2.4 A picture of the physical PAQ hardware refrencing blocks from Figure 2.3. Right: Components in the dashed and dotted box. Left: Components in the dashed box. Note that the T/M Receiver is not pictured. 6

2.5 A block diagram of the estimators in PAQ. 7

2.6 A block diagram of the computation and application of the equalizer and detection filters. The bold box emphasizes in the focus of this thesis. 8

2.7 An illustration of the discrete-time channel of length N_1+N_2+1 with a non-causal component comprising N_1 samples and a causal component comprising N_2 samples. 12

2.8 A diagram showing how the iNET packet is used as a cyclic prefix. 16

2.9 SOQPSK-TG power spectral density. 17

2.10 "Numerically optimized" SOQPSK detection filter $\mathbf{h}_{\text{NO}}$. 18

2.11 Offset Quadriture Phase Shift Keying symbol by symbol detector. 18

3.1 NVIDIA Tesla K40c and K20c. 22

3.2 A block diagram of how a CPU sequentially performs vector addition. 23

3.3 A block diagram of how a GPU performs vector addition in parallel. 23

3.4 32 threads launched in 4 thread blocks with 8 threads per block. 26

3.5 36 threads launched in 5 thread blocks with 8 threads per block with 4 idle threads. 26

3.6 Diagram comparing memory size and speed. Global memory is massive but extremely slow. Registers are extremely fast but there are very few. 27

3.7 Example of an NVIDIA GPU card. The GPU chip with registers and L1/shared memory is shown in the dashed box. The L2 cache and global memory is shown off chip in the solid boxes. 28

3.8 A block diagram where local, shared, and global memory is located. Each thread has private local memory. Each thread block has private shared memory. The GPU has global memory that all threads can access. 28

3.9 Plot showing how execution time is affected by changing the number of threads per block. The optimal execution time for an example GPU kernel is 0.1078 ms at the optimal 96 threads per block. 31

3.10 Plot showing the number of threads per block doesn't always drastically affect execution time. 32

3.11 The typical approach of CPU and GPU operations. This block diagram shows the profile of Listing 3.3. 33

3.12 GPU and CPU operations can be pipelined. This block diagram shows a Profile of Listing 3.4. 33

3.13 A block diagram of pipelining a CPU with three GPUs. 34

3.14 Block diagrams showing time-domain convolution and frequency-domain convolution. 37

3.15 Comparison of number of floating point operations (flops) required to convolve a variable length complex signal with a 186 tap complex filter. 39

3.16 Comparison of number of floating point operations (flops) required to convolve a variable length complex signal with a 23 tap complex filter. 40

3.17 Comparison of number of floating point operations (flops) required to convolve a 12672 sample complex signal with a variable length tap complex filter. 41

3.18 Comparison of a complex convolution on CPU and GPU. The signal length is variable and the filter is fixed at 186 taps. The comparison is messy with out lower bounding. 42

3.19 Comparison of a complex convolution on CPU and GPU. The signal length is variable and the filter is fixed at 186 taps. A lower bound was applied by searching for a local minimums in 15 sample width windows. 43

3.20 Comparison of a complex convolution on CPU and GPU. The signal length is variable and the filter is fixed at 23 taps. A lower bound was applied by searching for a local minimums in 5 sample width windows. 44

3.21 Comparison of a complex convolution on CPU and GPU. The filter length is variable and the signal is fixed at 12672 samples. A lower bound was applied by searching for a local minimums in 3 sample width windows. 45

3.22 Comparison of a batched complex convolution on a CPU and GPU. The number of batches is variable while the signal and filter length is set to 12672 and 186. . . . 47

3.23 Comparison on execution time per batch for complex convolution. The number of batches is variable while the signal and filter length is set to 12672 and 186. 48

3.24 Comparison of complex convolution using batch processing on a GPU. The signal length is variable and the filter is fixed at 186 taps. 49

3.25 Comparison of complex convolution using batch processing on a GPU. The signal length is variable and the filter is fixed at 23 taps. 50

3.26 Comparison of complex convolution using batch processing on a GPU. The filter length is variable and the signal length is set to 12672 samples. 51

3.27 Block diagrams showing showing cascaded time-domain convolution and frequency-domain convolution. 52

4.1 To simplify block diagrams, frequency-domain convolution is shown as one block. 66

4.2 To simplify block diagrams, frequency-domain cascaded convolution is shown as one block. 66

4.3 Block Diagram showing how the Zero-Forcing equalizer coefficients are implemented in the GPU. 72

4.4 Block Diagram showing how the Minimum Mean Squared Error equalizer coefficients are implemented in the GPU. 73

4.5 Diagram showing the relationships between $z(n)$, $\rho(n)$ and $m(n)$. 76

4.6 Block Diagram showing how the CMA equalizer filter is implemented in the GPU using frequency-domain convolution twice per iteration. 79

4.7 A diagram showing how the iNET packet is used as a cyclic prefix. 80

4.8 SOQPSK-TG power spectral density. 82

4.9 Block diagram showing Frequency Domain Equalizer One is implemented in the frequency domain in GPUs. 83

4.10 Block diagram showing Frequency Domain Equalizer Two is implemented in the frequency domain in GPUs. 83

Chapter 1

Introduction

1.1 Multipath in Aeronautical Telemetry

Multipath interference is one of the dominant causes for link loss in aeronautical telemetry. Strong multipath interference occurs in aeronautical telemetry when the transmitted signal is received via multiple paths because a test article is in a low elevation angle scenario as shown in Figure 1.1. Multipath propagation is modeled as linear, time-invariant system with a finite impulse response. Equalizers have been studied to combat multipath interference in aeronautical telemetry [1, 2]. There are two types of equalizers, blind and data-aided. Blind equalizers combat multipath using known properties of the transmitted signal but no knowledge of the data or multipath channel. Data-aided equalizers require knowledge of the propagation conditions. One method of obtaining an estimate of this knowledge is to periodically insert a known bit sequence called a "pilot" into the data stream. The receiver compares the received signal corresponding to the pilot with a locally stored copy of the pilot to estimate parameters such as the multipath channel, frequency offset, phase offset, and noise variance. Data-aided equalizers are finite-length impulse response (FIR) filters. The impulse response of the equalizer filter is computed using the estimated channel.

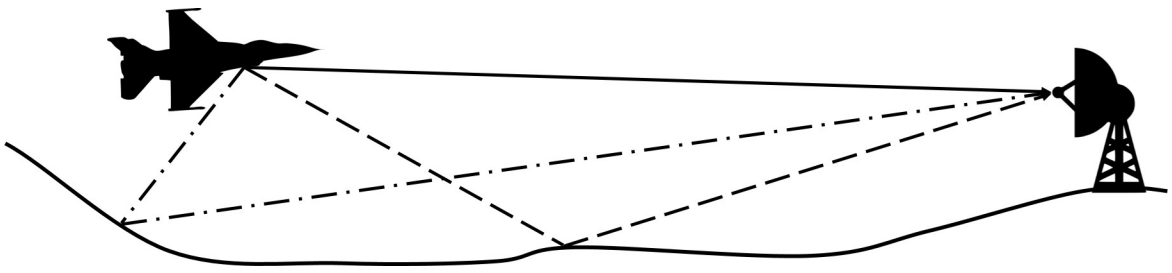

Figure 1.1: Multipath can occur when a signal is received multiple paths like line-of-sight or ground bounce or reflections.

1.2 Problem Statement

The real-time signal processing for a digital communications system with data-aided equalizers is computationally heavy. Digital communication algorithms implemented in a high powered Central Processing Unit (CPU) cannot meet the real-time requirement. Graphic Processing Units (GPUs) can be used to perform real-time processing because of their massively parallel architecture.

This thesis studies how signal processing can be reformulated to run quickly and efficiently in GPUs. Optimized libraries harness GPU resources to make signal processing implementation relatively easy and extremely fast. If algorithms can be reformulated for batch processing and use matrix/vector multiplication or Fast Fourier Transform libraries, GPUs can provide vast speed ups.

1.3 Organization

Chapter 2 describes the Preamble Assisted Equalization (PAQ) system and introduce the digital signal processing algorithms. Chapter 3 provides an overview of signal processing in GPUs. Chapter 4 describes how the five equalizers are implemented in GPUs. The thesis concludes with the summary and conclusions in Chapter 5.

Chapter 2

PAQ Project

Data-aided equalization in aeronautical telemetry has been studied and tested by the Preamble Assisted Equalization (PAQ) project [3]. PAQ built a system that compares five data-aided equalizers to blind equalization and no equalization. Laboratory tests were perfomed using a static RF multipath channel emulator and a noise source to produce Bit Error Rate (BER) curves. The five data-aided equalizers studied are

- zero-forcing (ZF) equalizer
- minimum mean square Error (MMSE) equalizer
- MMSE-initialized constant modulus algorithm (CMA) equalizer
- frequency domain equalizer one (FDE1)
- frequency domain equalizer two (FDE2).

Bit error statistics were be used as the figure or merit for the equalization algorithms.

2.1 System Overview

The system is summarized by the block diagram in Figure 2.1. The bit stream $\mathbf{b}$ modulates a SOQPSK-TG carrier. To enable data-aided equalization, the PAQ bit stream has a packetized structure shown in Figure 2.2. The bit stream has a pilot bit sequence, in the form of the iNET preamble and ASM, periodically inserted into the data bits. The iNET preamble comprises eight repetitions of the 16-bit sequence CD98_{hex} and the ASM field is

$$034776\text{C}7272895\text{B}0_{\text{hex}}. \tag{2.1}$$

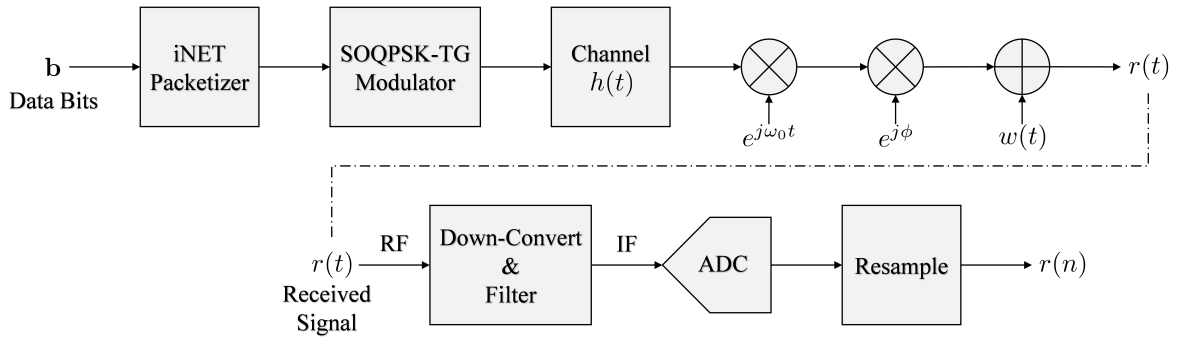

Figure 2.1: The Received signal has multipath interference, frequency offset, phase offset and additive white Gaussian noise. The received signal is down-converted, filtered, sampled, and resampled to produce the sample sequence $r(n)$.

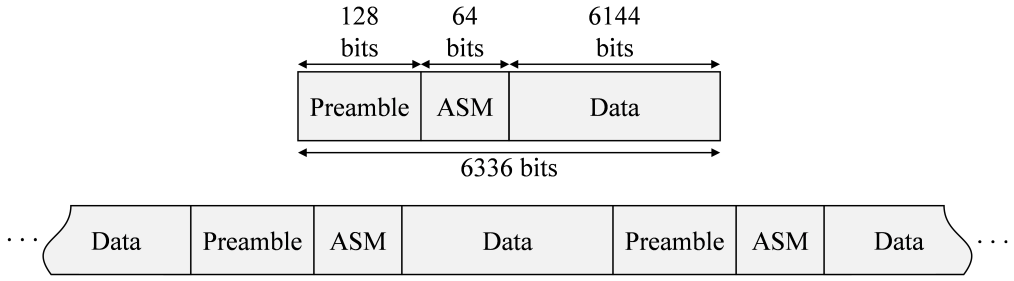

Figure 2.2: A diagram showing PAQ packetized sample structure.

The data payload is a known length-$(2^{11}-1)$ PN sequence. Each packet contains 128 preamble bits, 64 ASM bits and $6{,}144$ data bits making each iNET packet $6{,}336$ bits. The data bit rate is 10 Mbits/s. After preamble and ASM insertion, the bit rate presented to the modulator is 10.3125 Mbits/s.

After modulation, the transmitted signal experiences multipath interference modeled as an LTI system with the channel impulse response $h(t)$. The transmitted signal also experiences a frequency offset ω_0, a phase offset ϕ and additive white Gaussian noise $w(t)$. The received signal is down-converted, filtered in the T/M receiver, sampled at $93^1/_3$ Msamples/second by the ADC, and down-converted to baseband and resampled by $^{99}/_{448}$ in the GPUs in one step using a polyphase filterbank based on the principles outlined in [4, chap. (9)]. The result is $r(n)$, a sampled version of the complex-valued lowpass equivalent waveform at a sample rate of 20.625 Msamples/second or 2 samples/bit.

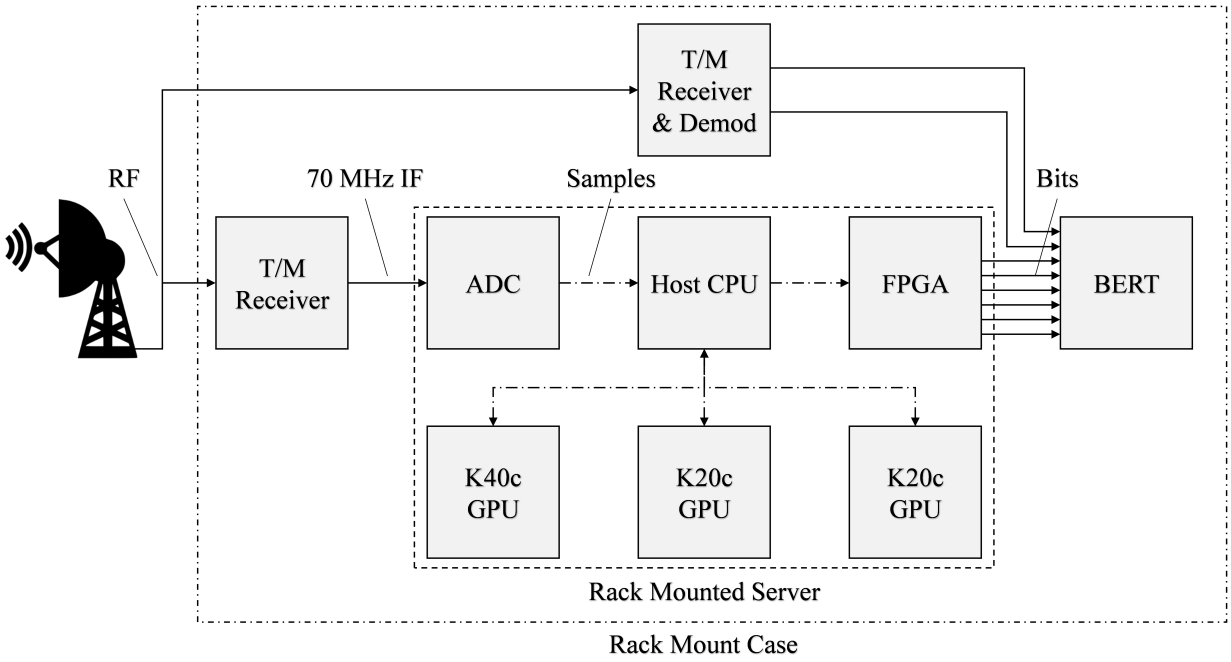

Figure 2.3: A block diagram of the physical PAQ hardware. The components inside the rack mounted server are in the dashed box. All the components in the dashed and dotted box are housed in a rack mounted case.

2.2 Hardware Overview

A block diagram of PAQ physical system is shown in Figure 2.3. A picture of the physical components is shown in Figure 2.4. The major components, and their functions are summarized as follows:

- The **T/M receiver** down-converts the received signal from L- or C-band RF to 70 MHz IF. The IF filter plays the role of an anti-aliasing filter.
- The **rack mounted server** is a high powered computer that houses an ADC, a FPGA and three GPUs slotted into a 32 pin PCIe bus.
- The **ADC** produces 14-bit samples of the real-valued bandpass IF signal. The sample rate is $93^1/_3$ Msamples/s. The samples are transferred to the host CPU via the PCIe bus.

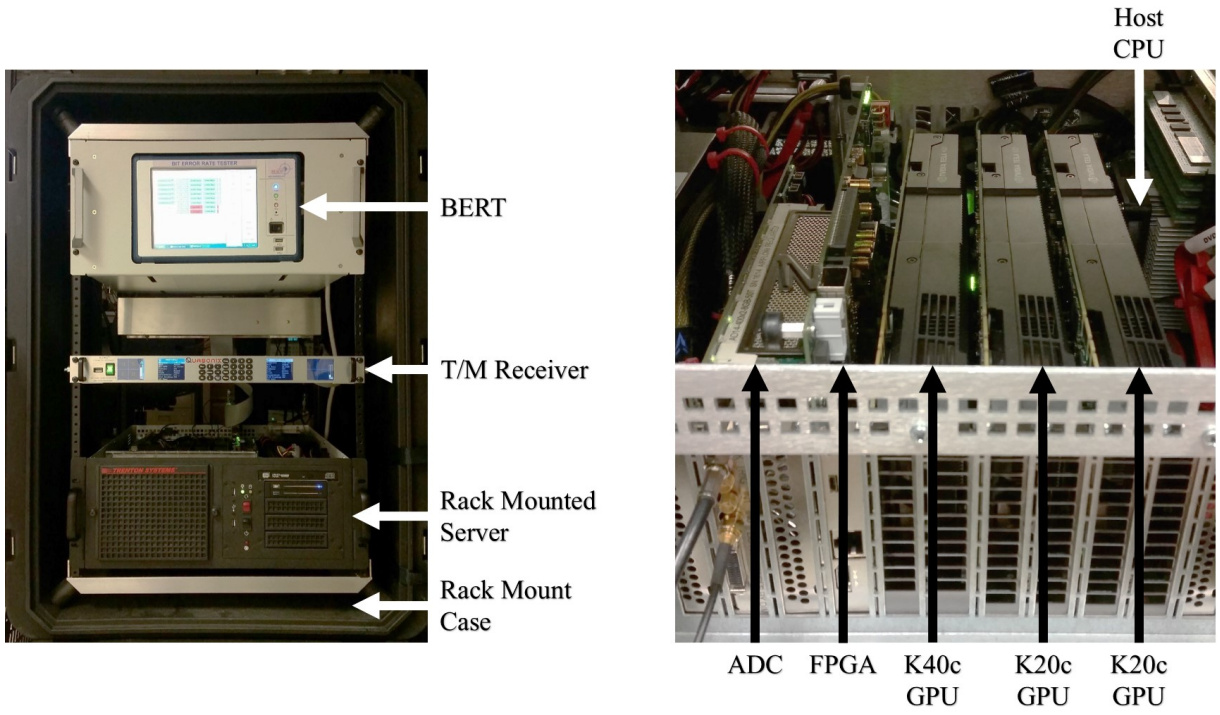

Figure 2.4: A picture of the physical PAQ hardware refrencing blocks from Figure 2.3. Right: Components in the dashed and dotted box. Left: Components in the dashed box. Note that the T/M Receiver is not pictured.

- The **host CPU** initiates memory transfers between itself and the ADC, GPUs and FPGA via the PCIe bus. The host CPU also launches the digital signal processing algorithms on the GPUs.
- The three **GPUs** are where the detection, estimation, equalization and demodulation resides.
- The bit error rate tester (**BERT**) counts the errors in each bit stream by comparing the streams to the transmitted PN sequence.
- The **FPGA** is the interface between the host CPU and the BERT. After the GPUs produce bit decisions, the host CPU transfers the decisions from the GPUs to the FPGA via the PCIe bus. The FPGA then clocks the bits out to the BERT for BER testing.
- The **T/M Receiver & Demodulator** demodulates the RF signal outputting two bit streams for blind equalization and no equalization for BER comparison.

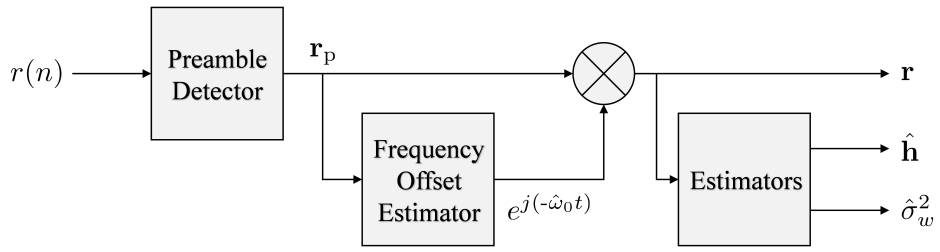

Figure 2.5: A block diagram of the estimators in PAQ.

2.3 Digital Signal Processing

A high-level digital signal processing flow is shown in Figure 2.5 and 2.6. The sequence $r(n)$ represents a continuous stream of samples. Because the frequency offset, channel, and noise variance are estimated using the preamble and ASM, the first step is to find the samples corresponding to the preamble in the received sample sequence $r(n)$. The preamble detector identifies the sample indices in the sequence $r(n)$ corresponding to the starting position of each occurrence of the waveform samples corresponding to the preamble. To simplify the notation used to describe the signal processing algorithms, we represent the output of the preamble detector by the vector $\mathbf{r}_{\mathrm{p}}$, a sequence of L_{pkt} samples starting the waveform samples corresponding to the preamble and ASM bits. In this way the signal processing algorithms are described on a packet-by-packet basis.

Starting with the block diagram of Figure 2.5, the preamble samples are used first to estimate the frequency offset. The estimated frequency offset $\hat{\omega}_0$ rads/sample is then used to "de-rotate" the vector of samples $\mathbf{r}_{\mathrm{p}}$ to produce a vector denoted $\mathbf{r}$. The de-rotated preamble and ASM samples in the vector $\mathbf{r}$ are used to estimate the channel $\hat{\mathbf{h}}$ and noise variance $\hat{\sigma}_w^2$ as shown.

The estimates produces in Figure 2.5 are used to compute the equalizer filter coefficients as illustrated in Figure 2.6. The figure shows five independent branches, each branch computing an equalizer filter. Lower case boldface $\mathbf{c}$ with a subscript on the top three branches represent impulse responses of the FIR equalizer filters. Upper case boldface $\mathbf{C}$ with a on the lower three branches subscript represents the transfer function (FFT) of the equalizer. In all five cases, the equalizer and a detection filter (described below) are applied to $\mathbf{r}$. The result is downsampled and processed by a symbol-by-symbol OQPSK detector to produce bit decisions for each equalizer.

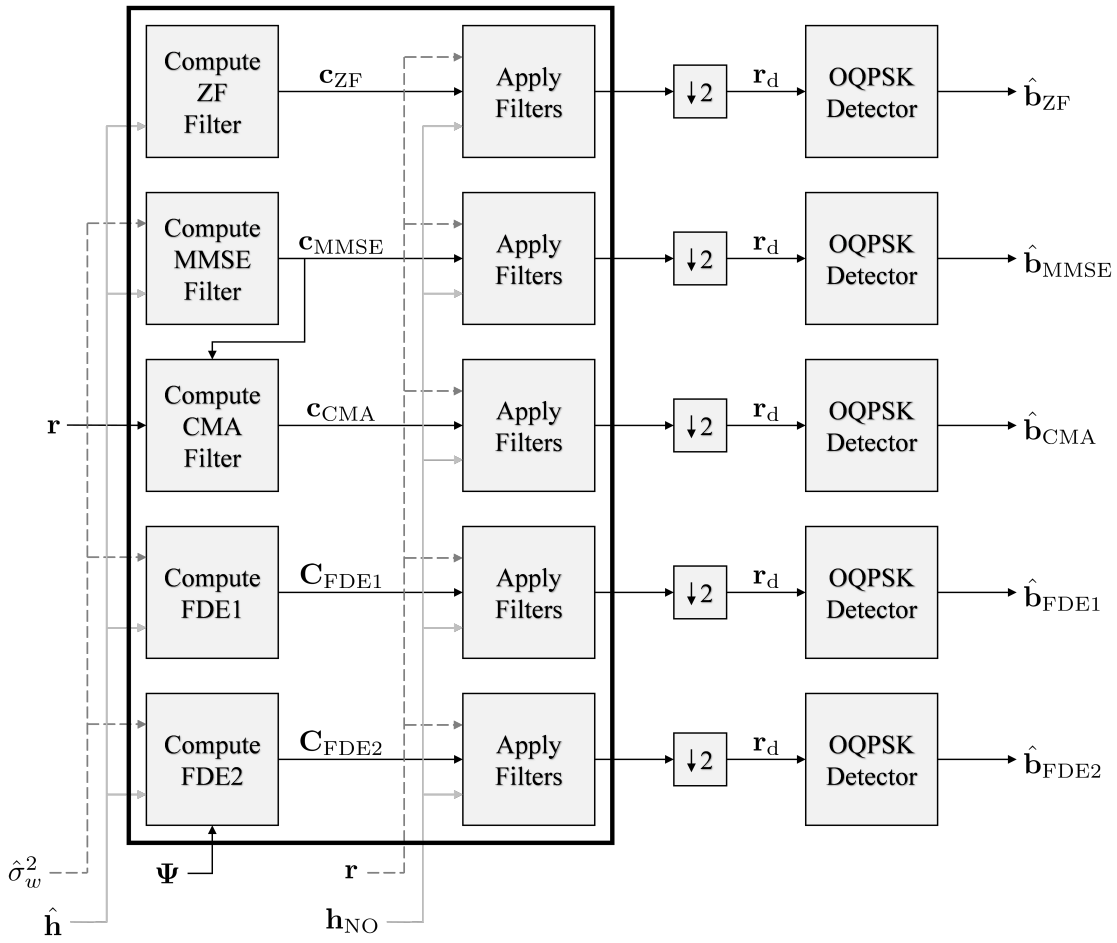

Figure 2.6: A block diagram of the computation and application of the equalizer and detection filters. The bold box emphasizes in the focus of this thesis.

The GPUs in Figure 2.3 and 2.4 perform all the digital signal processing in parallel. To introduce as much parallelism as possible, the received samples are processed in a batch comprising $39{,}321{,}600$ samples. At 20.625 Msamples/second, each batch of $39{,}321{,}600$ samples represents 1907 milliseconds of data. Each batch has at most 3104 $12{,}672$-sample iNET packets.[1] The GPU processes 3104 packets in parallel by leveraging batched processing. To meet the real-time requirement, **all** processing must be completed in less than 1907 ms.

This thesis, illustrates how the five PAQ data-aided equalizers were computed and applied in GPUs. The bold box in Figure 2.6 emphasizes processing blocks on which this thesis focuses.

[1] Each batch comprises 3103 or 3104 packets.

Even though the GPUs process 3104 packets in parallel, the signal processing algorithms are described on a packet-by-packet basis.

2.3.1 Preamble Detection

To compute the impulse responses or transfer functions of the five data-aided equalizers, an estimate of the channel and noise variance must be available. The required estimates are derived from the received waveform samples corresponding to the preamble and ASM bits. Consequently, the location of the waveform samples corresponding to the preamble and ASM bits must be found. The preamble detector identifies the sample indices in the sequence $r(n)$ corresponding to the starting position of each occurrence of the waveform samples corresponding to the preamble. The preamble detector computes the function $L(n)$ for each sample in the batch. Peaks in $L(n)$ identify the starting indices of the waveform samples corresponding to each occurrence of the preamble bits. The function $L(n)$ is given by

$$L(n) = \sum_{m=0}^{7} \left[I^2(n,m) + Q^2(n,m) \right] \tag{2.2}$$

where

$$\begin{aligned} I(n,m) \approx & \sum_{\ell \in \mathcal{L}_1} r_R(\ell+32m+n) - \sum_{\ell \in \mathcal{L}_2} r_R(\ell+32m+n) + \sum_{\ell \in \mathcal{L}_3} r_I(\ell+32m+n) - \sum_{\ell \in \mathcal{L}_4} r_I(\ell+32m+n) \\ & + 0.7071 \left[\sum_{\ell \in \mathcal{L}_5} r_R(\ell+32m+n) - \sum_{\ell \in \mathcal{L}_6} r_R(\ell+32m+n) \right. \\ & \left. + \sum_{\ell \in \mathcal{L}_7} r_I(\ell+32m+n) - \sum_{\ell \in \mathcal{L}_8} r_I(\ell+32m+n) \right], \end{aligned} \tag{2.3}$$

and

$$\begin{aligned} Q(n,m) \approx & \sum_{\ell \in \mathcal{L}_1} r_I(\ell+32m+n) - \sum_{\ell \in \mathcal{L}_2} r_I(\ell+32m+n) \\ & - \sum_{\ell \in \mathcal{L}_3} r_R(\ell+32m+n) + \sum_{\ell \in \mathcal{L}_4} r_R(\ell+32m+n) \end{aligned}$$

$$+ 0.7071 \left[\sum_{\ell \in \mathcal{L}_5} r_I(\ell + 32m + n) - \sum_{\ell \in \mathcal{L}_6} r_I(\ell + 32m + n) \right.$$
$$\left. - \sum_{\ell \in \mathcal{L}_7} r_R(\ell + 32m + n) + \sum_{\ell \in \mathcal{L}_8} r_R(\ell + 32m + n) \right] \quad (2.4)$$

with

$$\begin{aligned}
\mathcal{L}_1 &= \{0, 8, 16, 24\} \\
\mathcal{L}_2 &= \{4, 20\} \\
\mathcal{L}_3 &= \{2, 10, 14, 22\} \\
\mathcal{L}_4 &= \{6, 18, 26, 30\} \\
\mathcal{L}_5 &= \{1, 7, 9, 15, 17, 23, 25, 31\} \\
\mathcal{L}_6 &= \{3, 5, 11, 12, 13, 19, 21, 27, 28, 29\} \\
\mathcal{L}_7 &= \{1, 3, 9, 11, 12, 13, 15, 21, 23\} \\
\mathcal{L}_8 &= \{5, 7, 17, 19, 25, 27, 28, 29, 31\}.
\end{aligned} \quad (2.5)$$

A peak in $L(n)$ indicates the index n is the start of a preamble. Suppose $L(i)$ is a peak (i.e., i is the index of the peak). The vector $\mathbf{r}_\mathrm{p}$ is

$$\mathbf{r}_\mathrm{p} = \begin{bmatrix} r(i) \\ \vdots \\ r(i + L_\mathrm{pkt} - 1) \end{bmatrix} = \begin{bmatrix} r_\mathrm{p}(0) \\ \vdots \\ r_\mathrm{p}(L_\mathrm{pkt} - 1) \end{bmatrix} \quad (2.6)$$

The first $L_\mathrm{p} = 256$ samples of $\mathbf{r}_\mathrm{p}$ correspond to the preamble bits and the following $L_\mathrm{ASM} = 128$ samples of $\mathbf{r}_\mathrm{p}$ correspond to the ASM bits.

2.3.2 Frequency Offset Compensation

The preamble sequence comprises eight copies of the bit sequence $\mathrm{CD98}_\mathrm{hex}$. Consequently, the waveform samples $r_\mathrm{p}(0), \ldots, r_\mathrm{p}(L_\mathrm{p} - 1)$ comprise eight copies of $L_q = 32$ SOQPSK-TG waveform samples corresponding to $\mathrm{CD98}_\mathrm{hex}$.[2] The frequency offset estimator shown in Figure

[2]This statement is only approximately true. Because of the memory in SOQPSK-TG, the first block of L_q is a function of both the bit sequence $\mathrm{CD98}_\mathrm{hex}$ and the seven unknown bits preceding the first occurrence of $\mathrm{CD98}_\mathrm{hex}$.

2.5 is the estimator taken from [5, eq. (24)]. With the notation adjusted slightly, the frequency offset estimate is

$$\hat{\omega}_0 = \frac{1}{L_q} \arg \left\{ \sum_{n=i+2L_q}^{i+7L_q-1} r_{\mathrm{p}}(n) r_{\mathrm{p}}^*(n - L_q) \right\} \quad \text{for } i = 1, 2, 3, 4, 5. \tag{2.7}$$

The frequency offset is estimated for every packet or each vector of samples $\mathbf{r}_{\mathrm{p}}$ in the batch. Frequency offset compensation is performed by de-rotating the received samples by $-\hat{\omega}_0$:

$$r(n) = r_{\mathrm{p}}(n) e^{-j\hat{\omega}_0 n}. \tag{2.8}$$

Equations (2.7) and (2.8) are easily implemented into GPUs.

2.3.3 Channel Estimation

Let the SOQPSK-TG samples corresponding to the preamble and ASM bits be

$$\mathbf{p} = \begin{bmatrix} p(0) \\ p(1) \\ \vdots \\ p(L_{\mathrm{P}} + L_{\mathrm{ASM}} - 1) \end{bmatrix}. \tag{2.9}$$

The multipath channel is defined by the impulse response

$$\hat{\mathbf{h}} = \begin{bmatrix} \hat{h}(-N_1) \\ \vdots \\ \hat{h}(0) \\ \vdots \\ \hat{h}(N_2) \end{bmatrix}. \tag{2.10}$$

Note that at 2 samples/bit, the complex-valued lowpass equivalent channel impulse response is assumed to have a non-causal component comprising N_1 samples and a causal component comprising N_2 samples. Figure 2.7 shows the full discrete-time $L_h = N_1 + N_2 + 1$ sample channel. The ML estimate is [2, eq. 8]

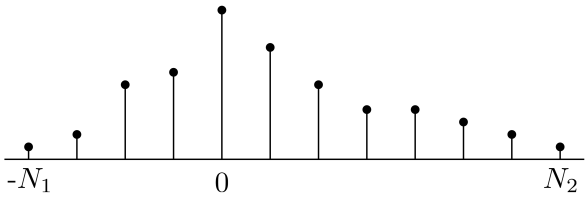

Figure 2.7: An illustration of the discrete-time channel of length $N_1 + N_2 + 1$ with a non-causal component comprising N_1 samples and a causal component comprising N_2 samples.

$$\hat{\mathbf{h}} = \underbrace{\left(\mathbf{X}^\dagger \mathbf{X}\right)^{-1} \mathbf{X}^\dagger}_{\mathbf{X}_{\text{lpi}}} \mathbf{r} \tag{2.11}$$

where

$$\mathbf{X} = \begin{bmatrix} p(N_2) & & & \\ \vdots & p(N_2) & & \\ p(L_{\text{p}} + L_{\text{ASM}} - N_1) & \vdots & \ddots & \\ & p(L_{\text{p}} + L_{\text{ASM}} - N_1) & p(N_2) & \\ & & \vdots & \\ & & p(L_{\text{p}} + L_{\text{ASM}} - N_1) & \end{bmatrix} \tag{2.12}$$

is the $(L_{\text{p}} + L_{\text{ASM}} - N_1 - N_2) \times (N_1 + N_2 + 1)$ convolution matrix formed from the SOQPSK-TG waveform samples corresponding to the preamble and ASM bits. The $(N_1 + N_2 + 1) \times (L_{\text{p}} + L_{\text{ASM}} - N_1 - N_2)$ matrix $\mathbf{X}_{\text{lpi}}$ is the left pseudo-inverse of $\mathbf{X}$. The matrix vector multiplication $\mathbf{X}_{\text{lpi}}\mathbf{r}$ is implemented simply and efficiently in GPUs.

2.3.4 Noise Variance Estimation

The noise variance estimator is [2, eq. 9]

$$\hat{\sigma}_w^2 = \frac{1}{2\rho} \left| \mathbf{r} - \mathbf{X}\hat{\mathbf{h}} \right|^2 \tag{2.13}$$

where

$$\rho = \text{Trace} \left\{ \mathbf{I} - \mathbf{X} \left(\mathbf{X}^\dagger \mathbf{X} \right)^{-1} \mathbf{X}^\dagger \right\} \tag{2.14}$$

where $\mathbf{X}$ is given by Equation (2.12). Equation (2.13) is easily implemented into GPUs.

2.3.5 Equalizers

Zero-Forcing Equalizer

The ZF equalizer is an FIR filter defined by the $L_{\text{eq}} = L_1 + L_2 + 1$ coefficients

$$\mathbf{c}_{\text{ZF}} = \begin{bmatrix} c_{\text{ZF}}(-L_1) \\ \vdots \\ c_{\text{ZF}}(0) \\ \vdots \\ c_{\text{ZF}}(L_2). \end{bmatrix}. \tag{2.15}$$

The filter coefficients are the solution to [3]

$$\mathbf{R}_{\hat{h}}\mathbf{c}_{\text{ZF}} = \hat{\mathbf{g}} \tag{2.16}$$

where

$$\mathbf{R}_{\hat{h}} = \begin{bmatrix} r_{\hat{h}}(0) & r^*_{\hat{h}}(1) & \cdots & r^*_{\hat{h}}(L_{eq}-1) \\ r_{\hat{h}}(1) & r_{\hat{h}}(0) & \cdots & r^*_{\hat{h}}(L_{eq}-2) \\ \vdots & \vdots & \ddots & \\ r_{\hat{h}}(L_{eq}-1) & r_{\hat{h}}(L_{eq}-2) & \cdots & r_{\hat{h}}(0) \end{bmatrix}, \tag{2.17}$$

$$\hat{\mathbf{g}} = \begin{bmatrix} \hat{h}^*(L_1) \\ \vdots \\ \hat{h}^*(0) \\ \vdots \\ \hat{h}^*(-L_2) \end{bmatrix}, \tag{2.18}$$

and

$$r_{\hat{h}}(k) = \sum_{n=-N_1}^{N_2} \hat{h}(n)\hat{h}^*(n-k), \tag{2.19}$$

MMSE Equalizer

The MMSE equalizer is an FIR filter defined by the $L_{\text{eq}} = L_1 + L_2 + 1$ coefficients

$$\mathbf{c}_{\text{MMSE}} = \begin{bmatrix} c_{\text{MMSE}}(-L_1) \\ \vdots \\ c_{\text{MMSE}}(0) \\ \vdots \\ c_{\text{MMSE}}(L_2). \end{bmatrix}. \tag{2.20}$$

The filter coefficients are the solution to [3]

$$\mathbf{R}\mathbf{c}_{\text{MMSE}} = \hat{\mathbf{g}} \tag{2.21}$$

where

$$\mathbf{R} = \mathbf{R}_{\hat{\mathbf{h}}} + \hat{\sigma}_w^2 \mathbf{I}, \tag{2.22}$$

$\mathbf{R}_{\hat{\mathbf{h}}}$ is given by (2.17), $\hat{\sigma}_w^2$ is given by (2.13), and $\hat{\mathbf{g}}$ is given by (2.18).

Constant Modulus Algorithm Equalizer

The CMA equalizer is an adaptive FIR filter where the $L_{\text{eq}} = L_1 + L_2 + 1$ coefficients at the b-th iteration are

$$\mathbf{c}_{\text{CMA}}^{(b)} = \begin{bmatrix} c_{\text{CMA}}^{(b)}(-L_1) \\ \vdots \\ c_{\text{CMA}}^{(b)}(0) \\ \vdots \\ c_{\text{CMA}}^{(b)}(L_2). \end{bmatrix}. \tag{2.23}$$

The equalizer output at the b-th iteration is

$$\mathbf{y}^{(b)} = \mathbf{c}_{\text{CMA}}^{(b)} * \mathbf{r}. \tag{2.24}$$

Note that in this implementation the CMA filter coefficients are constant for the duration of a packet [2]. The filter coefficients are updated on a packet-by-packet basis using a steepest descent

algorithm as follows:

$$\mathbf{c}_{\text{CMA}}^{(b+1)} = \mathbf{c}_{\text{CMA}}^{b} - \mu \nabla J \tag{2.25}$$

where

$$\nabla J = \frac{2}{L_{pkt}} \sum_{n=0}^{L_{pkt}-1} \left[y^{(b)}(n) \left(y^{(b)}(n) \right)^* - 1 \right] y^{(b)}(n) \mathbf{r}^*(n). \tag{2.26}$$

In Equation (2.26), $y^{(b)}(n)$ is the n-th element of the vector $\mathbf{y}^{(b)}$ and

$$\mathbf{r}(n) = \begin{bmatrix} r(n+L_1) \\ \vdots \\ r(n) \\ \vdots \\ r(n-L_2) \end{bmatrix}. \tag{2.27}$$

Frequency Domain Equalizer One

Frequency-domain equalization leverages the efficiency of the FFT algorithm to perform equalization filtering in the FFT domain. The difference between frequency-domain equalization and applying the previous three equalizer filters in the FFT domain is that the frequency-domain equalizer is computed directly in the FFT domain. To enable this, some provision must be made for the fact that point-by-point multiplication in the FFT domain corresponds to *circular* convolution in the time domain. This provision is most often in the form of a cyclic prefix prepended to the data packet [6–9]. Even though the PAQ format does not include any special provision for frequency-domain equalization such as a cyclic prefix, frequency-domain equalization is still possible using the ideas described by Coon et al [10]. Because of the repetitive nature of the preamble sequence, the second half of the preamble bits at the beginning of the packet are the same the first half of the preamble bits following the packet. Consequently, the second half of the preamble bits at the beginning of the packet form a cyclic prefix for the block comprising the ASM, the data, and the first half of the preamble following the packet as illustrated in Figure 2.8.

The FFT domain transfer function of FDE1 is [11, eq. (11)]

$$C_{\text{FDE1}}(e^{j\omega_k}) = \frac{\hat{H}^*(e^{j\omega_k})}{|\hat{H}(e^{j\omega_k})|^2 + \frac{1}{\hat{\sigma}_w^2}} \quad \omega_k = \frac{2\pi}{N_{\text{FFT}}} \text{ for } k = 0, 1, \cdots, N_{\text{FFT}} - 1 \tag{2.28}$$

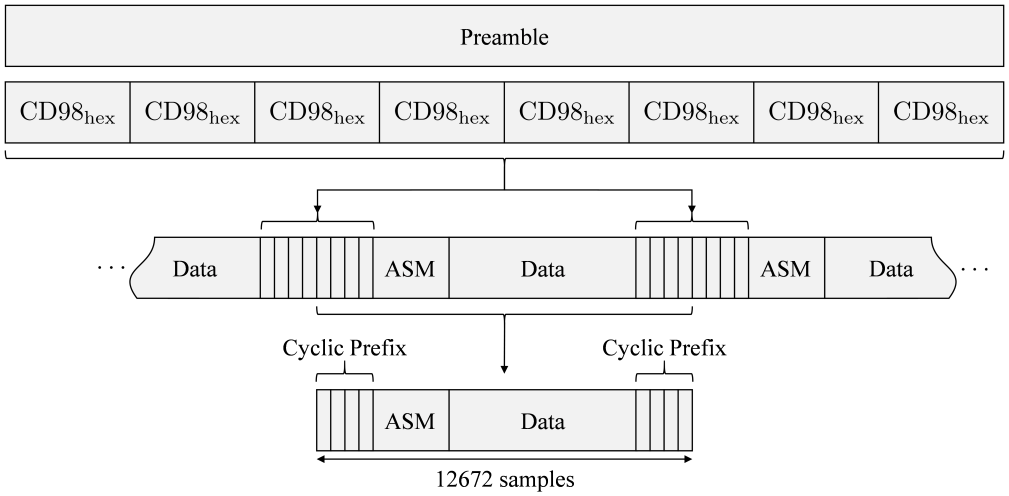

Figure 2.8: A diagram showing how the iNET packet is used as a cyclic prefix.

where $N_{\text{FFT}} = 2^u = 16{,}384$, where $u = \lceil \log_2 (L_{\text{pkt}}) \rceil = 14$, where $\lceil x \rceil$ means the smallest integer greater than or equal to x. In Equation (2.28), $\hat{H}(e^{j\omega_k})$ is the k-th element of the length-N_{FFT} FFT of $\hat{\mathbf{h}}$ and $\hat{\sigma}^2$ is given by (2.13). FDE1 is the MMSE equalizer formulated in the frequency domain where power spectral density of SOQPSK-TG is a constant.

Frequency Domain Equalizer Two

The FFT domain transfer function of FDE1 is [11, eq. (12)]

$$C_{\text{FDE2}}(e^{j\omega_k}) = \frac{\hat{H}^*(e^{j\omega_k})}{|\hat{H}(e^{j\omega_k})|^2 + \frac{\Psi(e^{j\omega_k})}{\hat{\sigma}_w^2}} \quad \omega_k = \frac{2\pi}{N_{\text{FFT}}} \text{ for } k = 0, 1, \cdots, N_{\text{FFT}} - 1 \tag{2.29}$$

where $N_{\text{FFT}} = 2^u = 16{,}384$, where $u = \lceil \log_2 (L_{\text{pkt}}) \rceil = 14$, where $\lceil x \rceil$ means the smallest integer greater than or equal to x. In Equation (2.29), $\hat{H}(e^{j\omega_k})$ is the k-th element of the length-N_{FFT} FFT of $\hat{\mathbf{h}}$ and $\hat{\sigma}^2$ is given by (2.13). Like FDE1, FDE2 is the MMSE equalizer formulated in the frequency domain. The difference is FDE2 uses an estimate of the true power spectral density of SOQPSK-TG. The SOQPSK-TG power spectral density $\Psi(e^{j\omega_k})$ is illustrated in Figure 2.9. $\Psi(e^{j\omega_k})$ was estimated using Welch's method periodogram averaging based on length-N_{FFT} FFTs of SOQPSK-TG sampled at 2 samples/bit and the Blackman window with 50% overlap.

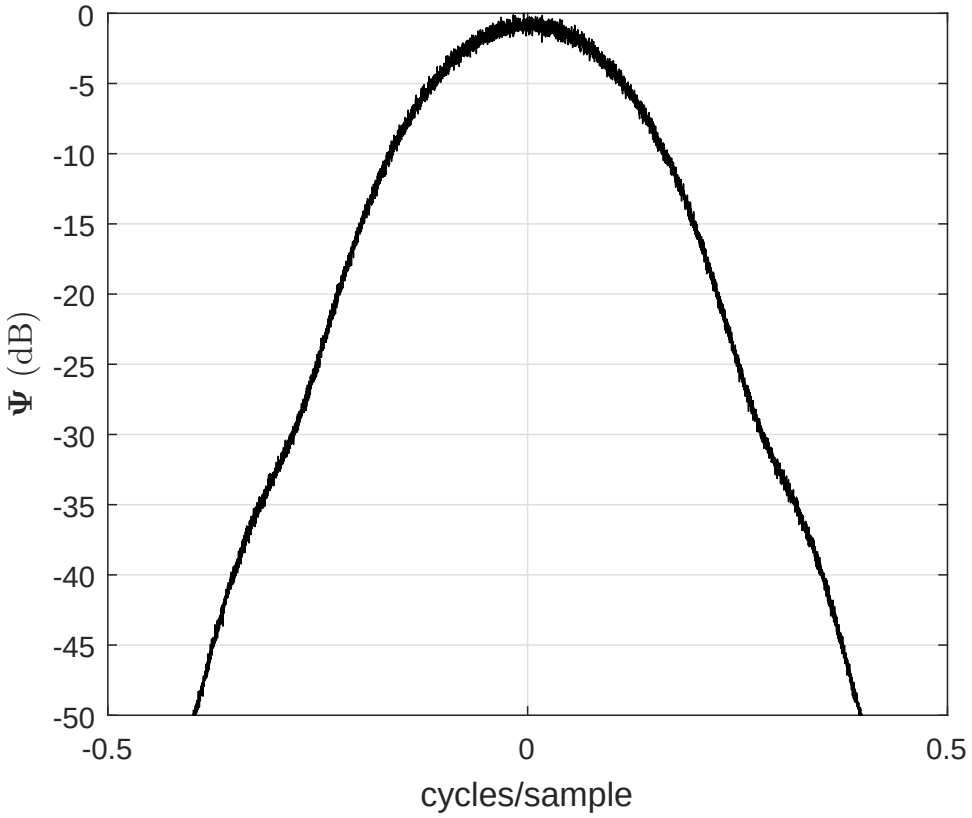

Figure 2.9: SOQPSK-TG power spectral density.

2.3.6 Symbol-by-Symbol Detector

Symbol-by-symbol detection comprises a detection filter and a phase lock loop (PLL) to track out the residual frequency offset. Before the symbols are detected, the equalized samples are passed through the detection filter then down-sampled by 2. The detection filter is a $L_{\text{df}} = 23$ sample "numerically optimized" SOQPSK detection filter $\mathbf{h}_{\text{NO}}$ shown in Figure 2.10 [12, Fig. 3]. The symbol-by-symbol detector block in Figure 2.6 is an OQPSK detector. Using the simple OQPSK detector in place of a complex MLSE SOQPSK-TG detector leads to less than 1 dB loss in detection efficency [12].

A Phase Lock Loop (PLL) is needed in the OQPSK detector to track out residual frequency offset. The residual frequency offset results from a frequency offset estimation error. Equalizers mitigate the effects of phase offset, timing offset, and ISI because all of these imparments form the composite channel seen by the equalizer. A frequency offset is different, and cannot be mitigated

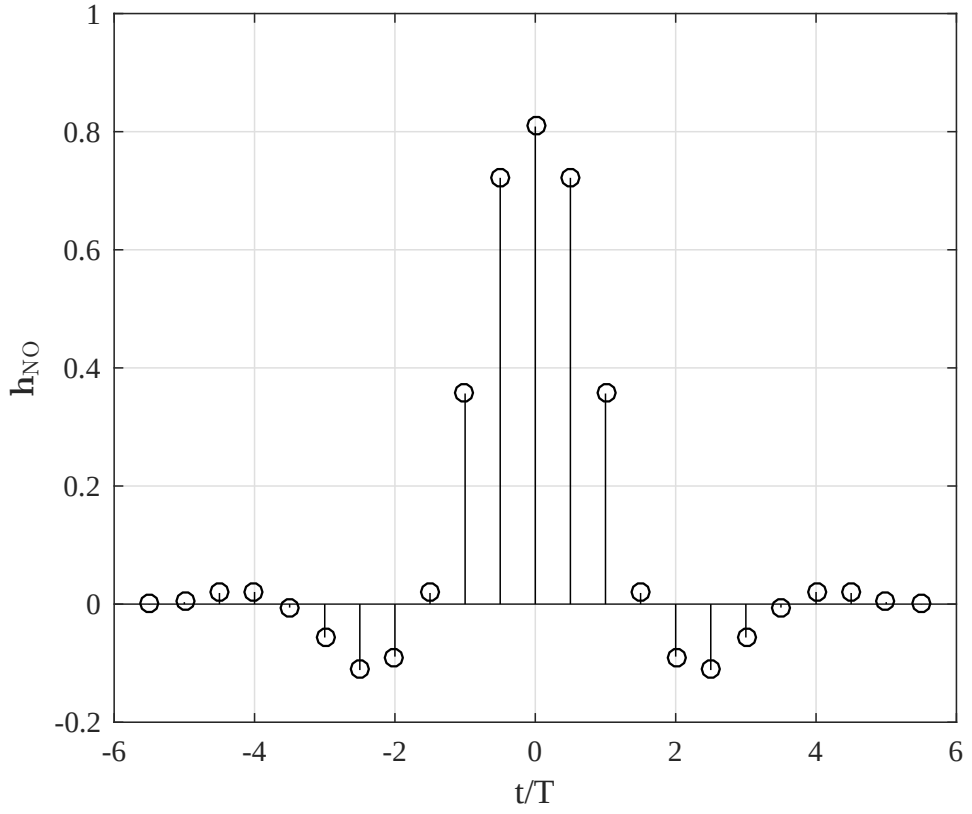

Figure 2.10: "Numerically optimized" SOQPSK detection filter $\mathbf{h}_{\mathrm{NO}}$.

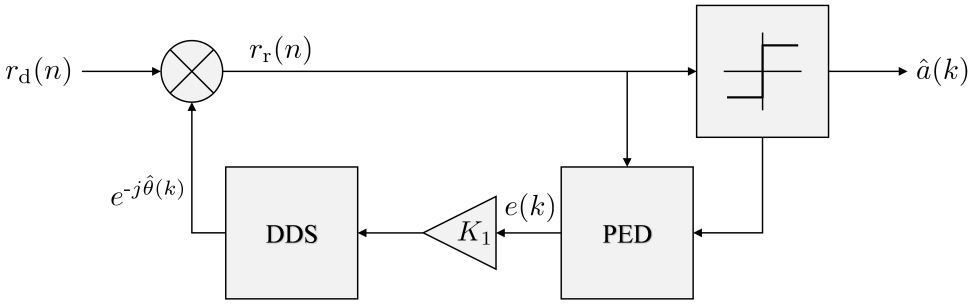

$$\hat{a}(k) = \begin{cases} p(k) & k < L_p + L_{\mathrm{asm}} \\ \mathrm{sgn}(\mathrm{Re}\{r_{\mathrm{r}}(k)\}) & k \geq L_p + L_{\mathrm{asm}} \quad \& \quad k \text{ even} \\ \mathrm{sgn}(\mathrm{Im}\{r_{\mathrm{r}}(k)\}) & k \geq L_p + L_{\mathrm{asm}} \quad \& \quad k \text{ odd} \end{cases}$$

$$e(k) = \begin{cases} 0 & k \text{ even} \\ \hat{a}(k-1)\mathrm{Im}\{r_{\mathrm{r}}(k-1)\} - \hat{a}(k)\mathrm{Re}\{r_{\mathrm{r}}(k)\} & k \text{ odd} \end{cases}$$

Figure 2.11: Offset Quadriture Phase Shift Keying symbol by symbol detector.

by the equalizer alone. The PLL tracks out the residual frequency offset using a feedback control loop.

Implementing a PLL may not seem feasible in GPUs because the feedback loop cannot be parallelized. But the PAQ system processes 3104 packets of data simultaneously in parallel. Running the PLL and detector serially through a full packet of samples is relatively fast because each iteration requires only 10 floating point operations and a few logic decisions.

Chapter 3

Signal Processing in GPUs

A Graphics Processing Unit (GPU) is a computational unit with a highly-parallel architecture well-suited for executing the same function on many data elements. In the past, GPUs were used to process graphics data but in 2008 NVIDIA released the Tesla GPU. Telsa GPUs are built for general purpose high performance computing. Figure 3.1 shows the form factor of a Tesla K40c and K20c.

In 2007 NVIDIA released an extension to C, C++ and Fortran called CUDA (Compute Unified Device Architecture). CUDA enables GPUs to be used for high performance computing in computer vision, deep learning, artificial intelligence and signal processing [13]. CUDA allows a programmer to write C++ like functions that are massively parallel called *kernels*. To invoke parallelism, a GPU kernel executed N times with the work distributed to N_{min} total *threads* that run concurrently. To achieve the full potential of high performance GPUs, kernels must be written with some basic concepts about GPU architecture and memory in mind. This chapter will show the following:

- Optimizing memory access leads to faster execution time rather than optimizing number of floating point operations.
- The number of threads per block can significantly affect execution time.
- CPU and GPU processing can be pipelined.
- Convolution maps very well to GPUs using the Fast Fourier Transform (FFT).
- Batched processing leads to faster execution time per batch.

Figure 3.1: NVIDIA Tesla K40c and K20c.

3.1 GPU and CUDA Introduction

3.1.1 An Example Comparing CPU and GPU

If a programmer has some C++ experience, learning how to program GPUs using CUDA comes fairly easily. GPU code still runs top to bottom and memory still has to be allocated. The only real difference is the physical location of the memory and how functions run on GPUs. To run functions or kernels on GPUs, the memory must be copied from the host (CPU) to the device (GPU). Once the memory has been copied, parallel GPU kernels operate on the data. After GPU kernel execution, results are usually copied back from the device (GPU) to the host (CPU).

Listing 3.1 shows a simple program that implements real-valued float vector addition in a CPU and a GPU. The vector $\mathbf{C}_1$ is the sum of the vectors $\mathbf{A}_1$ and $\mathbf{B}_1$ computed in the CPU. The vector $\mathbf{C}_2$ is the sum of the vectors $\mathbf{A}_2$ and $\mathbf{B}_2$ computed in the GPU. Line 42 the CPU computes $\mathbf{C}_1$ by summing elements of $\mathbf{A}_1$ and $\mathbf{B}_1$ together *sequentially*. Figure 3.2 shows how the

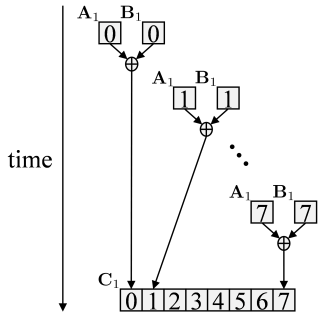

Figure 3.2: A block diagram of how a CPU sequentially performs vector addition.

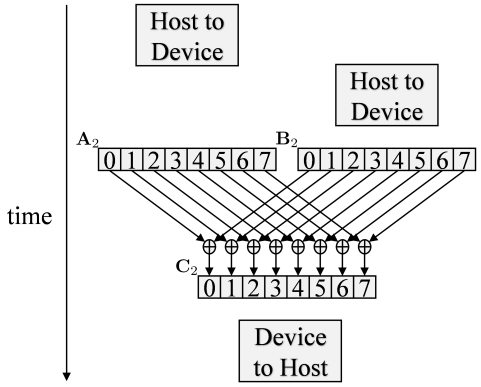

Figure 3.3: A block diagram of how a GPU performs vector addition in parallel.

CPU sequentially computes one element of $\mathbf{C}_1$ at time by summing one element from $\mathbf{A}_1$ and one element $\mathbf{B}_1$.

The GPU performs all the summations in parallel because each element of $\mathbf{C}_2$ is independent of all other elements. Before the computation of $\mathbf{C}_2$ can execute on the GPU, the vectors in host memory $\mathbf{A}_1$ and $\mathbf{B}_1$ are copied to device memory vectors $\mathbf{A}_2$ and $\mathbf{B}_2$ as shown on lines 60 and 61. Once $\mathbf{A}_2$ and $\mathbf{B}_2$ are on the GPU, the vector $\mathbf{C}_2$ is computed by calling the GPU kernel VecAddGPU on line 75. VecAddGPU computes all the elements of $\mathbf{C}_2$ by performing a summation of all the elements of $\mathbf{A}_2$ and $\mathbf{B}_2$. The vector $\mathbf{C}_2$ is then copied from device memory to host memory on line 78. Figure 3.3 shows how the GPU computes $\mathbf{C}_2$ *in parallel*.

Listing 3.1: Comparison of CPU and GPU code.

```
#include <iostream>
#include <stdlib.h>
#include <math.h>
using namespace std;

void VecAddCPU(float* destination,float* source0,float* source1,int myLength){
        for(int i = 0; i < myLength; i++)
                destination[i] = source0[i] + source1[i];
}

__global__ void VecAddGPU(float* destination, float* source0, float* source1, int lastThread){
        int i = blockIdx.x*blockDim.x + threadIdx.x;

        // don't access elements out of bounds
        if(i >= lastThread)
                return;

        destination[i] = source0[i] + source1[i];
}

int main(){
        int N = pow(2,22);
        cout << N << endl;
        /**
        * Vector Addition on CPU
        */
        // allocate memory on host
        float *A1;
        float *B1;
        float *C1;
        A1 = (float*) malloc (N*sizeof(float));
        B1 = (float*) malloc (N*sizeof(float));
        C1 = (float*) malloc (N*sizeof(float));

        // Initialize vectors 0-99
        for(int i = 0; i < N; i++){
                A1[i] = rand()%100;
                B1[i] = rand()%100;
        }

        // vector sum C1 = A1 + B1
        VecAddCPU(C1, A1, B1, N);

        /**
        * Vector Addition on GPU
        */
        // allocate memory on host for result
        float *C2;
        C2 = (float*) malloc (N*sizeof(float));

        // allocate memory on device for computation
        float *A2_gpu;
        float *B2_gpu;
        float *C2_gpu;
        cudaMalloc(&A2_gpu, sizeof(float)*N);
        cudaMalloc(&B2_gpu, sizeof(float)*N);
        cudaMalloc(&C2_gpu, sizeof(float)*N);

        // Copy vectors A and B from host to device
        cudaMemcpy(A2_gpu, A1, sizeof(float)*N, cudaMemcpyHostToDevice);
        cudaMemcpy(B2_gpu, B1, sizeof(float)*N, cudaMemcpyHostToDevice);

        // Set optimal number of threads per block
        int T_B = 32;

        // Compute number of blocks for set number of threads
```

```
67          int B = N/T_B;
68
69          // If there are left over points, run an extra block
70          if(N % T_B > 0)
71                  B++;
72
73          // Run computation on device
74          //for(int i = 0; i < 100; i++)
75          VecAddGPU<<<B, T_B>>>(C2_gpu, A2_gpu, B2_gpu, N);
76
77          // Copy vector C2 from device to host
78          cudaMemcpy(C2, C2_gpu, sizeof(float)*N, cudaMemcpyDeviceToHost);
79
80          // Compare C2 to C1
81          bool equal = true;
82          for(int i = 0; i < N; i++)
83                  if(C1[i] != C2[i])
84                          equal = false;
85          if(equal)
86                  cout << "C2 is equal to C1." << endl;
87          else
88                  cout << "C2 is NOT equal to C1." << endl;
89
90          // Free vectors on CPU
91          free(A1);
92          free(B1);
93          free(C1);
94          free(C2);
95
96          // Free vectors on GPU
97          cudaFree(A2_gpu);
98          cudaFree(B2_gpu);
99          cudaFree(C2_gpu);
100 }
```

3.1.2 GPU kernel using threads and thread blocks

A GPU kernel is executed by launching blocks with a set number of threads per block. In the Listing 3.1, VecAddGPU is launched on line 75 with 32 threads per block. The total number of threads launched on the GPU is the number of blocks times the number of threads per block. VecAddGPU needs to be launched with at least $N = 2^{22}$ (line 22) threads or $2^{22}/32$ blocks of 32 threads.

CUDA gives each thread launched in a GPU kernel a set of unique indices called threadIdx and blockIdx. threadIdx is the thread index inside the assigned thread block. blockIdx is the index of the block to which the thread is assigned. Both threadIdx and blockIdx are three dimensional (i.e. they both have x, y, and z components). In this thesis only the x dimension is used because the GPU kernels operate only on one dimensional vectors. blockDim is the number of threads assigned

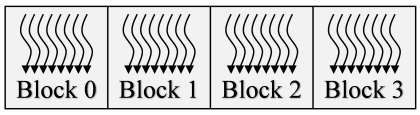

Figure 3.4: 32 threads launched in 4 thread blocks with 8 threads per block.

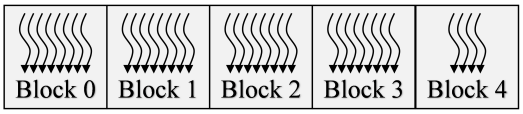

Figure 3.5: 36 threads launched in 5 thread blocks with 8 threads per block with 4 idle threads.

per block, in fact blockDim is equal to the number of threads per block because the vectors are one dimensional.

To convert the CPU "for loop" on line 7 to a GPU kernel, at least N threads are launched with T threads per thread block. The number of blocks needed is $B = \frac{N}{T_B}$ or $B = \frac{N}{T} + 1$ if N is not an integer multiple of T. Figure 3.4 shows $N = 32$ threads launched in $B = 4$ thread blocks with $T = 8$ threads per block. Figure 3.5 shows $N = 36$ threads launched in $B = 5$ thread blocks with $T = 8$ threads per block. An full extra thread block is launched with $T = 8$ threads but 4 threads are idle. Note that thread blocks are executed independent of other thread blocks. The GPU does not guarantee Block 0 will execute before Block 2.

3.1.3 GPU Memory

GPUs have plenty of computational resources but most GPU kernels are limited by memory bandwidth to feed the computational units. GPU kernels execute faster if the kernel is designed to access memory efficiently rather than reducing the computational burden. NVIDIA GPUs have many different types of memory to maximize speed and efficiency.

The fastest memory is private local memory, in the form of Registers and L1 Cache/shared memory. Local memory is fast but only kilobytes are available. The slowest memory is public memory in the form of the L2 Cache and Global Memory. Public memory is slow but gigabytes

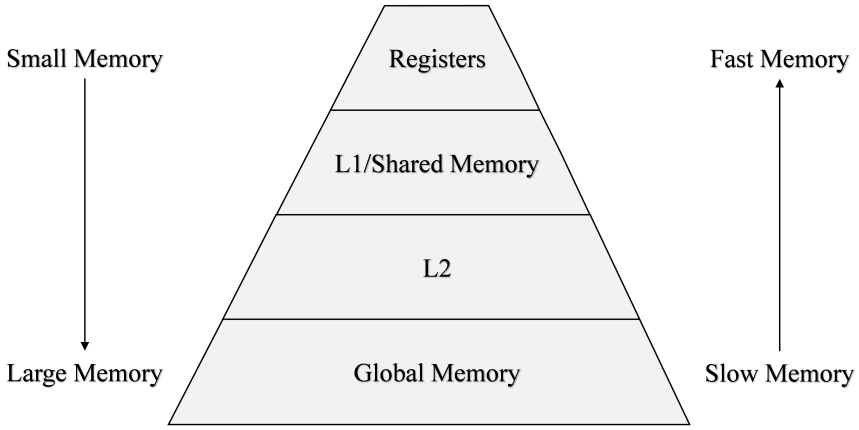

Figure 3.6: Diagram comparing memory size and speed. Global memory is massive but extremely slow. Registers are extremely fast but there are very few.

are available. Figure 3.6 shows the trade-off of memory speed and the size of different types of memory.

Figure 3.7 shows a picture of the GPU hardware. The solid boxes show that the L2 cache and Global Memory are physically located *off* the GPU chip. The dashed box shows that Registers and L1 Cache/Shared Memory are physically located *on* the GPU chip. A public access takes over 60 clock cycles because the memory is off chip. A local memory access is only a few clock cycles because the memory is on chip.

Figure 3.8 illustrates where each type of memory is located. Threads have access to their own Registers and the L1 Cache. Threads in a block can coordinate using shared memory because shared memory is private to the thread block. All threads have access to the L2 Cache and Global Memory. The figure also shows that thread blocks are assigned to streaming multiprocessors (SMs). CUDA handles all the thread block assignments to SMs. Table 3.1 lists Telsa K40c and K20c resources.

3.1.4 Thread Optimization

Most resources listed in Table 3.1 show how much memory per thread block is available. The number of threads per block and the amount of resources available have an inverse relationship.

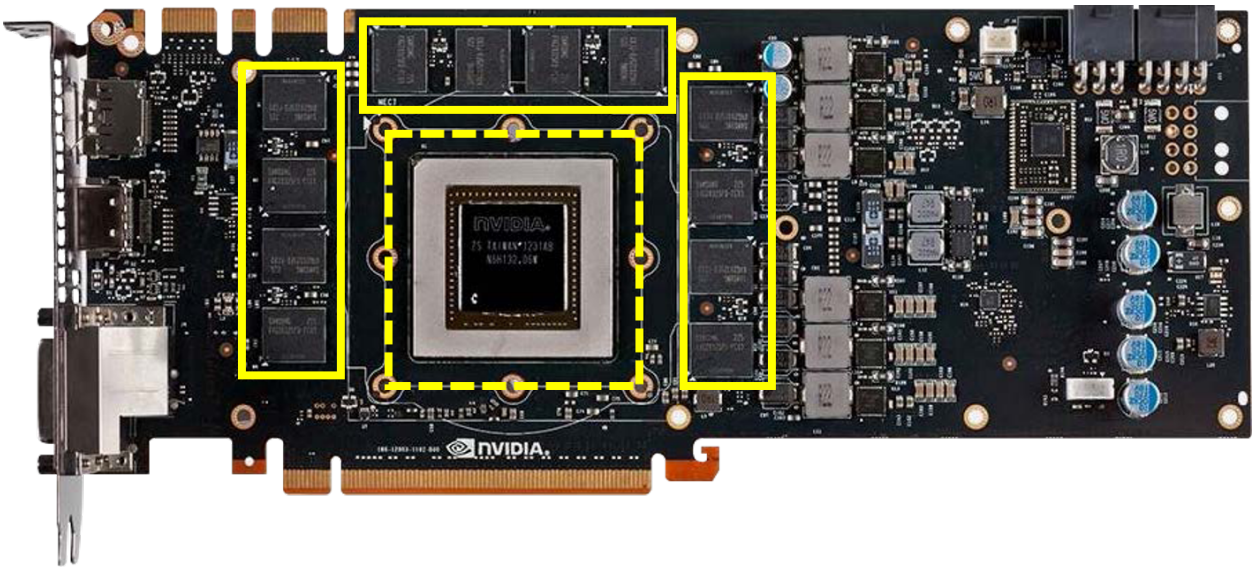

Figure 3.7: Example of an NVIDIA GPU card. The GPU chip with registers and L1/shared memory is shown in the dashed box. The L2 cache and global memory is shown off chip in the solid boxes.

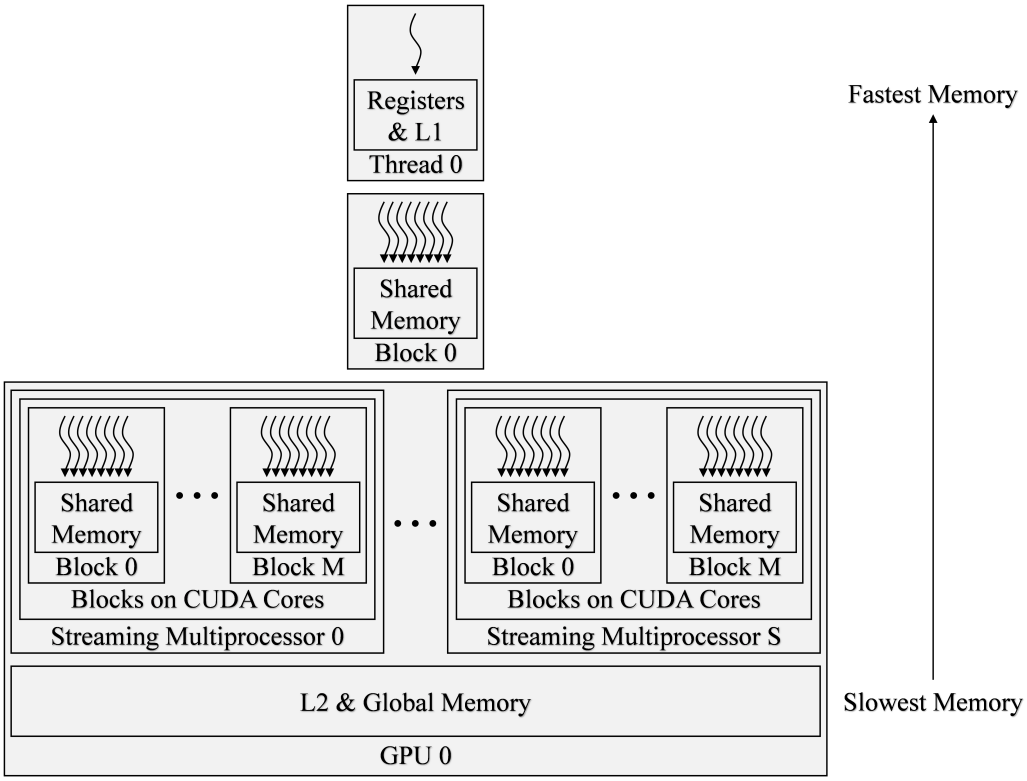

Figure 3.8: A block diagram where local, shared, and global memory is located. Each thread has private local memory. Each thread block has private shared memory. The GPU has global memory that all threads can access.

Table 3.1: The resources available with three NVIDIA GPUs used in this thesis (1x Tesla K40c 2x Tesla K20c). Note that CUDA configures the size of the L1 cache needed.

Feature	Per	Tesla K40c	Tesla K20c
Global Memory	GPU	12 GB	5 GB
L2 Cache Size	GPU	1.6 GB	1.3 GB
Memory Bandwidth		288 GB/s	208 GB/s
Shared Memory	Thread Block	49 kB	49 kB
L1 Cache Size	Thread Block	variable	variable
Registers	Thread Block	65536	65536
Maximum Threads	Thread Block	1024	1024
CUDA Cores	GPU	2880	2496
Base Core Clock		745 MHz	732 MHz

Threads have very little memory resources available if a GPU kernel launches 1024 threads per block. Threads have a lot of memory resources available if a GPU kernel launches 32 threads per block. This section shows that finding the optimum number of threads per block can dramatically speed up GPU kernels.

Improving memory accesses should always be the first optimization when a GPU kernel needs to be faster. The next step is to find the optimal number of threads per block to launch. Knowing the perfect number of threads per block to launch is challenging to calculate. Fortunately, the maximum number of possible threads per block is 1024 in the Tesla K40c and K20c GPUs. Listing 3.2 shows a simple test program that measures GPU kernel execution time while varying the number of possible threads per block. The number of threads per block with the fastest computation time is the optimal number of threads per block for that specific GPU kernel.

Listing 3.2: Code snippet for thread optimization.

```
float milliseconds_opt = pow(2,10); // initiaize to "big" number
int T_B_opt;
int minNumTotalThreads = pow(2,20); // set to minimum number of required threads
for(int T_B = 1; T_B<=1024; T_B++){
        int B = minNumTotalThreads/T_B;
        if(minNumTotalThreads % T_B > 0)
                B++;
        cudaEvent_t start, stop;
        cudaEventCreate(&start);
        cudaEventCreate(&stop);
        cudaEventRecord(start);

        GPUkernel<<<B, T_B>>>(dev_vec0, dev_vec1);

        cudaEventRecord(stop);
        cudaEventSynchronize(stop);
        float milliseconds = 0;
        cudaEventElapsedTime(&milliseconds, start, stop);
        cudaEventDestroy(start);
        cudaEventDestroy(stop);
        if(milliseconds<milliseconds_opt){
                milliseconds_opt = milliseconds;
                T_B_opt = T_B;
        }
}
cout << "Optimal Threads Per Block " << T_B_opt << endl
cout << "Optimal Execution Time    " << milliseconds_opt << endl;
```

Most of the time the optimal number of threads per block is a multiple of 32 this is because at the lowest level of architecture, GPUs perform computations in *warps*. Warps are groups of 32 threads that perform every computation together in lock step. If the number of threads per block is not a multiple of 32, some threads in a warp are idle and the GPU has unused computational resources.

Figure 3.9 shows the execution time of an example GPU kernel. The optimal execution time is 0.1078 ms at the optimal 96 threads per block. By simply adjusting the number of threads per block, the execution time of this example kernel can be reduced by 2.

Adjusting the number of threads per block does not always dramatically reduce execution time. Figure 3.10 shows the execution time for another GPU kernel with varying threads per block. The execution time of this example kernel can be reduced by 1.12 by launching 560 threads per block.

While designing a custom GPU kernel to obtain a major speed up is satisfying, CUDA has optimized GPU libraries that are extremely useful and efficient with exceptional documentation.

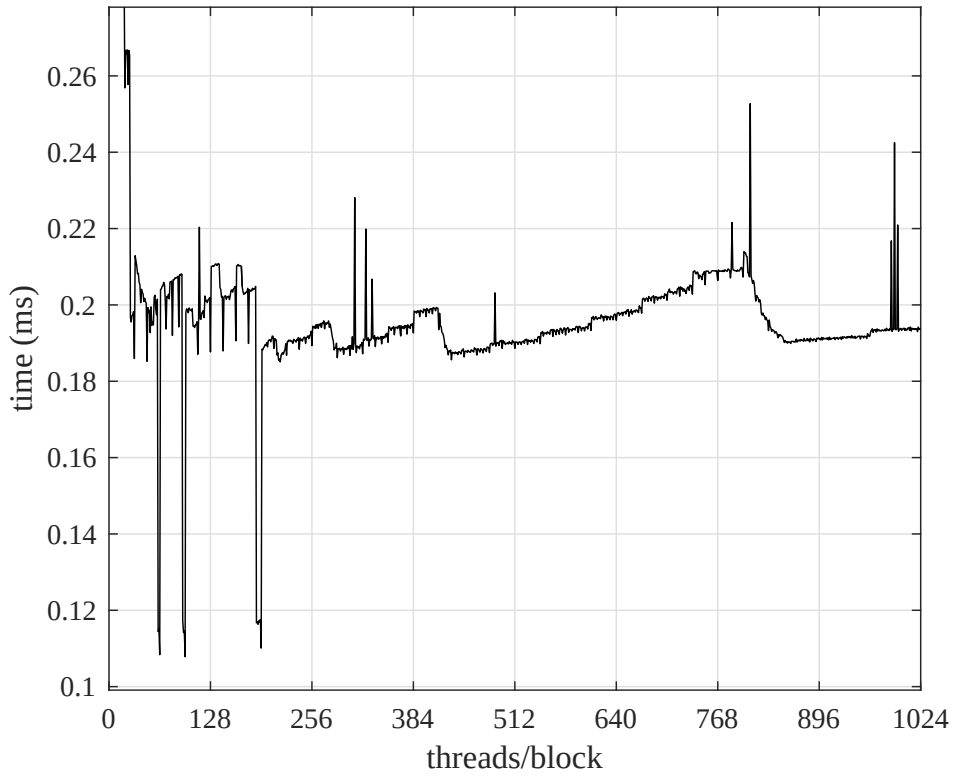

Figure 3.9: Plot showing how execution time is affected by changing the number of threads per block. The optimal execution time for an example GPU kernel is 0.1078 ms at the optimal 96 threads per block.

The CUDA libraries are written by NVIDIA engineers to maximize the performance of NVIDIA GPUs. The libraries explained in this thesis include cuFFT, cuBLAS and cuSolverSp.

3.1.5 CPU and GPU Pipelining

While GPU kernels execute physically on the GPU, the GPU only executes instructions received from the host CPU. The CPU is idle while it waits for GPU kernels to execute. To introduce CPU and GPU pipelining, the CPU can be pipelined by performing other operations while waiting for the GPU to finish executing kernels.

A basic CPU GPU program with no pipelining is shown in Listing 3.3. The CPU acquires data from myADC on Line 5. After the CPU takes time to acquire data, the data is copied from the host (CPU) to the device (GPU) on line 8. The data is processed on the GPU once then the result

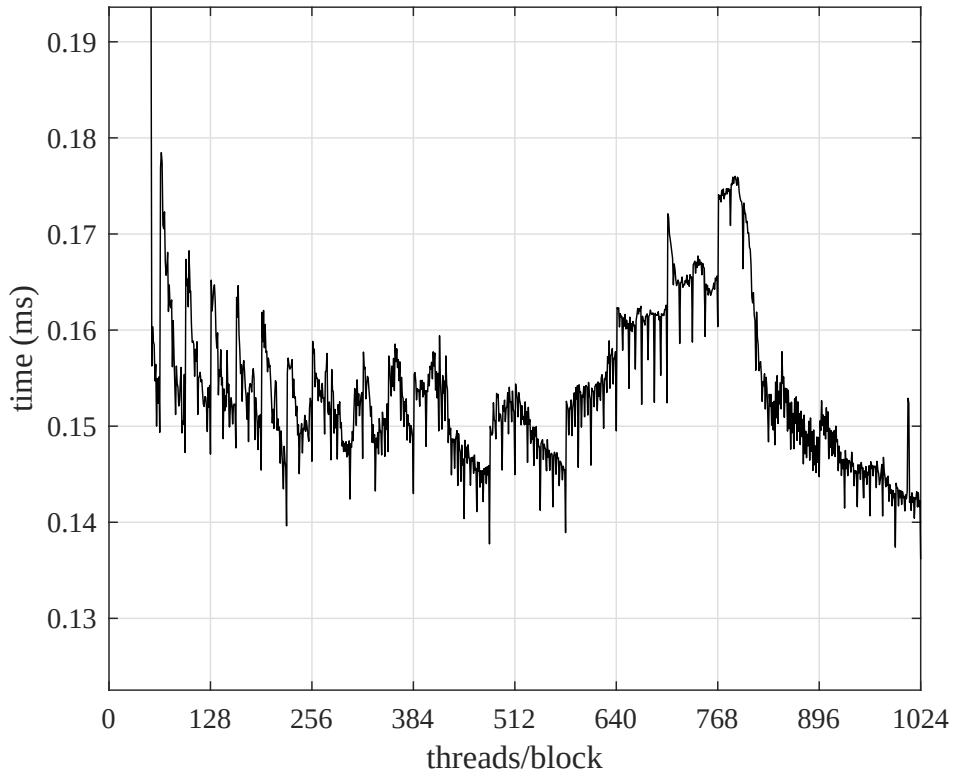

Figure 3.10: Plot showing the number of threads per block doesn't always drastically affect execution time.

is copied back to the device to host on line 9 and 10. The cudaDeviceSynchronize function on line 13 blocks CPU until all GPU instructions are finished executing. Note that the CPU is blocked during any host to device or device to host transfer. Acquiring and copying data takes processing time on the CPU and GPU. Figure 3.11 shows a block diagram of what is happening on the CPU and GPU in Listing 3.3 (end of the section). The GPU is idle while the CPU is acquiring data and the CPU is idle while the GPU is processing.

Listing 3.4 (end of the section) shows how to CPU and GPU operations can be pipelined. Assuming data is already on the GPU from a prior computation, the CPU gives processing instructions to the GPU then acquires data. The CPU then does an asynchronous data transfer to a temporary vector on the GPU. The GPU first performs a device to device transfer from the temporary vector. The GPU then runs the GPUkernel and transfers the result to the host. Note that device to device transfers do not block the CPU. This system suffers a full cycle latency.

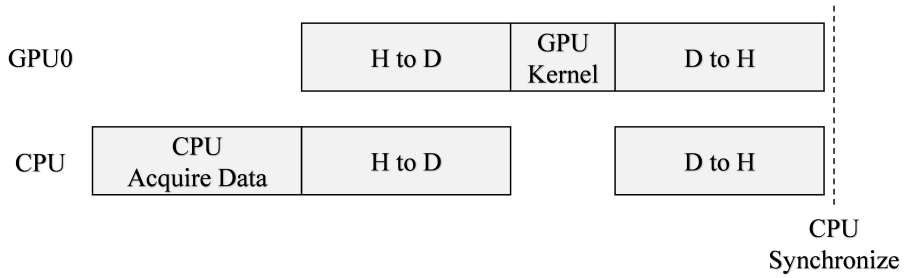

Figure 3.11: The typical approach of CPU and GPU operations. This block diagram shows the profile of Listing 3.3.

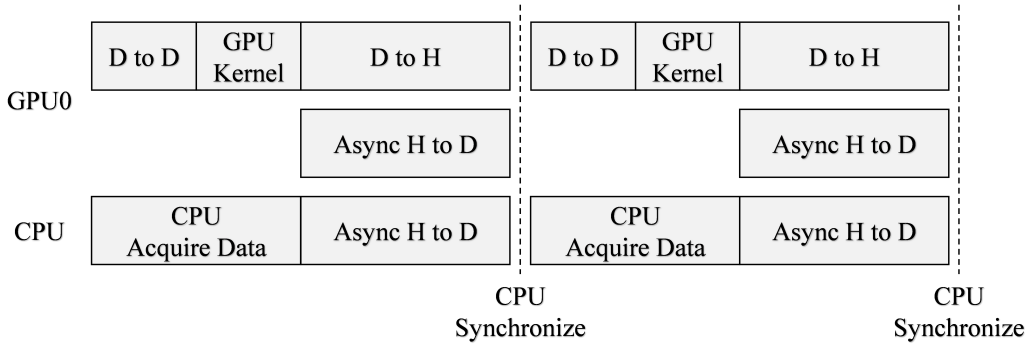

Figure 3.12: GPU and CPU operations can be pipelined. This block diagram shows a Profile of Listing 3.4.

Pipelineing can be extended to multiple GPUs for even more throughput but only suffer latency of copying memory to one GPU. Figure 3.13 shows a block diagram of how three GPUs can be pipelined. A strong understanding of the full system is required to pipeline at this level.

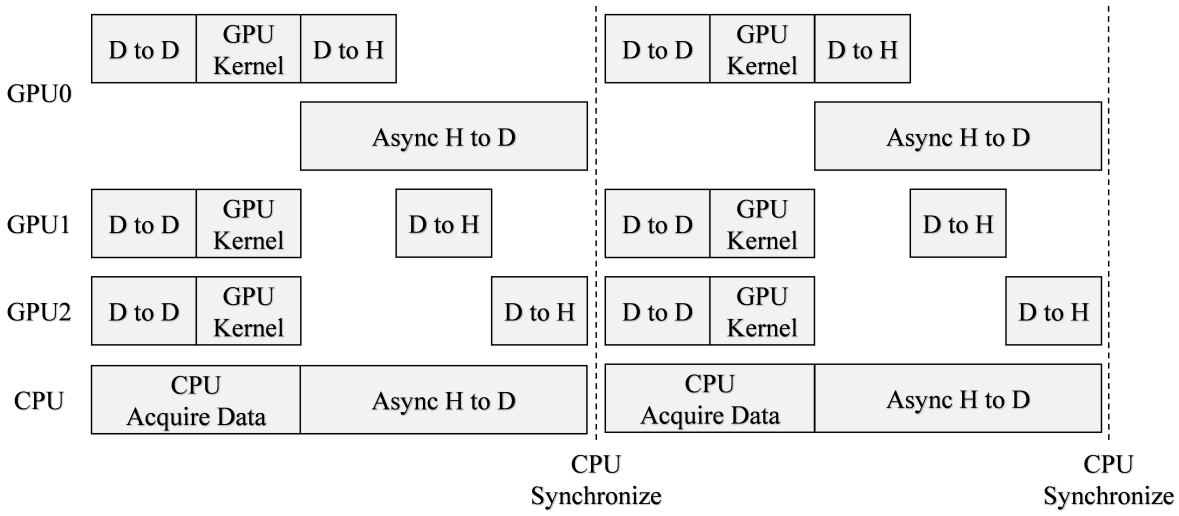

Figure 3.13: A block diagram of pipelining a CPU with three GPUs.

Listing 3.3: Example code Simple example of the CPU acquiring data from myADC, copying from host to device, processing data on the device then copying from device to host. No processing occurs on device while CPU is acquiring data.

```
int main()
{
        ...
        // CPU Acuire Data
        myADC.acquire(vec);

        // Launch instructions on GPU
        cudaMemcpy(dev_vec0, vec,      numBytes, cudaMemcpyHostToDevice);
        GPUkernel<<<1, N>>>(dev_vec0);
        cudaMemcpy(vec,      dev_vec0, numBytes, cudaMemcpyDeviceToHost);

        // Synchronize CPU with GPU
        cudaDeviceSynchronize();
        ...
}
```

Listing 3.4: Example code Simple of the CPU acquiring data from myADC, copying from host to device, processing data on the device then copying from device to host. No processing occurs on device while CPU is acquiring data.

```
int main()
{
        ...
        // Launch instructions on GPU
        cudaMemcpy(dev_vec, dev_temp, numBytes, cudaMemcpyDeviceToDevice);
        GPUkernel<<<N, M>>>(dev_vec);
        cudaMemcpy(vec,     dev_vec,  numBytes, cudaMemcpyDeviceToHost);

        // CPU Acuire Data
        myADC.acquire(vec);
        cudaMemcpyAsync(dev_temp, vec, numBytes, cudaMemcpyHostToDevice);

        // Synchronize CPU with GPU
        cudaDeviceSynchronize();
        ...

        ...
        // Launch instructions on GPU
        cudaMemcpy(dev_vec, dev_temp, numBytes, cudaMemcpyDeviceToDevice);
        GPUkernel<<<N, M>>>(dev_vec);
        cudaMemcpy(vec,     dev_vec,  numBytes, cudaMemcpyDeviceToHost);

        // CPU Acuire Data
        myADC.acquire(vec);
        cudaMemcpyAsync(dev_temp, vec, numBytes, cudaMemcpyHostToDevice);

        // Synchronize CPU with GPU
        cudaDeviceSynchronize();
        ...
}
```

3.2 GPU Convolution

Convolution is one of the most important tools in digital signal processing. The PAQ system explained uses convolution up to 26 times per packet, depending on the number of CMA iterations. If convolution execution time can be reduced by 10 ms, the full system execution time can reduced by 260 ms. This section will use the following notation:

- The signal $\mathbf{x}$ is a vector of N complex samples indexed by $x(n)$ where $0 \leq\leq N-1$.
- The filter $\mathbf{h}$ is a vector of L complex samples indexed by $h(n)$ where $0 \leq\leq L-1$.
- The filtered signal $\mathbf{y}$ is a vector resulting from the convolution of $\mathbf{x}$ and $\mathbf{h}$. $\mathbf{y}$ is $C = N+L-1$ complex samples and is indexed by $y(n)$ where $0 \leq n \leq C-1$.
- The forward Fast Fourier Transform (FFT) of the vector $\mathbf{x}$ is denoted $\mathscr{F}(\mathbf{x})$.
- The inverse Fast Fourier Transform (IFFT) of the vector $\mathbf{x}$ is denoted $\mathscr{F}^{-1}(\mathbf{x})$.

Discrete time convolution applies the filter $\mathbf{h}$ to the signal $\mathbf{x}$ resulting in the filter signal $\mathbf{y}$. Convolution in the time domain is

$$y(n) = \sum_{m=0}^{L-1} x(m)h(n-m) \tag{3.1}$$

and the frequency domain is

$$\mathbf{y} = \mathscr{F}^{-1}(\mathscr{F}(\mathbf{x}) \times \mathscr{F}(\mathbf{h})). \tag{3.2}$$

Figure 3.14 shows block diagrams for time-domain and frequency domain convolution. This section will show:

- GPU convolution is faster than CPU convolution with large data sets using execution time as a metric.
- GPU convolution execution time is dependent more on memory access than floating point operations.

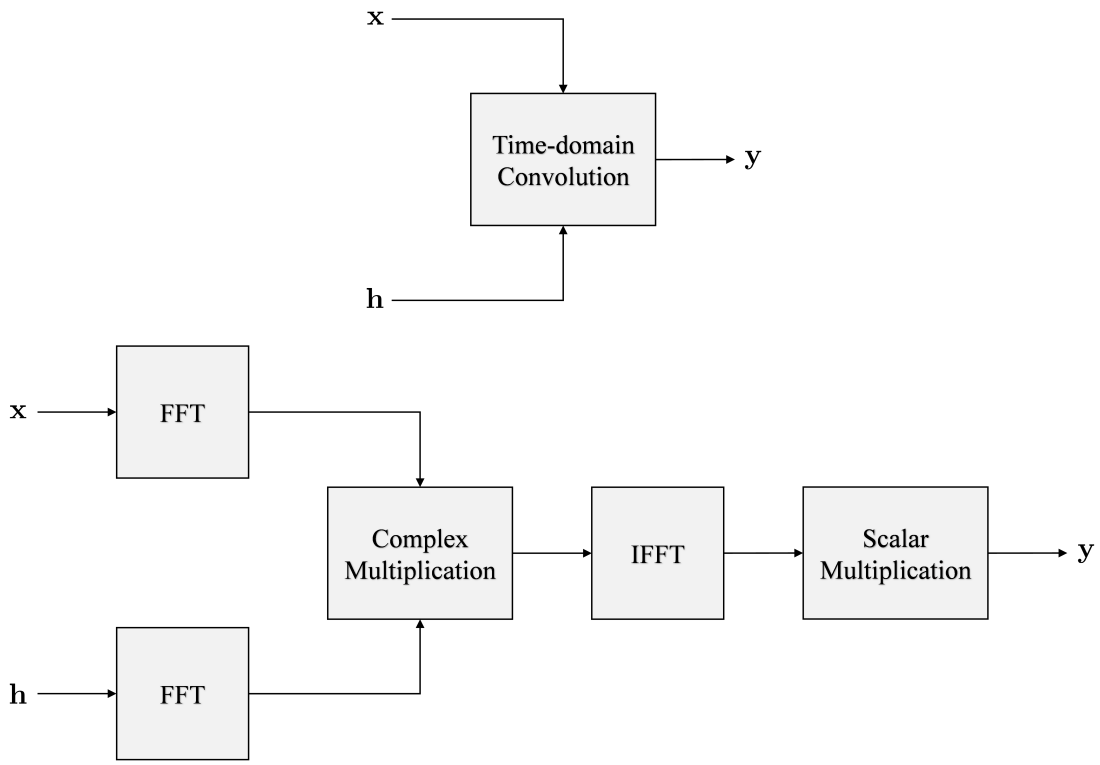

Figure 3.14: Block diagrams showing time-domain convolution and frequency-domain convolution.

- Performing batched GPU convolution invokes more parallelism and decreases execution time per batch.
- Batched GPU frequency-domain convolution executes faster than batched GPU time-domain convolution.

3.2.1 Floating Point Operation Comparison

Traditionally the number of floating point operations (flops) is used to estimate how computationally intense an algorithm is. Each complex multiplication

$$(A + jB) \times (C + jD) = (AC - BD) + j(AD + BC) \tag{3.3}$$

requires 6 flops, 4 multiplications and 2 additions/subtractions. Output elements of $\mathbf{y}$ in Equation (3.1) requires $8L = (6+2)L$ flops, 2 extra flops are required for each summand. The time-domain convolution requires

$$8LC \text{ flops} \tag{3.4}$$

where $C = N + L - 1$ is the length of the convolution result.

To leverage the Cooley-Tukey radix 2 Fast Fourier Transform (FFT) in frequency-domain convolution, common practice is to compute the M point FFT where $M = 2^u$ and $u = \lceil \log_2(C) \rceil$. Both the CPU based Fastest Fourier Transform in the West (FFTW) library and the NVIDIA GPU cuFFT library use the Cooley-Tukey radix 2 FFT. Each FFT or IFFT requires $5M \log_2(M)$ flops [14, 15]. As shown by Equation (3.2), frequency-domain convolution requires

$$3 \times 5M \log_2(M) + 6M \text{ flops} \tag{3.5}$$

from 3 FFTs and M point-to-point multiplications.

Sections 2.2 and 2.3.6 show the PAQ system has one signal length, $N = L_{\text{pkt}} = 12672$ samples and two filter lengths $L = L_{\text{df}} = 23$ and $L = L_{\text{eq}} = 186$. Figures 3.15 through 3.17 compare the number of flops required for time-domain and frequency-domain convolution. The figures compare flops by fixing the signal length with variable filter length or visa versa. These figures show applying a 186 tap filter to a 12672 sample signal requires less flops in the frequency domain and applying a 23 tap filter to a 12672 sample signal requires less flops in the time domain.

3.2.2 CPU and GPU Single convolution using batch processing Comparison

This section will show GPU convolution execution time is dependent more on memory access than the number of required floating point operations while CPU convolution execution time is dependent on the number of floating point operations. To illustrate these points, the execution

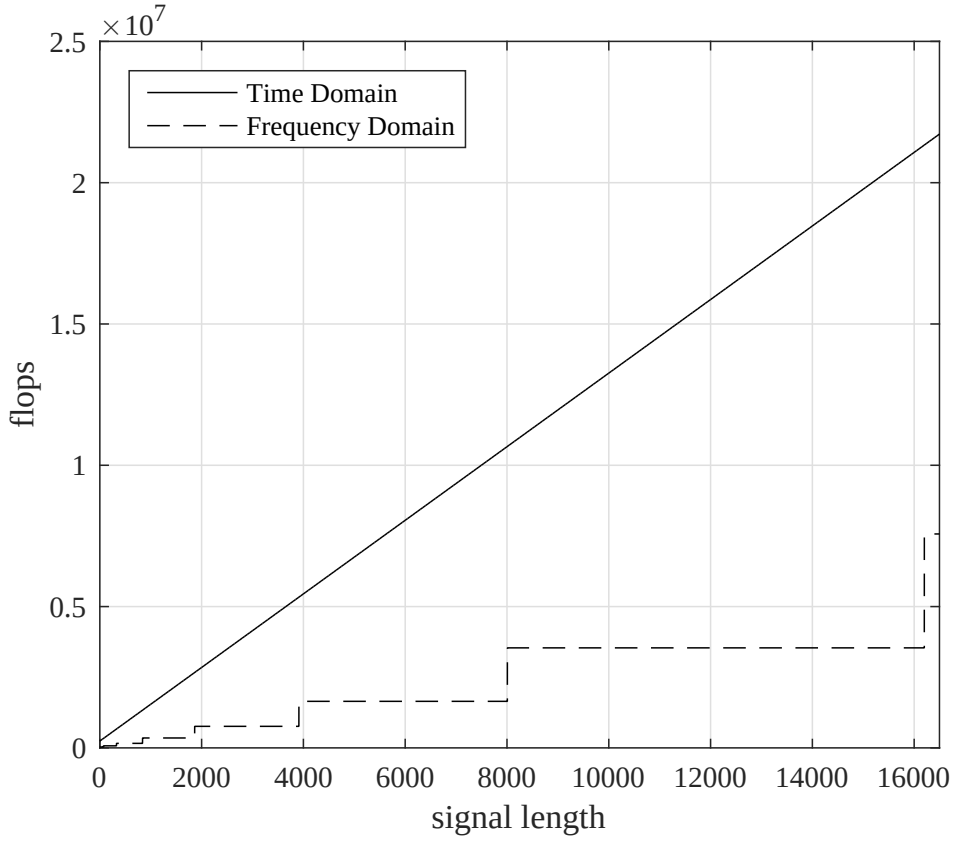

Figure 3.15: Comparison of number of floating point operations (flops) required to convolve a variable length complex signal with a 186 tap complex filter.

time of the code in Listing 3.5 (at the end of the chapter) was measured. The code implements convolution five different ways:

- time-domain convolution in a CPU
- frequency-domain convolution in a CPU using the FFTW library
- time-domain convolution in a GPU using global memory
- time-domain convolution in a GPU using shared memory
- frequency-domain convolution in a GPU using the cuFFT library

The three time-domain convolution implementations compute (3.1) directly. The two frequency-domain convolution implementations compute (3.2) using the CPU FFTW library and

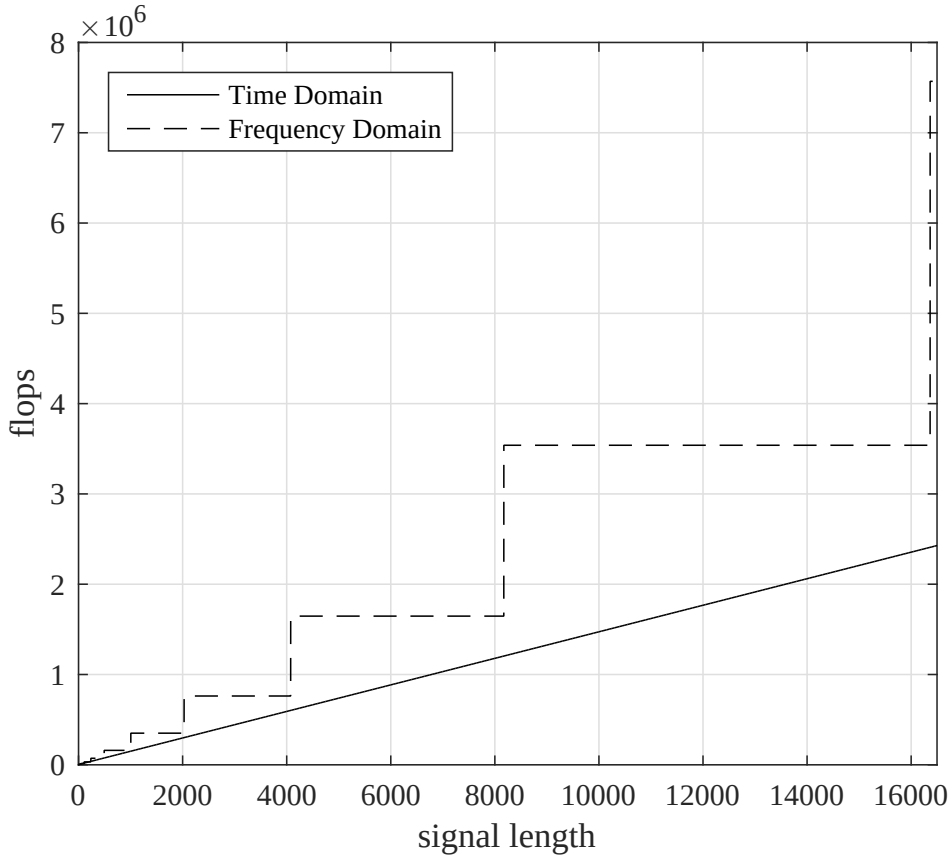

Figure 3.16: Comparison of number of floating point operations (flops) required to convolve a variable length complex signal with a 23 tap complex filter.

the GPU based cuFFT library. The cuFFT library uses global memory and shared memory to be as fast and efficient as possible. For a given signal and filter length, a good CUDA programmer can make an educated guess on which algorithm is faster. There is no clear conclusion until all the algorithms have been implemented and measured.

All the memory transfers to and from the GPU were timed for a fair comparison of GPU to CPU execution time. Table 3.2 shows how the execution time was measured for each convolution implementation. Figures 3.18 through 3.21 compare execution time of the five different convolution implementations by fixing the filter length with variable signal length or visa versa. Sub-windows emphasize points that are of interest to the PAQ system. The variations in the time-domain CPU execution times are du to the claims on the host CPU resources by the operating

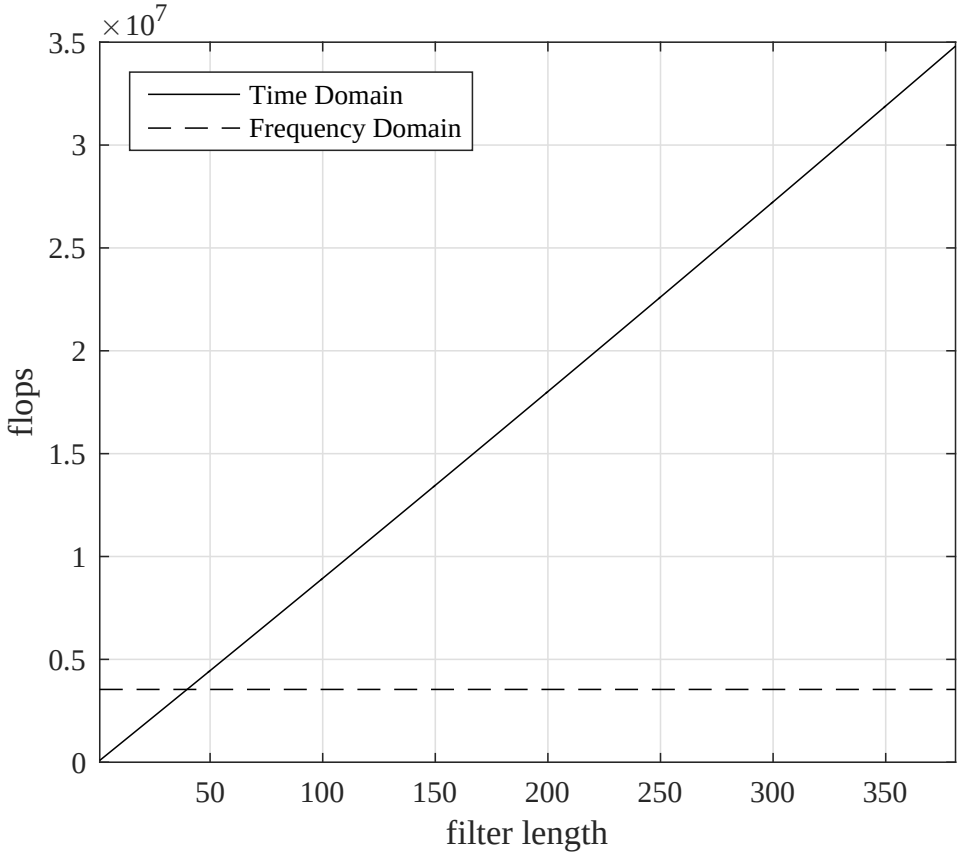

Figure 3.17: Comparison of number of floating point operations (flops) required to convolve a 12672 sample complex signal with a variable length tap complex filter.

Table 3.2: Defining start and stop lines for timing comparison in Listing 3.5.

Algorithm	Function	Start Line	Stop Line
CPU time domain	ConvCPU	208	210
CPU frequency domain	FFTW	213	259
GPU time domain global	ConvGPU	267	278
GPU time domain shared	ConvGPUshared	282	293
GPU frequency domain	cuFFT	301	327

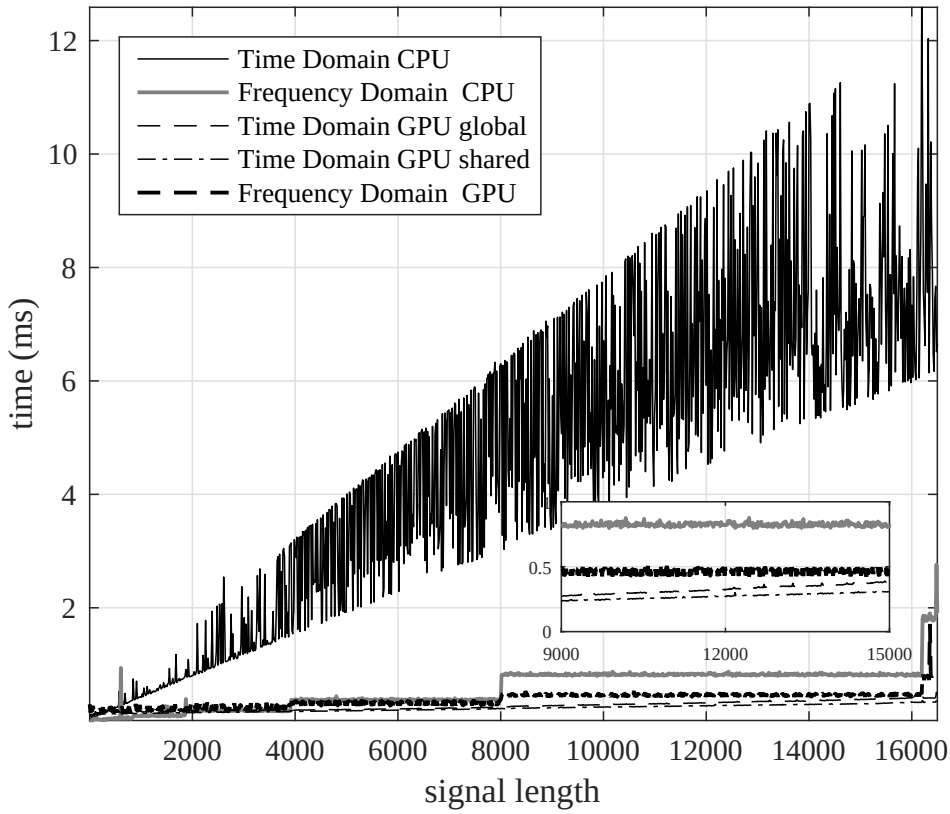

Figure 3.18: Comparison of a complex convolution on CPU and GPU. The signal length is variable and the filter is fixed at 186 taps. The comparison is messy with out lower bounding.

system. To clean up the time samples, local minimums were found in windows ranging from 3 to 15 samples. The smallest windows possible were used to produce the results.

Comparing Figures 3.19 through 3.21 to Figures 3.15 through 3.17 shows CPU and GPU convolution have the same structure that the number of flops predicted except GPU convolution is not affected as much by varied signal or filter lengths. The convolution execution time comparison demonstrates the observation that most GPU kernels execution time is limited by memory bandwidth not computational resources. Tables 3.3 and 3.4 show the GPU time-domain algorithm using shared memory is fastest for the signal length and filter lengths of the PAQ system when performing a single complex convolution.

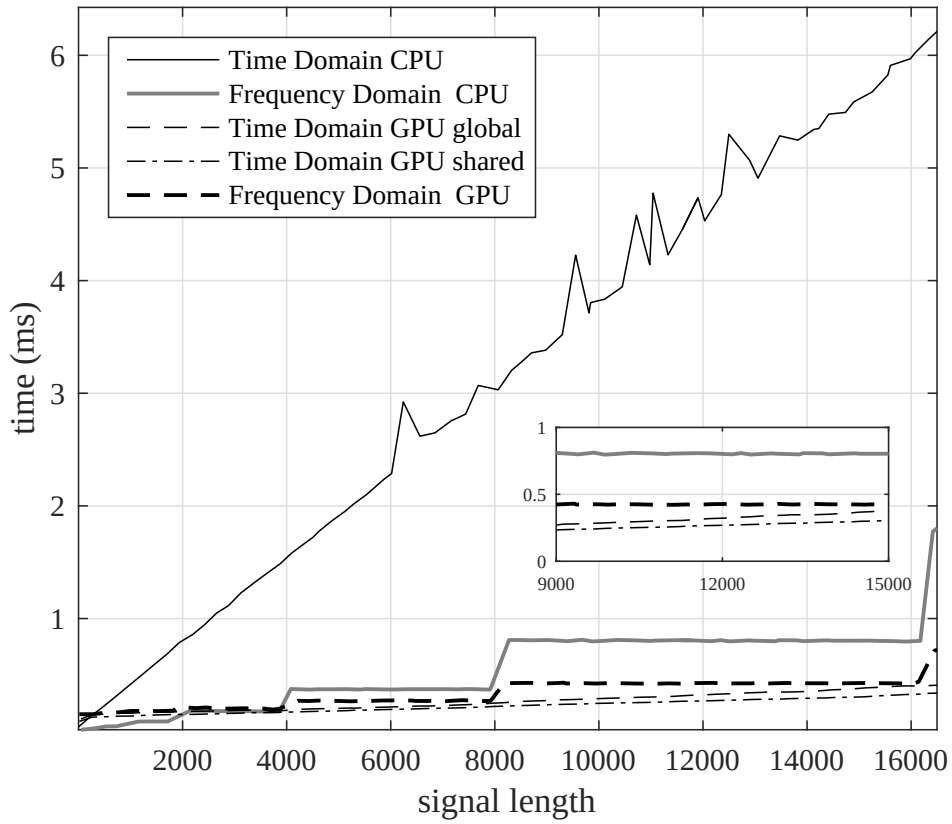

Figure 3.19: Comparison of a complex convolution on CPU and GPU. The signal length is variable and the filter is fixed at 186 taps. A lower bound was applied by searching for a local minimums in 15 sample width windows.

Table 3.3: Convolution computation times with signal length 12672 and filter length 186 on a Tesla K40c GPU.

Algorithm	Function or Library	Execution Time (ms)
CPU time domain	ConvCPU	5.3000
CPU frequency domain	FFTW	0.7972
GPU time domain global	ConvGPU	0.3321
GPU time domain shared	ConvGPUshared	0.2748
GPU frequency domain	cuFFT	0.4224

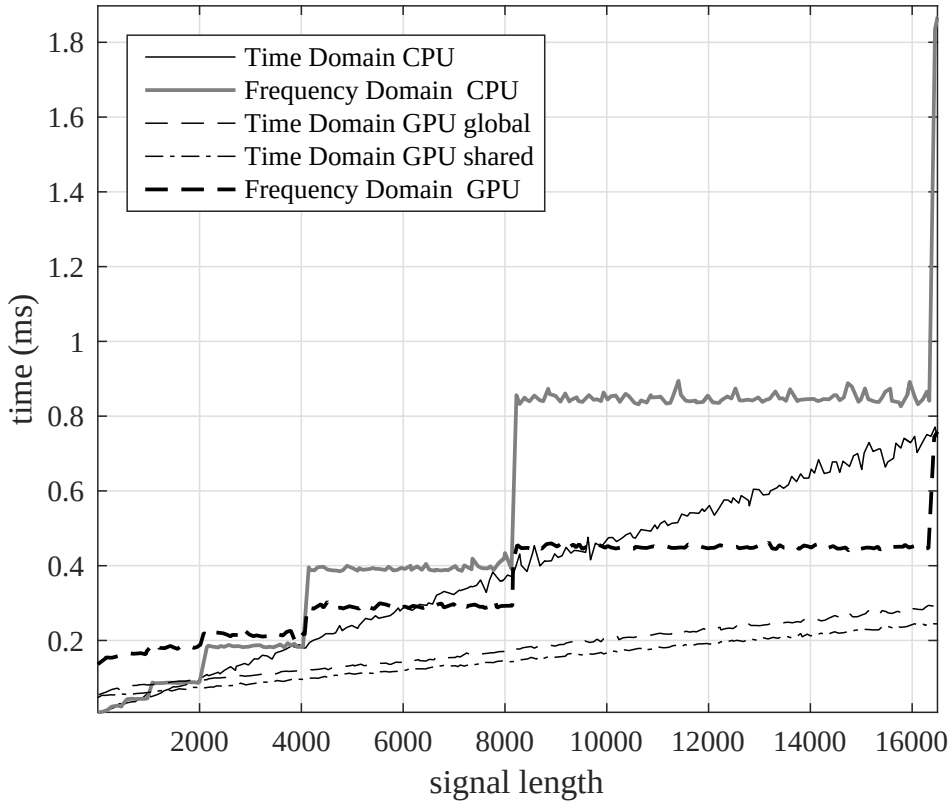

Figure 3.20: Comparison of a complex convolution on CPU and GPU. The signal length is variable and the filter is fixed at 23 taps. A lower bound was applied by searching for a local minimums in 5 sample width windows.

Table 3.4: Convolution computation times with signal length 12672 and filter length 23 on a Tesla K40c GPU.

Algorithm	Function or Library	Execution Time (ms)
CPU time domain	ConvCPU	0.5878
CPU frequency domain	FFTW	0.8417
GPU time domain global	ConvGPU	0.4476
GPU time domain shared	ConvGPUshared	0.1971
GPU frequency domain	cuFFT	0.3360

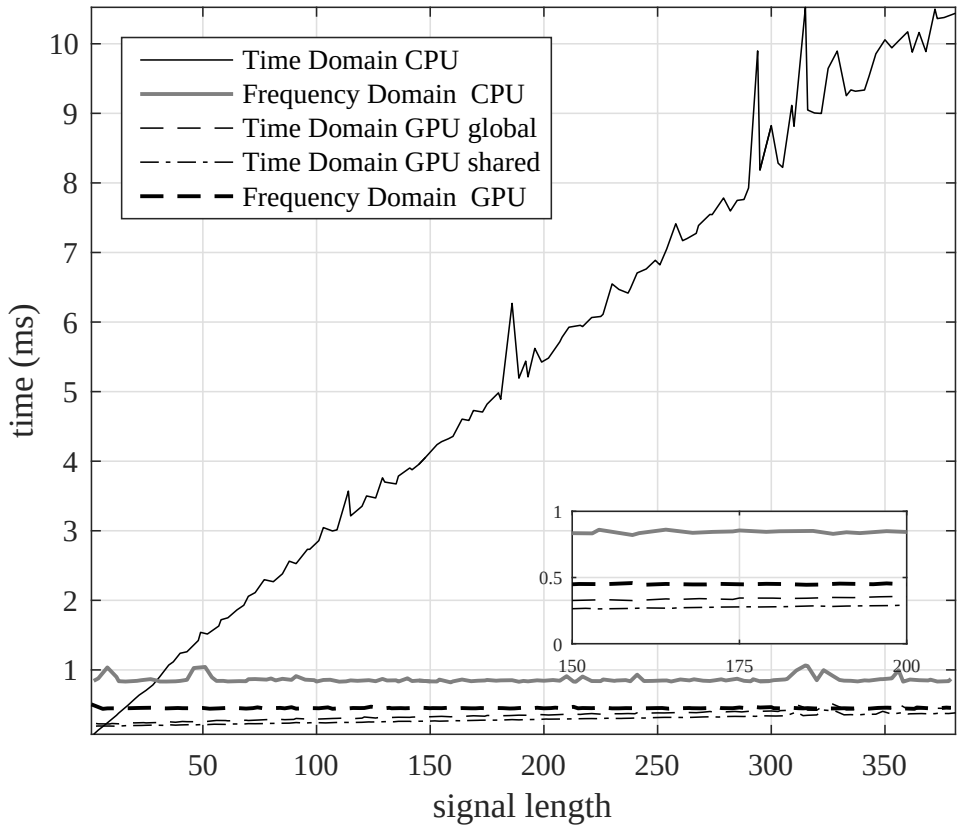

Figure 3.21: Comparison of a complex convolution on CPU and GPU. The filter length is variable and the signal is fixed at 12672 samples. A lower bound was applied by searching for a local minimums in 3 sample width windows.

3.2.3 Convolution Using Batch Processing

Section 3.2.2 illustrated convolving one signal with one filter does not leverage the full power of parallel processing in GPUs. The received signal in the PAQ system has a packetized structure with 3104 packets per 1907 ms. Rather than processing each packet separately, the packets may be buffered and processed in a "batch." Batch processing in GPUs has less CPU overhead and introduces an extra level of parallelism. Batch processing has faster execution time per packet than processing packets separately. CUDA has many libraries that have batch processing, including cuFFT, cuBLAS and cuSolverSp. Haidar et al. [16] showed batched libaries achive more Gflops than calling GPU kernels multiple times. Listing 3.6 (at the end of the chapter) shows three GPU

Table 3.5: Defining start and stop lines for execution time comparison in Listing 3.6.

Algorithm	Function	Start Line	Stop Line
GPU time domain global	ConvGPU	197	204
GPU time domain shared	ConvGPUshared	212	219
GPU frequency domain	cuFFT	227	245

implementations of convolution using batch processing and Table 3.5 shows how the execution time of the code was measured.

Figure 3.22 compares execution time of convolution using batch processing as the number of packets increases, note that no lower bounding was used. This figure shows that frequency-domain convolution leverages batch processing better than time-domain convolution. As expected, CPU-based convolution using batch processing is not competitive with GPU-based convolution using batch processing and thus CPU-batched processing is not explored any further.

Now that the GPU and CPU execution time is not being compared, Table 3.5 shows execution times include only GPU kernels and exclude memory transfers. Figure 3.23 compares GPU convolution using batch processing execution time per batch as the number of packets increases. The figure shows execution time per batch decreases as the number of packets increases but stops improving after 70 packets.

Figures 3.24 through 3.26 compare execution time of the three GPU convolution implementations by fixing the filter length with variable signal length or visa versa. Tables 3.6 and 3.7 show the execution times for the signal length and filter lengths of the PAQ system when performing convolution using batch processing. Frequency-domain convolution using batch processing is fastest for 186 tap filters while time-domain convolution using batch processing and shared memory is fastest for 23 tap filters.

Until now, convolving one signal with only one filter has been considered. Figure 2.6 showed the received signal is filtered by two cascaded filters: an equalizer filter and a detection

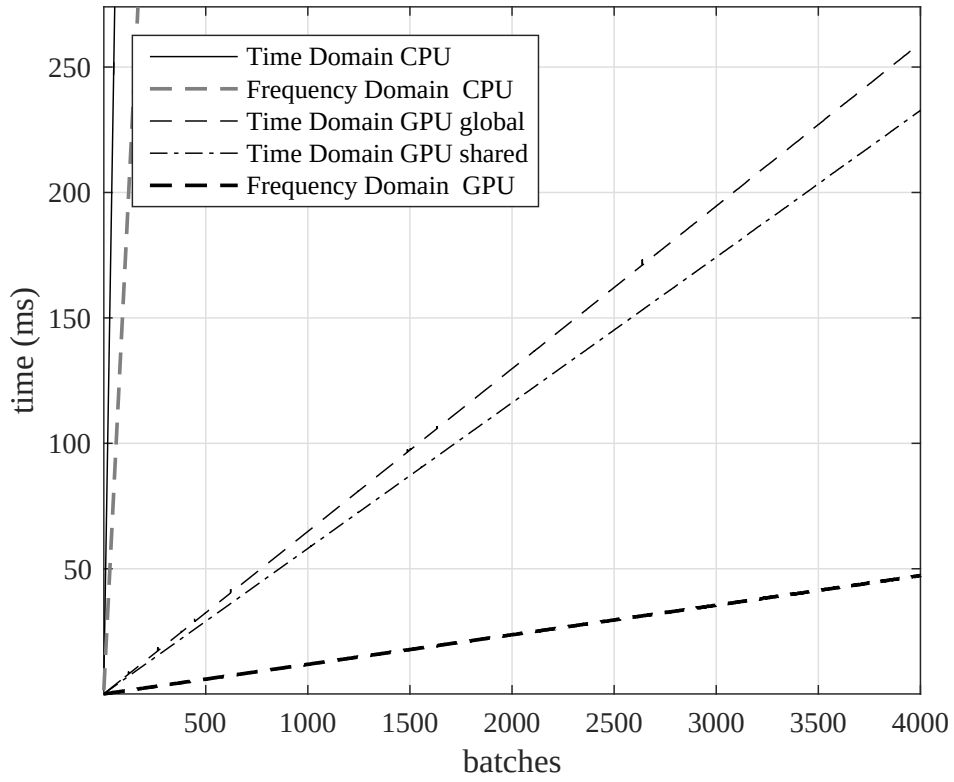

Figure 3.22: Comparison of a batched complex convolution on a CPU and GPU. The number of batches is variable while the signal and filter length is set to 12672 and 186.

Table 3.6: Convolution using batch processing execution times with for a 12672 sample signal and 186 tap filter on a Tesla K40c GPU.

Algorithm	Function or Library	Execution Time (ms)
GPU time domain global	ConvGPU	201.29
GPU time domain shared	ConvGPUshared	180.272
GPU frequency domain	cuFFT	36.798

Table 3.7: Convolution using batch processing execution times with for a 12672 sample signal and 23 tap filter on a Tesla K40c GPU.

Algorithm	Function or Library	Execution Time (ms)
GPU time domain global	ConvGPU	27.642
GPU time domain shared	ConvGPUshared	20.4287
GPU frequency domain	cuFFT	36.7604

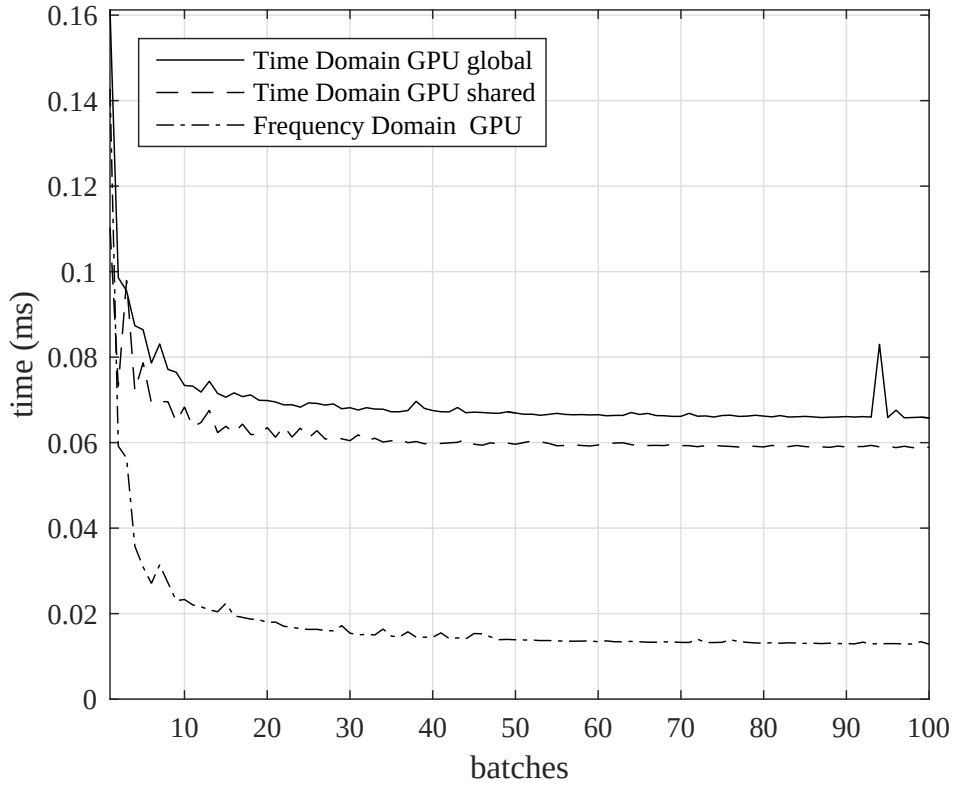

Figure 3.23: Comparison on execution time per batch for complex convolution. The number of batches is variable while the signal and filter length is set to 12672 and 186.

filter. The block diagrams in Figure 3.27 show the steps required for cascading time-domain and frequency-domain convolution.

Comparing the block diagrams in Figures 3.27 and 3.14, cascading two filters in the frequency domain only requires an extra FFT and point-by-point complex multiplication while cascading filters in the time domain requires two time-domain convolutions. The first time-domain convolution produces a composite filter from the convolution of the 186 sample equalizer filter with the 23 tap detection filter. The second time-domain convolution applies the composite $208 = 186 + 23 - 1$ tap filter to a 12672 sample signal. Table 3.8 shows the execution times for the signal length and filter lengths of the PAQ system when performing cascaded convolution using batch processing. Cascaded-convolution using batch processing in the frequency domain is fastest.

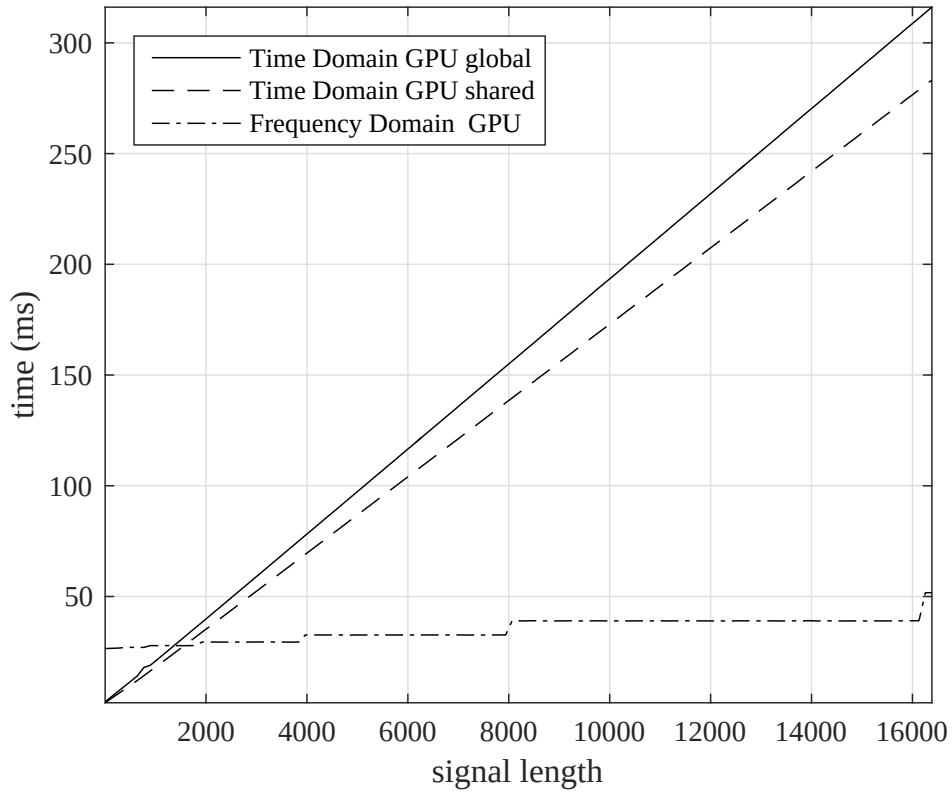

Figure 3.24: Comparison of complex convolution using batch processing on a GPU. The signal length is variable and the filter is fixed at 186 taps.

Table 3.8: Batched convolution execution times with for a 12672 sample signal and cascaded 23 and 186 tap filter on a Tesla K40c GPU.

Algorithm	Function or Library	Execution Time (ms)
GPU time domain global	ConvGPU	223.307
GPU time domain shared	ConvGPUshared	200.018
GPU frequency domain	cuFFT	39.0769

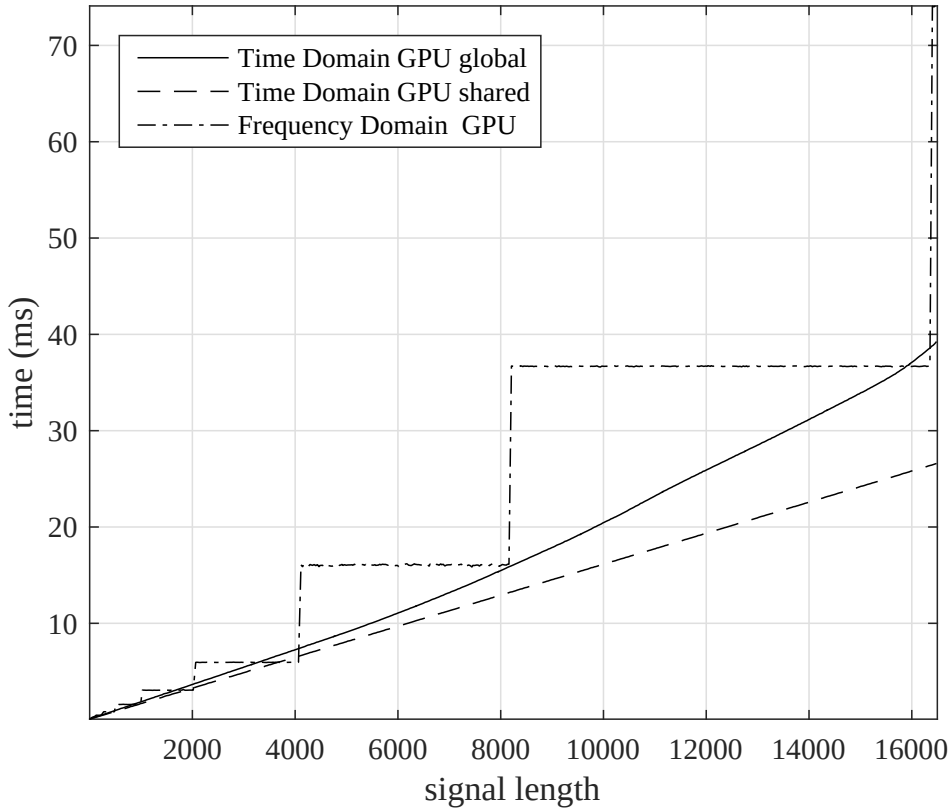

Figure 3.25: Comparison of complex convolution using batch processing on a GPU. The signal length is variable and the filter is fixed at 23 taps.

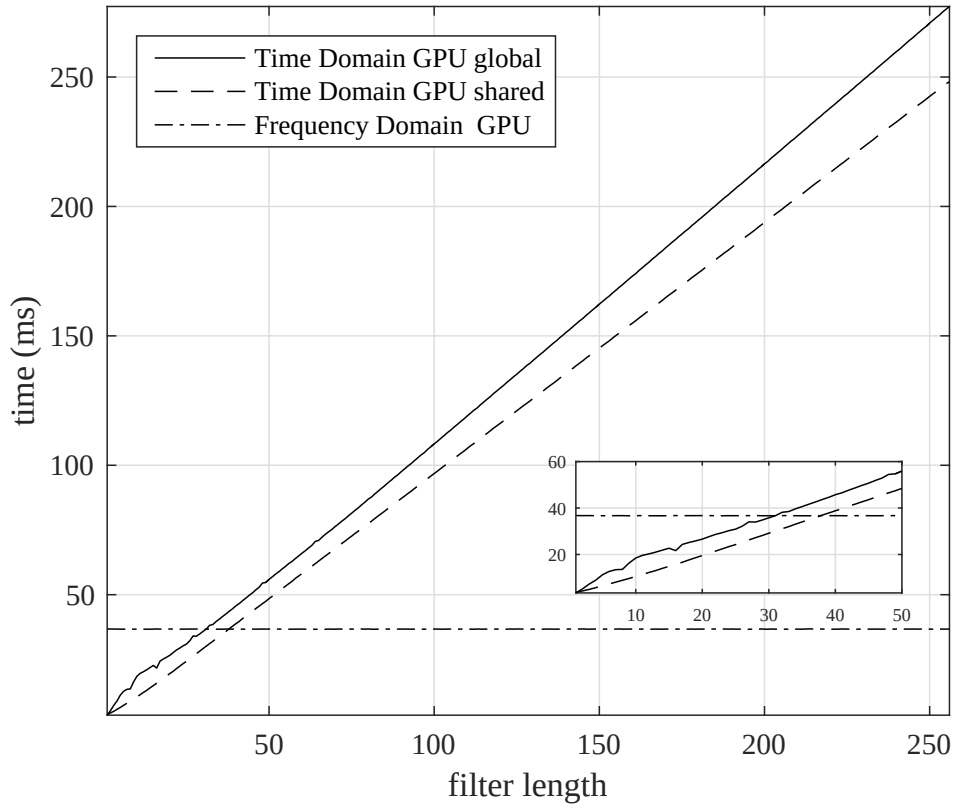

Figure 3.26: Comparison of complex convolution using batch processing on a GPU. The filter length is variable and the signal length is set to 12672 samples.

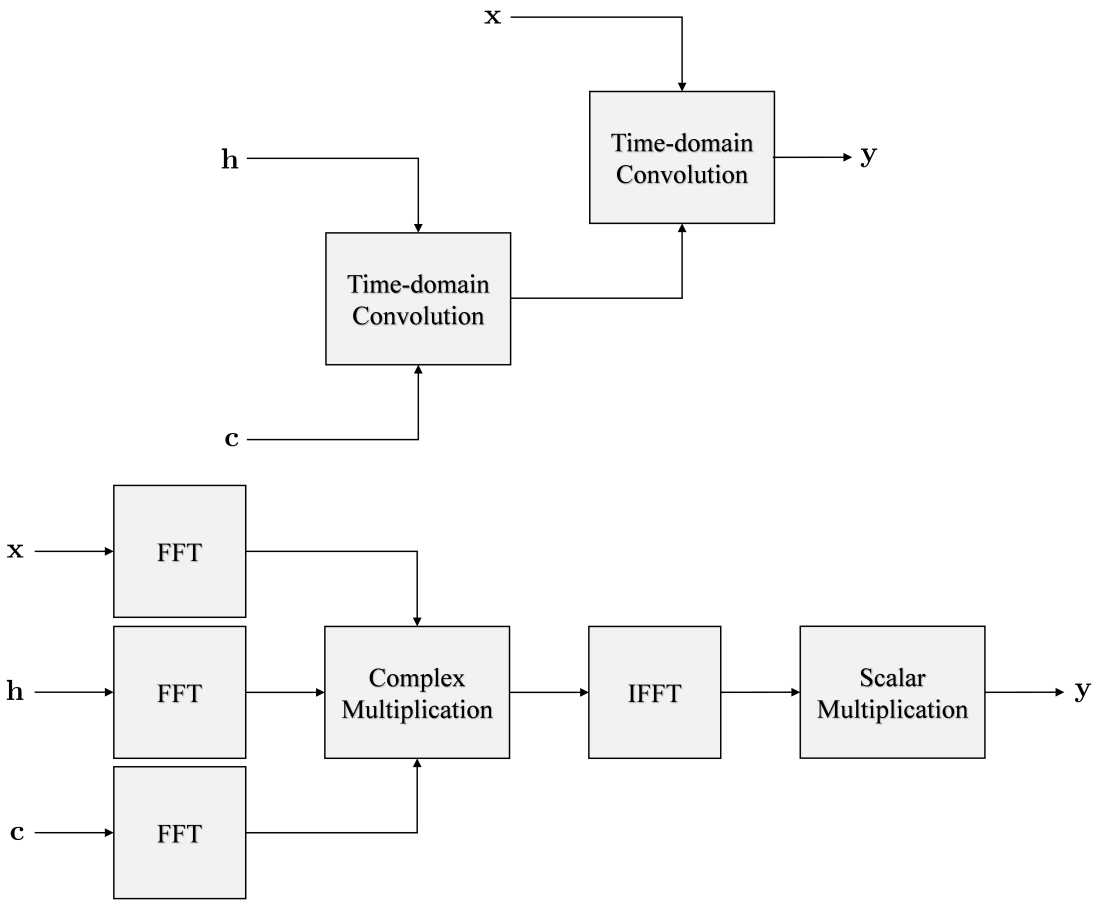

Figure 3.27: Block diagrams showing showing cascaded time-domain convolution and frequency-domain convolution.

Listing 3.5: CUDA code to performing complex convolution five different ways: time domain CPU, frequency domain CPU time domain GPU, time domain GPU using shared memory and frequency domain GPU.

```
#include <iostream>
#include <stdlib.h>
#include <math.h>
#include <cufft.h>
#include <fstream>
#include <string>
#include <fftw3.h>
using namespace std;


void ConvCPU(cufftComplex* y,cufftComplex* x,cufftComplex* h,int Lx,int Lh){
        for(int yIdx = 0; yIdx < Lx+Lh-1; yIdx++){
                cufftComplex temp;
                temp.x = 0;
                temp.y = 0;
                for(int hIdx = 0; hIdx < Lh; hIdx++){
                        int xAccessIdx = yIdx-hIdx;
                        if(xAccessIdx>=0 && xAccessIdx<Lx){
                                // temp += x[xAccessIdx]*h[hIdx];
                                float A = x[xAccessIdx].x;
                                float B = x[xAccessIdx].y;
                                float C = h[hIdx].x;
                                float D = h[hIdx].y;
                                cufftComplex result;
                                result.x = A*C-B*D;
                                result.y = A*D+B*C;
                                temp.x += result.x;
                                temp.y += result.y;
                        }
                }
                y[yIdx] = temp;
        }

}

__global__ void ConvGPU(cufftComplex* y,cufftComplex* x,cufftComplex* h,int Lx,int Lh){
        int yIdx = blockIdx.x*blockDim.x + threadIdx.x;

        int lastThread = Lx+Lh-1;

        // don't access elements out of bounds
        if(yIdx >= lastThread)
                return;

        cufftComplex temp;
        temp.x = 0;
        temp.y = 0;
        for(int hIdx = 0; hIdx < Lh; hIdx++){
                int xAccessIdx = yIdx-hIdx;
                if(xAccessIdx>=0 && xAccessIdx<Lx){
                        // temp += x[xAccessIdx]*h[hIdx];
                        float A = x[xAccessIdx].x;
                        float B = x[xAccessIdx].y;
                        float C = h[hIdx].x;
                        float D = h[hIdx].y;
                        cufftComplex result;
                        result.x = A*C-B*D;
                        result.y = A*D+B*C;
                        temp.x += result.x;
                        temp.y += result.y;
                }
        }
        y[yIdx] = temp;
```

```
}


__global__ void ConvGPUshared(cufftComplex* y,cufftComplex* x,cufftComplex* h,int Lx,int Lh){
        int yIdx = blockIdx.x*blockDim.x + threadIdx.x;

        int lastThread = Lx+Lh-1;

        extern __shared__ cufftComplex h_shared[];
        if(threadIdx.x < Lh){
                h_shared[threadIdx.x] = h[threadIdx.x];
        }
        __syncthreads();

        // don't access elements out of bounds
        if(yIdx >= lastThread)
                return;

        cufftComplex temp;
        temp.x = 0;
        temp.y = 0;
        for(int hIdx = 0; hIdx < Lh; hIdx++){
                int xAccessIdx = yIdx-hIdx;
                if(xAccessIdx>=0 && xAccessIdx<Lx){
                        // temp += x[xAccessIdx]*h[hIdx];
                        float A = x[xAccessIdx].x;
                        float B = x[xAccessIdx].y;
                        float C = h_shared[hIdx].x;
                        float D = h_shared[hIdx].y;
                        cufftComplex result;
                        result.x = A*C-B*D;
                        result.y = A*D+B*C;
                        temp.x += result.x;
                        temp.y += result.y;
                }
        }
        y[yIdx] = temp;
}

__global__ void PointToPointMultiply(cufftComplex* v0, cufftComplex* v1, int lastThread){
        int i = blockIdx.x*blockDim.x + threadIdx.x;

        // don't access elements out of bounds
        if(i >= lastThread)
                return;
        float A = v0[i].x;
        float B = v0[i].y;
        float C = v1[i].x;
        float D = v1[i].y;

        // (A+jB)(C+jD) = (AC-BD) + j(AD+BC)
        cufftComplex result;
        result.x = A*C-B*D;
        result.y = A*D+B*C;

        v0[i] = result;
}

__global__ void ScalarMultiply(cufftComplex* vec0, float scalar, int lastThread){
        int i = blockIdx.x*blockDim.x + threadIdx.x;

        // Don't access elements out of bounds
        if(i >= lastThread)
                return;
        cufftComplex scalarMult;
        scalarMult.x = vec0[i].x*scalar;
        scalarMult.y = vec0[i].y*scalar;
        vec0[i] = scalarMult;
```

```
132 }
133
134 int main(){
135         int N = 1000;
136         int L = 186;
137         int C = N + L - 1;
138         int M = pow(2, ceil(log(C)/log(2)));
139
140         cufftComplex *mySignal1;
141         cufftComplex *mySignal2;
142         cufftComplex *mySignal2_fft;
143
144         cufftComplex *myFilter1;
145         cufftComplex *myFilter2;
146         cufftComplex *myFilter2_fft;
147
148         cufftComplex *myConv1;
149         cufftComplex *myConv2;
150         cufftComplex *myConv2_timeReversed;
151         cufftComplex *myConv3;
152         cufftComplex *myConv4;
153         cufftComplex *myConv5;
154
155         mySignal1               = (cufftComplex*)malloc(N*sizeof(cufftComplex));
156         mySignal2               = (cufftComplex*)malloc(M*sizeof(cufftComplex));
157         mySignal2_fft           = (cufftComplex*)malloc(M*sizeof(cufftComplex));
158
159         myFilter1               = (cufftComplex*)malloc(L*sizeof(cufftComplex));
160         myFilter2               = (cufftComplex*)malloc(M*sizeof(cufftComplex));
161         myFilter2_fft           = (cufftComplex*)malloc(M*sizeof(cufftComplex));
162
163         myConv1                 = (cufftComplex*)malloc(C*sizeof(cufftComplex));
164         myConv2                 = (cufftComplex*)malloc(M*sizeof(cufftComplex));
165         myConv2_timeReversed= (cufftComplex*)malloc(M*sizeof(cufftComplex));
166         myConv3                 = (cufftComplex*)malloc(C*sizeof(cufftComplex));
167         myConv4                 = (cufftComplex*)malloc(C*sizeof(cufftComplex));
168         myConv5                 = (cufftComplex*)malloc(M*sizeof(cufftComplex));
169
170         srand(time(0));
171         for(int i = 0; i < N; i++){
172                 mySignal1[i].x = rand()%100-50;
173                 mySignal1[i].y = rand()%100-50;
174         }
175
176         for(int i = 0; i < L; i++){
177                 myFilter1[i].x = rand()%100-50;
178                 myFilter1[i].y = rand()%100-50;
179         }
180
181         cufftComplex *dev_mySignal3;
182         cufftComplex *dev_mySignal4;
183         cufftComplex *dev_mySignal5;
184
185         cufftComplex *dev_myFilter3;
186         cufftComplex *dev_myFilter4;
187         cufftComplex *dev_myFilter5;
188
189         cufftComplex *dev_myConv3;
190         cufftComplex *dev_myConv4;
191         cufftComplex *dev_myConv5;
192
193         cudaMalloc(&dev_mySignal3, N*sizeof(cufftComplex));
194         cudaMalloc(&dev_mySignal4, N*sizeof(cufftComplex));
195         cudaMalloc(&dev_mySignal5, M*sizeof(cufftComplex));
196
197         cudaMalloc(&dev_myFilter3, L*sizeof(cufftComplex));
198         cudaMalloc(&dev_myFilter4, L*sizeof(cufftComplex));
199         cudaMalloc(&dev_myFilter5, M*sizeof(cufftComplex));
```

```
200
201         cudaMalloc(&dev_myConv3,   C*sizeof(cufftComplex));
202         cudaMalloc(&dev_myConv4,   C*sizeof(cufftComplex));
203         cudaMalloc(&dev_myConv5,   M*sizeof(cufftComplex));
204
205
206         /**
207          * Time-domain Convolution CPU
208          */
209         ConvCPU(myConv1,mySignal1,myFilter1,N,L);
210
211         /**
212          * Frequency Domain Convolution CPU
213          */
214         fftwf_plan forwardPlanSignal = fftwf_plan_dft_1d(M, (fftwf_complex*)mySignal2,    (
                fftwf_complex*)mySignal2_fft,           FFTW_FORWARD, FFTW_MEASURE);
215         fftwf_plan forwardPlanFilter = fftwf_plan_dft_1d(M, (fftwf_complex*)myFilter2,   (
                fftwf_complex*)myFilter2_fft,           FFTW_FORWARD, FFTW_MEASURE);
216         fftwf_plan backwardPlanConv  = fftwf_plan_dft_1d(M, (fftwf_complex*)mySignal2_fft,(
                fftwf_complex*)myConv2_timeReversed, FFTW_FORWARD, FFTW_MEASURE);
217
218         cufftComplex zero; zero.x = 0; zero.y = 0;
219         for(int i = 0; i < M; i++){
220                 if(i<N)
221                         mySignal2[i] = mySignal1[i];
222                 else
223                         mySignal2[i] = zero;
224
225                 if(i<L)
226                         myFilter2[i] = myFilter1[i];
227                 else
228                         myFilter2[i] = zero;
229         }
230
231         fftwf_execute(forwardPlanSignal);
232         fftwf_execute(forwardPlanFilter);
233
234         for (int i = 0; i < M; i++){
235                 // mySignal2_fft = mySignal2_fft*myFilter2_fft;
236                 float A = mySignal2_fft[i].x;
237                 float B = mySignal2_fft[i].y;
238                 float C = myFilter2_fft[i].x;
239                 float D = myFilter2_fft[i].y;
240                 cufftComplex result;
241                 result.x = A*C-B*D;
242                 result.y = A*D+B*C;
243                 mySignal2_fft[i] = result;
244         }
245
246         fftwf_execute(backwardPlanConv);
247
248         // myConv2 from fftwf must be time reversed and scaled
249         // to match Matlab, myConv1, myConv3, myConv4 and myConv5
250         cufftComplex result;
251         for (int i = 0; i < M; i++){
252                 result.x = myConv2_timeReversed[M-i].x/M;
253                 result.y = myConv2_timeReversed[M-i].y/M;
254                 myConv2[i] = result;
255         }
256         result.x = myConv2_timeReversed[0].x/M;
257         result.y = myConv2_timeReversed[0].y/M;
258         myConv2[0] = result;
259
260         fftwf_destroy_plan(forwardPlanSignal);
261         fftwf_destroy_plan(forwardPlanFilter);
262         fftwf_destroy_plan(backwardPlanConv);
263
264
```

```
265         /**
266          * Time-domain Convolution GPU Using Global Memory
267          */
268         cudaMemcpy(dev_mySignal3, mySignal1, sizeof(cufftComplex)*N, cudaMemcpyHostToDevice);
269         cudaMemcpy(dev_myFilter3, myFilter1, sizeof(cufftComplex)*L, cudaMemcpyHostToDevice);
270 
271         int T_B = 512;
272         int B = C/T_B;
273         if(C % T_B > 0)
274                 B++;
275         ConvGPU<<<B, T_B>>>(dev_myConv3, dev_mySignal3, dev_myFilter3, N, L);
276 
277         cudaMemcpy(myConv3, dev_myConv3, C*sizeof(cufftComplex), cudaMemcpyDeviceToHost);
278 
279 
280         /**
281          * Time-domain Convolution GPU Using Shared Memory
282          */
283         cudaMemcpy(dev_mySignal4, mySignal1, sizeof(cufftComplex)*N, cudaMemcpyHostToDevice);
284         cudaMemcpy(dev_myFilter4, myFilter1, sizeof(cufftComplex)*L, cudaMemcpyHostToDevice);
285 
286         T_B = 512;
287         B = C/T_B;
288         if(C % T_B > 0)
289                 B++;
290         ConvGPUshared<<<B, T_B,L*sizeof(cufftComplex)>>>(dev_myConv4, dev_mySignal4,
                dev_myFilter4, N, L);
291 
292         cudaMemcpy(myConv4, dev_myConv4, C*sizeof(cufftComplex), cudaMemcpyDeviceToHost);
293 
294 
295         /**
296          * Frequency-domain Convolution GPU
297          */
298         cufftHandle plan;
299         int n[1] = {M};
300         cufftPlanMany(&plan,1,n,NULL,1,1,NULL,1,1,CUFFT_C2C,1);
301 
302         cudaMemset(dev_mySignal5, 0,         M*sizeof(cufftComplex));
303         cudaMemset(dev_myFilter5, 0,         M*sizeof(cufftComplex));
304 
305         cudaMemcpy(dev_mySignal5, mySignal2, M*sizeof(cufftComplex), cudaMemcpyHostToDevice);
306         cudaMemcpy(dev_myFilter5, myFilter2, M*sizeof(cufftComplex), cudaMemcpyHostToDevice);
307 
308         cufftExecC2C(plan, dev_mySignal5, dev_mySignal5, CUFFT_FORWARD);
309         cufftExecC2C(plan, dev_myFilter5, dev_myFilter5, CUFFT_FORWARD);
310 
311         T_B = 512;
312         B = M/T_B;
313         if(M % T_B > 0)
314                 B++;
315         PointToPointMultiply<<<B, T_B>>>(dev_mySignal5, dev_myFilter5, M);
316 
317         cufftExecC2C(plan, dev_mySignal5, dev_mySignal5, CUFFT_INVERSE);
318 
319         T_B = 128;
320         B = M/T_B;
321         if(M % T_B > 0)
322                 B++;
323         float scalar = 1.0/((float)M);
324         ScalarMultiply<<<B, T_B>>>(dev_mySignal5, scalar, M);
325 
326         cudaMemcpy(myConv5, dev_mySignal5, M*sizeof(cufftComplex), cudaMemcpyDeviceToHost);
327 
328         cufftDestroy(plan);
329 
330         free(mySignal1);
331         free(mySignal2);
```

```
332
333         free(myFilter1);
334         free(myFilter2);
335
336         free(myConv1);
337         free(myConv2);
338         free(myConv2_timeReversed);
339         free(myConv3);
340         free(myConv4);
341         free(myConv5);
342         fftwf_cleanup();
343
344         cudaFree(dev_mySignal3);
345         cudaFree(dev_mySignal4);
346         cudaFree(dev_mySignal5);
347
348         cudaFree(dev_myFilter3);
349         cudaFree(dev_myFilter4);
350         cudaFree(dev_myFilter5);
351
352         cudaFree(dev_myConv3);
353         cudaFree(dev_myConv4);
354         cudaFree(dev_myConv5);
355
356         return 0;
357 }
```

Listing 3.6: CUDA code to perform batched complex convolution three different ways in a GPU: time domain using global memory, time domain using shared memory and frequency domain GPU.

```
#include <cufft.h>
#include <iostream>
using namespace std;

__global__ void ConvGPU(cufftComplex* y_out,cufftComplex* x_in,cufftComplex* h_in,int Lx,int Lh,
    int maxThreads){
        int threadNum = blockIdx.x*blockDim.x + threadIdx.x;
        int convLength = Lx+Lh-1;

        // Don't access elements out of bounds
        if(threadNum >= maxThreads)
                return;

        int batch = threadNum/convLength;
        int yIdx  = threadNum%convLength;
        cufftComplex* x = &x_in[Lx*batch];
        cufftComplex* h = &h_in[Lh*batch];
        cufftComplex* y = &y_out[convLength*batch];

        cufftComplex temp;
        temp.x = 0;
        temp.y = 0;
        for(int hIdx = 0; hIdx < Lh; hIdx++){
                int xAccessIdx = yIdx-hIdx;
                if(xAccessIdx>=0 && xAccessIdx<Lx){
                        // temp += x[xAccessIdx]*h[hIdx];
                        // (A+jB)(C+jD) = (AC-BD) + j(AD+BC)
                        float A = x[xAccessIdx].x;
                        float B = x[xAccessIdx].y;
                        float C = h[hIdx].x;
                        float D = h[hIdx].y;
                        cufftComplex complexMult;
                        complexMult.x = A*C-B*D;
                        complexMult.y = A*D+B*C;

                        temp.x += complexMult.x;
                        temp.y += complexMult.y;
                }
        }
        y[yIdx] = temp;
}

__global__ void ConvGPUshared(cufftComplex* y_out,cufftComplex* x_in,cufftComplex* h_in,int Lx,
    int Lh,int maxThreads){

        int threadNum = blockIdx.x*blockDim.x + threadIdx.x;
        int convLength = Lx+Lh-1;
        // Don't access elements out of bounds
        if(threadNum >= maxThreads)
                return;

        int batch = threadNum/convLength;
        int yIdx  = threadNum%convLength;
        cufftComplex* x = &x_in[Lx*batch];
        cufftComplex* h = &h_in[Lh*batch];
        cufftComplex* y = &y_out[convLength*batch];

        extern __shared__ cufftComplex h_shared[];
        if(threadIdx.x < Lh)
                h_shared[threadIdx.x] = h[threadIdx.x];

        __syncthreads();

        cufftComplex temp;
        temp.x = 0;
```

```
64          temp.y = 0;
65          for(int hIdx = 0; hIdx < Lh; hIdx++){
66                  int xAccessIdx = yIdx-hIdx;
67                  if(xAccessIdx>=0 && xAccessIdx<Lx){
68                          // temp += x[xAccessIdx]*h[hIdx];
69                          // (A+jB)(C+jD) = (AC-BD) + j(AD+BC)
70                          float A = x[xAccessIdx].x;
71                          float B = x[xAccessIdx].y;
72                          float C = h_shared[hIdx].x;
73                          float D = h_shared[hIdx].y;
74                          cufftComplex complexMult;
75                          complexMult.x = A*C-B*D;
76                          complexMult.y = A*D+B*C;
77
78                          temp.x += complexMult.x;
79                          temp.y += complexMult.y;
80                  }
81          }
82          y[yIdx] = temp;
83  }
84
85  __global__ void PointToPointMultiply(cufftComplex* vec0, cufftComplex* vec1, int maxThreads){
86          int i = blockIdx.x*blockDim.x + threadIdx.x;
87          // Don't access elements out of bounds
88          if(i >= maxThreads)
89                  return;
90          // vec0[i] = vec0[i]*vec1[i];
91          // (A+jB)(C+jD) = (AC-BD) + j(AD+BC)
92          float A = vec0[i].x;
93          float B = vec0[i].y;
94          float C = vec1[i].x;
95          float D = vec1[i].y;
96          cufftComplex complexMult;
97          complexMult.x = A*C-B*D;
98          complexMult.y = A*D+B*C;
99          vec0[i] = complexMult;
100 }
101
102 __global__ void ScalarMultiply(cufftComplex* vec0, float scalar, int lastThread){
103         int i = blockIdx.x*blockDim.x + threadIdx.x;
104         // Don't access elements out of bounds
105         if(i >= lastThread)
106                 return;
107         cufftComplex scalarMult;
108         scalarMult.x = vec0[i].x*scalar;
109         scalarMult.y = vec0[i].y*scalar;
110         vec0[i] = scalarMult;
111 }
112
113 int main(){
114         int numBatches = 3104;
115         int N = 12672;
116         int L = 186;
117         int C = N + L - 1;
118         int M = pow(2, ceil(log(C)/log(2)));
119         int maxThreads;
120         int T_B;
121         int B;
122
123         cufftHandle plan;
124         int n[1] = {M};
125         cufftPlanMany(&plan,1,n,NULL,1,1,NULL,1,1,CUFFT_C2C,numBatches);
126
127         // Allocate memory on host
128         cufftComplex *mySignal1;
129         cufftComplex *mySignal1_pad;
130         cufftComplex *myFilter1;
131         cufftComplex *myFilter1_pad;
```

```
132         cufftComplex *myConv1;
133         cufftComplex *myConv2;
134         cufftComplex *myConv3;
135         mySignal1      = (cufftComplex*) malloc(N*numBatches*sizeof(cufftComplex));
136         mySignal1_pad  = (cufftComplex*) malloc(M*numBatches*sizeof(cufftComplex));
137         myFilter1      = (cufftComplex*) malloc(L*numBatches*sizeof(cufftComplex));
138         myFilter1_pad  = (cufftComplex*) malloc(M*numBatches*sizeof(cufftComplex));
139         myConv1        = (cufftComplex*) malloc(C*numBatches*sizeof(cufftComplex));
140         myConv2        = (cufftComplex*) malloc(C*numBatches*sizeof(cufftComplex));
141         myConv3        = (cufftComplex*) malloc(M*numBatches*sizeof(cufftComplex));
142
143         srand(time(0));
144         for(int i = 0; i < N; i++){
145                 mySignal1[i].x = rand()%100-50;
146                 mySignal1[i].y = rand()%100-50;
147         }
148
149         for(int i = 0; i < L; i++){
150                 myFilter1[i].x = rand()%100-50;
151                 myFilter1[i].y = rand()%100-50;
152         }
153
154         cufftComplex zero;
155         zero.x = 0;
156         zero.y = 0;
157         for(int i = 0; i<M*numBatches; i++){
158                 mySignal1_pad[i] = zero;
159                 myFilter1_pad[i] = zero;
160         }
161         for(int batch=0; batch < numBatches; batch++){
162                 for(int i = 0; i < N; i++){
163                         mySignal1[batch*N+i] = mySignal1[i];
164                         mySignal1_pad[batch*M+i] = mySignal1[i];
165                 }
166                 for(int i = 0; i < L; i++){
167                         myFilter1[batch*L+i] = myFilter1[i];
168                         myFilter1_pad[batch*M+i] = myFilter1[i];
169                 }
170         }
171
172         // Allocate memory on device
173         cufftComplex *dev_mySignal1;
174         cufftComplex *dev_mySignal2;
175         cufftComplex *dev_mySignal3;
176         cufftComplex *dev_myFilter1;
177         cufftComplex *dev_myFilter2;
178         cufftComplex *dev_myFilter3;
179         cufftComplex *dev_myConv1;
180         cufftComplex *dev_myConv2;
181         cufftComplex *dev_myConv3;
182         cudaMalloc(&dev_mySignal1, N*numBatches*sizeof(cufftComplex));
183         cudaMalloc(&dev_mySignal2, N*numBatches*sizeof(cufftComplex));
184         cudaMalloc(&dev_mySignal3, M*numBatches*sizeof(cufftComplex));
185         cudaMalloc(&dev_myFilter1, L*numBatches*sizeof(cufftComplex));
186         cudaMalloc(&dev_myFilter2, L*numBatches*sizeof(cufftComplex));
187         cudaMalloc(&dev_myFilter3, M*numBatches*sizeof(cufftComplex));
188         cudaMalloc(&dev_myConv1,   C*numBatches*sizeof(cufftComplex));
189         cudaMalloc(&dev_myConv2,   C*numBatches*sizeof(cufftComplex));
190         cudaMalloc(&dev_myConv3,   M*numBatches*sizeof(cufftComplex));
191
192         /**
193          * Time-domain Convolution GPU Using Global Memory
194          */
195         cudaMemcpy(dev_mySignal1, mySignal1, numBatches*sizeof(cufftComplex)*N,
                cudaMemcpyHostToDevice);
196         cudaMemcpy(dev_myFilter1, myFilter1, numBatches*sizeof(cufftComplex)*L,
                cudaMemcpyHostToDevice);
197
```

```
198         maxThreads = C*numBatches;
199         T_B = 128;
200         B = maxThreads/T_B;
201         if(maxThreads % T_B > 0)
202                 B++;
203         ConvGPU<<<B, T_B>>>(dev_myConv1, dev_mySignal1, dev_myFilter1, N, L, maxThreads);
204
205         cudaMemcpy(myConv1, dev_myConv1, C*numBatches*sizeof(cufftComplex),
                cudaMemcpyDeviceToHost);
206
207         /**
208          * Time-domain Convolution GPU Using Shared Memory
209          */
210         cudaMemcpy(dev_mySignal2, mySignal1, numBatches*sizeof(cufftComplex)*N,
                cudaMemcpyHostToDevice);
211         cudaMemcpy(dev_myFilter2, myFilter1, numBatches*sizeof(cufftComplex)*L,
                cudaMemcpyHostToDevice);
212
213         maxThreads = C*numBatches;
214         T_B = 256;
215         B = maxThreads/T_B;
216         if(maxThreads % T_B > 0)
217                 B++;
218         ConvGPUshared<<<B, T_B, L*sizeof(cufftComplex)>>>(dev_myConv2, dev_mySignal2,
                dev_myFilter2, N, L,maxThreads);
219
220         cudaMemcpy(myConv2, dev_myConv2, C*numBatches*sizeof(cufftComplex),
                cudaMemcpyDeviceToHost);
221
222         /**
223          * Frequency-domain Convolution GPU
224          */
225         cudaMemcpy(dev_mySignal3, mySignal1_pad, M*numBatches*sizeof(cufftComplex),
                cudaMemcpyHostToDevice);
226         cudaMemcpy(dev_myFilter3, myFilter1_pad, M*numBatches*sizeof(cufftComplex),
                cudaMemcpyHostToDevice);
227
228         cufftExecC2C(plan, dev_mySignal3, dev_mySignal3, CUFFT_FORWARD);
229         cufftExecC2C(plan, dev_myFilter3, dev_myFilter3, CUFFT_FORWARD);
230
231         maxThreads = M*numBatches;
232         T_B = 96;
233         B = maxThreads/T_B;
234         if(maxThreads % T_B > 0)
235                 B++;
236         PointToPointMultiply<<<B, T_B>>>(dev_mySignal3, dev_myFilter3, maxThreads);
237         cufftExecC2C(plan, dev_mySignal3, dev_mySignal3, CUFFT_INVERSE);
238
239         T_B = 640;
240         B = maxThreads/T_B;
241         if(maxThreads % T_B > 0)
242                 B++;
243         float scalar = 1.0/((float)M);
244         ScalarMultiply<<<B, T_B>>>(dev_mySignal3, scalar, maxThreads);
245
246         cudaMemcpy(myConv3, dev_mySignal3, M*numBatches*sizeof(cufftComplex),
                cudaMemcpyDeviceToHost);
247
248         cufftDestroy(plan);
249
250         // Free vectors on CPU
251         free(mySignal1);
252         free(myFilter1);
253         free(myConv1);
254         free(myConv2);
255         free(myConv3);
256
257         // Free vectors on GPU
```

```
258         cudaFree(dev_mySignal1);
259         cudaFree(dev_mySignal2);
260         cudaFree(dev_mySignal3);
261         cudaFree(dev_myFilter1);
262         cudaFree(dev_myFilter2);
263         cudaFree(dev_myFilter3);
264         cudaFree(dev_myConv1);
265         cudaFree(dev_myConv2);
266         cudaFree(dev_myConv3);
267 
268         return 0;
269 }
```

Chapter 4

Equalizer GPU Implementation

Each equalizer in the PAQ system presents an interesting challenge from a GPU implementation perspective. The equations for each equalizer in Section **??** were reformulated in preparation for fast and efficient GPU implementation. This chapter is explain how the FIR equalizer filter coefficients are computed and applied.

Every equalizer filter is computed using batch processing. In batch processing, each packet is totally independent of all other packets. To simplify figures, every block diagram in this chapter shows how one packet is processed. Each packet in a batch is processed exactly the same way with different data. If a block diagram shows how to compute one equalizer filter, the block diagram is repeated 3104 times compute a full batch of equalizer filters.

Convolution is used many times in this chapter. Section 3.2.3 showed that GPU frequency-domain batch convolution performs best for the PAQ system. To simplify block diagrams, frequency -domain batch convolution is shown as one block. Figures 4.1 and 4.2 show how frequency-domain batch convolution is represented in this chapter.

Note that the "numerically optimized" detection filter $\mathbf{h}_{\text{NO}}$ and the SOQPSK-TG power spectral density $\mathbf{\Psi}$ are defined constants. The SOQPSK-TG power spectral density $\mathbf{\Psi}$ and $\mathbf{H}_{\text{NO}}$ are pre-computed and stored where $\mathbf{H}_{\text{NO}}$ is the $16{,}384$ point FFT of $\mathbf{h}_{\text{NO}}$. Applying $\mathbf{h}_{\text{NO}}$ in the frequency domain does not require an extra FFT, only extra complex multiplies.

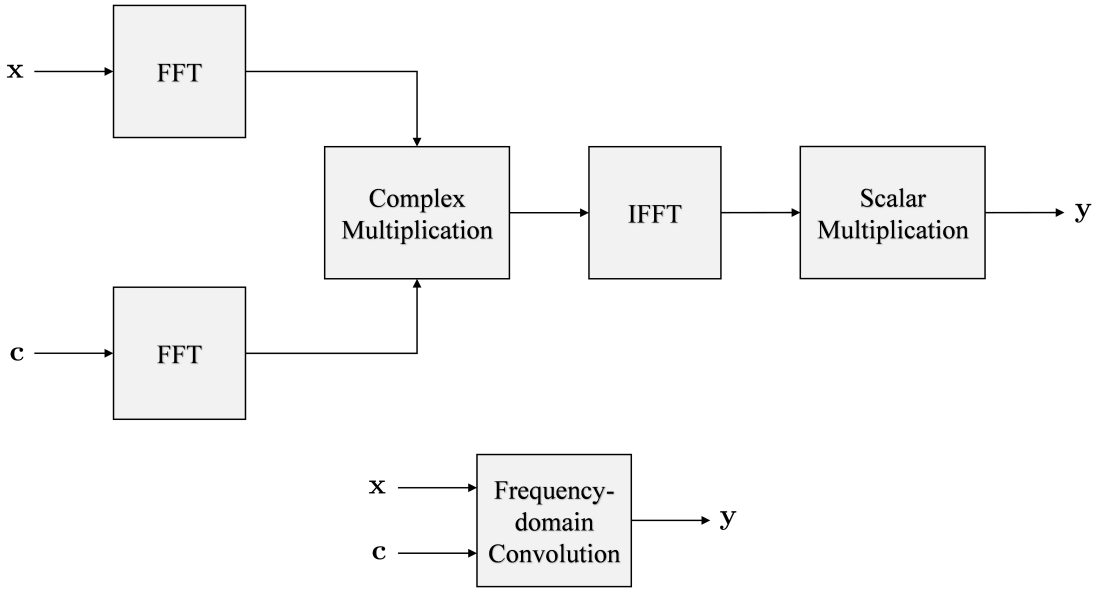

Figure 4.1: To simplify block diagrams, frequency-domain convolution is shown as one block.

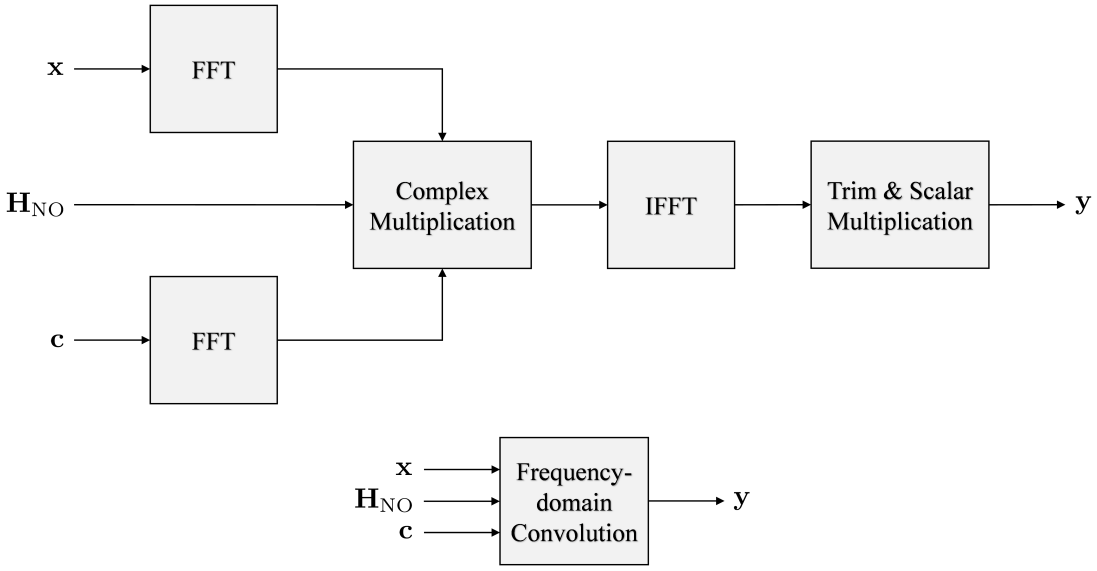

Figure 4.2: To simplify block diagrams, frequency-domain cascaded convolution is shown as one block.

4.1 Zero-Forcing and MMSE GPU Implementation

The ZF and MMSE equalizers are treated together here because they have many common features. Both equalizers are found by solving linear equations

$$\mathbf{A}\mathbf{c} = \mathbf{b} \tag{4.1}$$

where $\mathbf{c}$ is a vector of desired equalizer coefficients and the square matrix $\mathbf{A}$ and vector $\mathbf{b}$ are known. It will be shown that the only difference between ZF and MMSE lies in the matrix $\mathbf{A}$.

Zero-Forcing

The ZF equalizer is an FIR filter defined by the coefficients

$$c_{\text{ZF}}(-L_1) \quad \cdots \quad c_{\text{ZF}}(0) \quad \cdots \quad c_{\text{ZF}}(L_2). \tag{4.2}$$

The filter coefficients are the solution to the matrix vector equation [**?**, eq. (311)]

$$\mathbf{R}_{\hat{h}}\mathbf{c}_{\text{ZF}} = \hat{\mathbf{h}}_{n_0} \tag{4.3}$$

where

$$\mathbf{c}_{\text{ZF}} = \begin{bmatrix} c_{\text{ZF}}(-L_1) \\ \vdots \\ c_{\text{ZF}}(0) \\ \vdots \\ c_{\text{ZF}}(L_2) \end{bmatrix}, \tag{4.4}$$

$$\mathbf{R}_{\hat{h}} = \mathbf{H}^{\dagger}\mathbf{H} = \begin{bmatrix} r_{\hat{h}}(0) & r^*_{\hat{h}}(1) & \cdots & r^*_{\hat{h}}(L_{eq}-1) \\ r_{\hat{h}}(1) & r_{\hat{h}}(0) & \cdots & r^*_{\hat{h}}(L_{eq}-2) \\ \vdots & \vdots & \ddots & \\ r_{\hat{h}}(L_{eq}-1) & r_{\hat{h}}(L_{eq}-2) & \cdots & r_{\hat{h}}(0) \end{bmatrix} \tag{4.5}$$

and

$$\hat{\mathbf{h}}_{n_0} = \mathbf{H}^{\dagger}\mathbf{u}_{n_0} = \begin{bmatrix} \hat{h}^*(L_1) \\ \vdots \\ \hat{h}^*(0) \\ \vdots \\ \hat{h}^*(-L_2) \end{bmatrix}, \tag{4.6}$$

where

$$r_{\hat{h}}(k) = \sum_{n=-N_1}^{N_2} \hat{h}(n)\hat{h}^*(n-k), \tag{4.7}$$

$$\mathbf{u}_{n_0} = \begin{bmatrix} 0 \\ \vdots \\ 0 \end{bmatrix} \Bigg\} n_0 - 1 \text{ zeros} \\ \begin{bmatrix} 1 \end{bmatrix} \\ \begin{bmatrix} 0 \\ \vdots \\ 0 \end{bmatrix} \Bigg\} N_1 + N_2 + L_1 + L_2 - n_0 + 1 \text{ zeros}, \tag{4.8}$$

$n_0 = N_1 + L_1 + 1$ and

$$\mathbf{H} = \begin{bmatrix} \hat{h}(-N_1) & & & \\ \hat{h}(-N_1+1) & \hat{h}(-N_1) & & \\ \vdots & \vdots & \ddots & \\ \hat{h}(N_2) & \hat{h}(N_2-1) & & \hat{h}(-N_1) \\ & \hat{h}(N_2) & & \hat{h}(-N_1+1) \\ & & & \vdots \\ & & & \hat{h}(N_2) \end{bmatrix}. \tag{4.9}$$

The $(L_{\text{EQ}} \times L_{\text{EQ}})$ auto-correlation matrix $\mathbf{R}_{\hat{h}}$ comprises the sample auto-correlation $r_{\hat{h}}(k)$. Building $\mathbf{R}_{\hat{h}}$ using $r_{\hat{h}}(k)$ eliminates the need for the matrix matrix multiplication $\mathbf{H}^{\dagger}\mathbf{H}$. Note that

the sample auto-correlation $r_{\hat{h}}(k)$ only has support on $-(L_{ch}-1) \leq k \leq L_{ch}-1$, making the auto-correlation matrix $\mathbf{R}_{\hat{h}}$ sparse or 63% zero.

The MMSE equalizer is an FIR filter defined by the coefficients

$$c_{\text{MMSE}}(-L_1) \quad \cdots \quad c_{\text{MMSE}}(0) \quad \cdots \quad c_{\text{MMSE}}(L_2). \tag{4.10}$$

The filter coefficients are the solution to the matrix vector equation [**?**, eq. (330) and (333)]

$$\mathbf{R}\mathbf{c}_{\text{MMSE}} = \mathbf{g}^{\dagger} \tag{4.11}$$

where

$$\mathbf{c}_{\text{MMSE}} = \begin{bmatrix} c_{\text{MMSE}}(-L_1) \\ \vdots \\ c_{\text{MMSE}}(0) \\ \vdots \\ c_{\text{MMSE}}(L_2) \end{bmatrix}, \tag{4.12}$$

$$\mathbf{R} = \mathbf{G}\mathbf{G}^{\dagger} + 2\hat{\sigma}_w^2 \mathbf{I}_{L_1+L_2+1} = \begin{bmatrix} r_h(0)+2\hat{\sigma}_w^2 & r_h^*(1) & \cdots & r_h^*(L_{eq}-1) \\ r_h(1) & r_h(0)+2\hat{\sigma}_w^2 & \cdots & r_h^*(L_{eq}-2) \\ \vdots & \vdots & \ddots & \\ r_h(L_{eq}-1) & r_h(L_{eq}-2) & \cdots & r_h(0)+2\hat{\sigma}_w^2 \end{bmatrix} \tag{4.13}$$

and

$$\mathbf{g}^{\dagger} = \hat{\mathbf{h}}_{n0} = \begin{bmatrix} \hat{h}^*(L_1) \\ \vdots \\ \hat{h}^*(0) \\ \vdots \\ \hat{h}^*(-L_2) \end{bmatrix}, \tag{4.14}$$

where

$$r_{\hat{h}}(k) = \sum_{n=-N_1}^{N_2} \hat{h}(n)\hat{h}^*(n-k) \tag{4.15}$$

and

$$\mathbf{G} = \begin{bmatrix} \hat{h}(N_2) & \cdots & \hat{h}(-N_1) & & & \\ & \hat{h}(N_2) & \cdots & \hat{h}(-N_1) & & \\ & & \ddots & & \ddots & \\ & & & \hat{h}(N_2) & \cdots & \hat{h}(-N_1) \end{bmatrix}. \tag{4.16}$$

The $(L_{\text{EQ}} \times L_{\text{EQ}})$ auto-correlation matrix $\mathbf{R}$ comprises the sample auto-correlation $r_{\hat{h}}(k)$ and the noise variance estimate $\hat{\sigma}_w^2$. Building $\mathbf{R}$ using $r_{\hat{h}}(k)$ and $\hat{\sigma}_w^2$ eliminates the need for the matrix matrix multiplication $\mathbf{G}\mathbf{G}^\dagger$. Note that the sample auto-correlation $r_{\hat{h}}(k)$ only has support on $-(L_{ch}-1) \leq k \leq L_{ch}-1$ and the addition of $\hat{\sigma}_w^2$ does not increase that support, making the auto-correlation matrix $\mathbf{R}$ sparse or 63% zero.

The ZF and MMSE FIR equalizer filter coefficient computations have exactly the same form as shown in Equations (4.3) and (4.11). Any ZF equalizer filter computation restructuring can also be applied directly to the MMSE equalizer filter computation. To simplify the conversation, the following section will explain the investigation only the ZF equalizer filter GPU implementation.

The ZF equalizer filter can be computed two ways: solve the system of linear equations

$$\mathbf{R}_{\hat{h}}\mathbf{c}_{\text{ZF}} = \hat{\mathbf{h}}_{n_0} \tag{4.17}$$

or compute the inverse of $\mathbf{R}_{\hat{h}}$ then perform matrix vector multiplication

$$\mathbf{c}_{\text{ZF}} = \mathbf{R}_{\hat{h}}^{-1}\hat{\mathbf{h}}_{n_0}. \tag{4.18}$$

Both techniques require $\mathcal{O}(n^3)$ operations making the computation of the ZF and MMSE equalizer filter coefficients extremely heavy. Computing a matrix inverse or solving linear systems in GPUs

is especially challenging because common algorithms for matrix inversion and solving linear systems are serial. Three approaches to computing the equalizer filter coefficients were explored

- Using the Levinson-Durbin recursion algorithm to solve the system of equations
- Using the cuBLAS LU decomposition library to compute the inverse and matrix vector multiplication
- Using the cuSolver library to solve the system of equations.

The Levinson-Durbin recursion algorithm avoids $\mathcal{O}(n^3)$ inverse or solving operations by leveraging the Toeplitz or diagonal-constant structure of $\mathbf{R}_{\hat{h}}$ [17, Chap. 5]. The first GPU implementation of the Levinson-Durbin recursion algorithm computed the ZF equalizer filter assuming the matrix $\mathbf{R}_{\hat{h}}$ and the vector $\hat{\mathbf{h}}_{n_0}$ were *real-valued*. The Levinson-Durbin recursion algorithm showed promise by computing 3104 real-valued ZF equalizer filters in 500 ms.

The GPU implementation of Levinson-Durbin recursion was then converted from computing real-valued ZF equalizer filters to computing *complex-valued* ZF equalizer filters. Converting from real-valued to complex-valued filters requires more memory accesses and flops. The Levinson-Durbin recursion computed 3104 complex-valued ZF equalizer filters in $2{,}500$ ms, in excess of the 1907 ms maximum for all processing time.

The next algorithm explored computed the inverse of $\mathbf{R}_{\hat{h}}$ using the cuBLAS batch processing library. The cuBLAS library computes a *complex-valued* inverse using the LU decomposition in 600 ms. cuBLAS executed faster than the Levinson-Durbin recursion algorithm but 600 ms is still 31% of the total 1907 ms processing time.

The final and fastest algorithm explored solves the linear system in Equation (4.17)using a GPU sparse complex-valued solver library called cuSolverSp. A sparse solver can be used because section **??** showed that $\mathbf{R}_{\hat{h}}$ is sparse comprising 63% zeros because the matrix comprises of the vector $\mathbf{r}_{\hat{h}}$ with finite support on $-(L_{ch}-1) \leq k \leq L_{ch}-1$.

"cusolverSpCcsrqrsvBatched" is the GPU function used from the cuSolverSp library. cusolverSpCcsrqrsvBatched is a complex-valued batch solver that leverages the sparse properties of

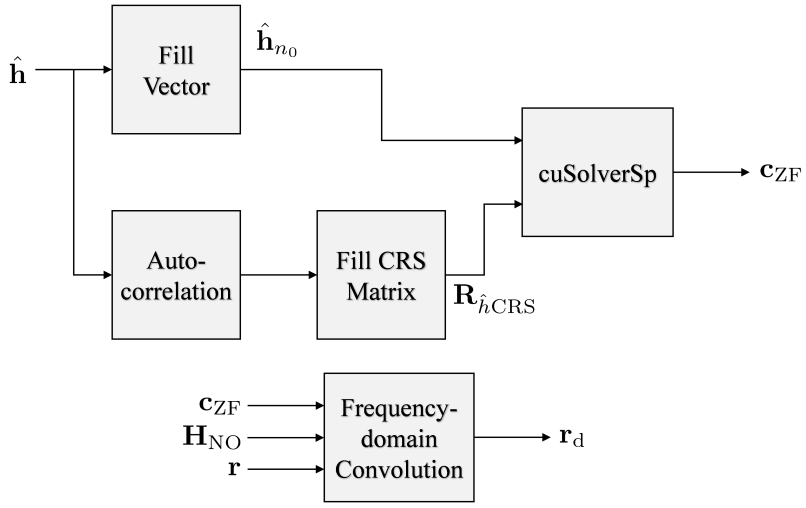

Figure 4.3: Block Diagram showing how the Zero-Forcing equalizer coefficients are implemented in the GPU.

$\mathbf{R}_{\hat{h}}$ by exploiting Compressed Row Storage (CRS) [18]. Compressed Row Storage reduces the large 186×186 matrices to a 12544 element CSR matrix $\mathbf{R}_{\hat{h}\mathrm{CRS}}$. Before cusolverSpCcsrqrsv-Batched can be called, the CSR matrix $\mathbf{R}_{\hat{h}\mathrm{CRS}}$ has to be built using $\mathbf{r}_{\hat{h}}$. An example of how to use the CUDA cusolverSp library can be found in [19]. Before the cuSolverSp library can be called, the CSR matrix $\mathbf{R}_{\hat{h}\mathrm{CRS}}$ must be built from the estimated channel auto-correlation and the vector $\hat{\mathbf{h}}_{n_0}$ is built with the conjugated and time-reversed estimated channel $\hat{\mathbf{h}}$.

Figures 4.3 and 4.4 show how the ZF and MMSE equalizer filters are computed and applied to the received samples. Note that the equalizer filters are applied in the frequency-domain with the detection filter. Table 4.1 lists the algorithms researched and their respective execution times.

4.2 Constant Modulus Algorithm GPU Implementation

The bth CMA equalizer is an FIR filter defined by the coefficients

$$c^b_{\mathrm{CMA}}(-L_1) \quad \cdots \quad c^b_{\mathrm{CMA}}(0) \quad \cdots \quad c^b_{\mathrm{CMA}}(L_2). \tag{4.19}$$

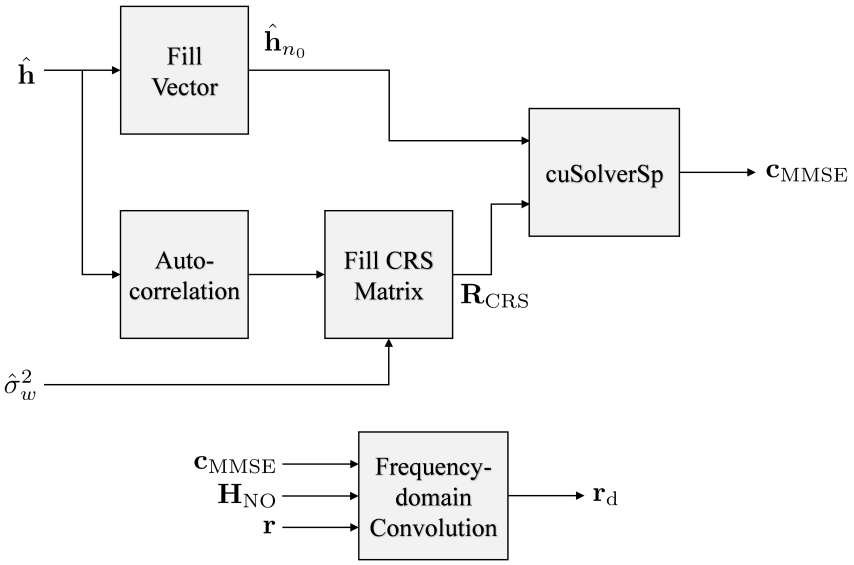

Figure 4.4: Block Diagram showing how the Minimum Mean Squared Error equalizer coefficients are implemented in the GPU.

Table 4.1: Three different algorithms were explored to compute the ZF and MMSE equalizer filters.

Algorithm	Data type	Execution Time (ms)
Levinson Recursion	floats	500
Levinson Recursion	Complex	2500
LU Decomposition	Complex	600
cuSolver	Complex	355.96

The filter coefficients are calculated by a steepest decent algorithm

$$\mathbf{c}_{\mathrm{CMA}}^{b+1} = \mathbf{c}_{\mathrm{CMA}}^{b} - \mu \nabla J \tag{4.20}$$

initialized by the MMSE equalizer coefficients

$$\mathbf{c}_{\mathrm{CMA}}^{0} = \mathbf{c}_{\mathrm{MMSE}}. \tag{4.21}$$

The vector **J** is the cost function and ∇J is the cost function gradient [**?**, eq. (352)]

$$\nabla J = \frac{2}{L_{pkt}} \sum_{n=0}^{L_{pkt}-1} \Big[y(n)y^*(n) - 1 \Big] \, y(n)\mathbf{r}^*(n). \tag{4.22}$$

where

$$\mathbf{r}(n) = \begin{bmatrix} r(n+L_1) \\ \vdots \\ r(n) \\ \vdots \\ r(n-L_2) \end{bmatrix}. \tag{4.23}$$

This means ∇J is defined by

$$\nabla J = \begin{bmatrix} \nabla J(-L_1) \\ \vdots \\ \nabla J(0) \\ \vdots \\ \nabla J(L_2) \end{bmatrix}. \tag{4.24}$$

A DSP engineer could implement the steepest decent algorithm by computing the cost function gradient directly. The L_{pkt} sample summation for ∇J in (4.22) does not map well to GPUs. Chapter 3 will show how well convolution performs in GPUs. The computation for ∇J can be massaged and re-expressed as convolution.

To begin messaging ∇J, the term

$$z(n) = 2 \Big[y(n)y^*(n) - 1 \Big] \, y(n) \tag{4.25}$$

is defined to simplify the expression of ∇J to

$$\nabla J = \frac{1}{L_{pkt}} \sum_{n=0}^{L_{pkt}-1} z(n)\mathbf{r}^*(n). \tag{4.26}$$

Expanding the expression of ∇J into vector form

$$\nabla J = \frac{z(0)}{L_{pkt}} \begin{bmatrix} r^*(L_1) \\ \vdots \\ r^*(0) \\ \vdots \\ r^*(L_2) \end{bmatrix} + \frac{z(1)}{L_{pkt}} \begin{bmatrix} r^*(1+L_1) \\ \vdots \\ r^*(1) \\ \vdots \\ r^*(1-L_2) \end{bmatrix} + \cdots \frac{z(L_{pkt}-1)}{L_{pkt}} \begin{bmatrix} r^*(L_{pkt}-1+L_1) \\ \vdots \\ r^*(L_{pkt}-1) \\ \vdots \\ r^*(L_{pkt}-1-L_2) \end{bmatrix} \quad (4.27)$$

shows a pattern in $z(n)$ and $\mathbf{r}(n)$. The kth value of ∇J is

$$\nabla J(k) = \frac{1}{L_{pkt}} \sum_{m=0}^{L_{pkt}-1} z(m) r^*(m-k), \quad -L_1 \leq k \leq L_2. \quad (4.28)$$

The summation almost looks like a convolution accept the conjugate on the element $r(n)$. To put the summation into the familiar convolution form, define

$$\rho(n) = r^*(n). \quad (4.29)$$

Now

$$\nabla J(k) = \frac{1}{L_{pkt}} \sum_{m=0}^{L_{pkt}-1} z(m) \rho(k-m). \quad (4.30)$$

Note that $z(n)$ has support on $0 \leq n \leq L_{\text{pkt}}-1$ and $\rho(n)$ has support on $-L_{\text{pkt}}+1 \leq n \leq 0$, the long result of the convolution sum $m(n)$ has support on $-L_{\text{pkt}}+1 \leq n \leq L_{\text{pkt}}-1$. Putting all the pieces together, we have

$$\begin{aligned} m(n) &= \sum_{m=0}^{L_{pkt}-1} z(m) \rho(n-m) \\ &= \sum_{m=0}^{L_{pkt}-1} z(m) r^*(m-n) \end{aligned} \quad (4.31)$$

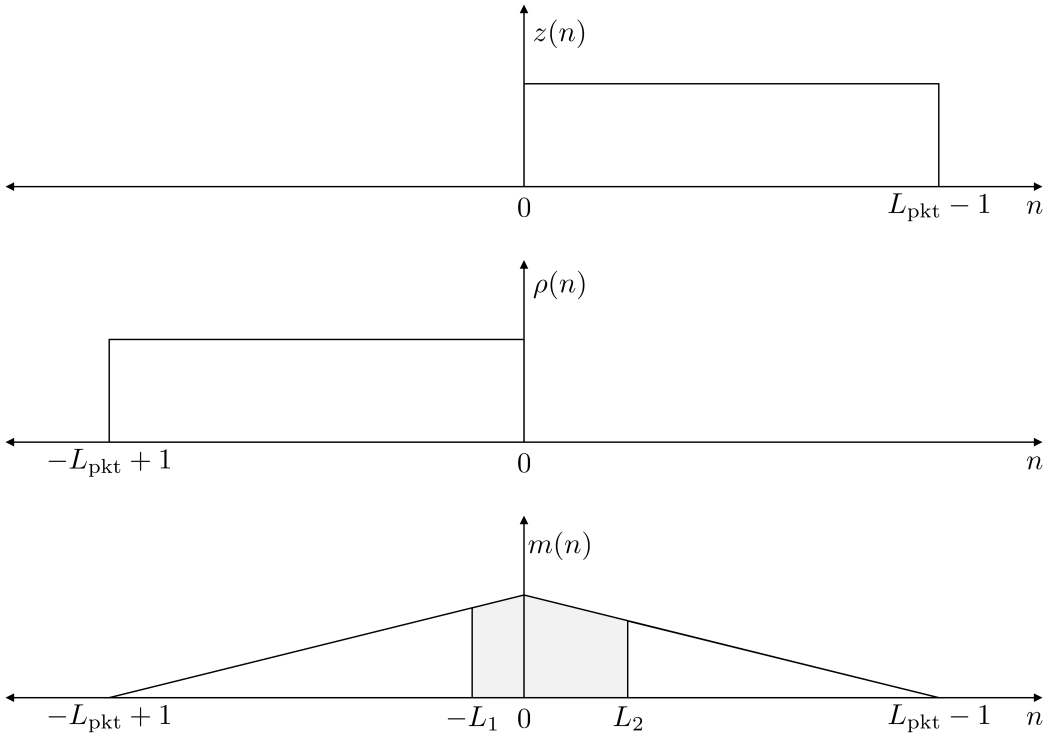

Figure 4.5: Diagram showing the relationships between $z(n)$, $\rho(n)$ and $m(n)$.

Comparing Equation (4.30) and (4.31) shows that

$$\nabla J(k) = \frac{1}{L_{pkt}} m(k), \quad -L_1 \leq k \leq L_2. \tag{4.32}$$

The values of interest are shown in Figure 4.5.

This suggest the following matlab code for computing computing the gradient vector ∇J and implementing CMA.

The Constant Modulus Algorithm (CMA) computes FIR equalizer filter coefficients by a steepest decent algorithm in Equation (4.20)

$$\mathbf{c}_{\rm CMA}^{b+1} = \mathbf{c}_{\rm CMA}^{b} - \mu \nabla J. \tag{4.33}$$

The more iterations a steepest decent algorithm executes, the better the CMA equalizer file will be. The cost function gradient used in the steepest decent algorithm is ∇J shown in Equation (4.26).

Table 4.2: CMA

```
 1 c_CMA = c_MMSE;
 2 for i = 1:its
 3     yy = conv(r,c_CMA);
 4     y = yy(L1+1:end-L2); % trim yy
 5     z = 2*(y.*conj(y)-1).*y;
 6     Z = fft(z,Nfft);
 7     R = fft(conj(r(end:-1:1)),Nfft)
 8     m = ifft(Z.*R);
 9     delJ = m(Lpkt-L1:Lpkt+L2)/Lpkt;
10     c_CMA = c_CMA-mu*delJ;
11 end
12 yy = conv(r,c_CMA);
13 y = yy(L1+1:end-L2); % trim yy
```

The most computationally heavy portion of the CMA equalizer filter implementation is computing the cost function gradient ∇J. Section **??** showed there is two approaches to computing ∇J: directly or using convolution.

To compute the cost function gradient directly the L_{pkt} sample summation

$$\nabla J = \frac{1}{L_{pkt}} \sum_{n=0}^{L_{pkt}-1} z(n)\mathbf{r}^*(n) \tag{4.34}$$

computes the cost function gradient where

$$z(n) = 2\left[y(n)y^*(n) - 1\right] y(n). \tag{4.35}$$

This approach did not allow for multiple iterations because each equalizer filter coefficient required a 12672-sample summation. The summation in GPU kernels performs poorly because every equalizer filter coefficient accesses the full packet of received samples. One CMA iteration took 421.317 ms to execute computing ∇J directly also applying $\mathbf{c}_{\text{CMA}}^{b}$ and computing $\mathbf{c}_{\text{CMA}}^{b+1}$.

Table 4.3: Two different algorithms were explored to compute the cost function gradient ∇J.

CMA Iteration Algorithm	Execution Time (ms)
∇J directly	421.317
∇J using convolution	88.774

Using convolution to compute ∇J decreased execution time significantly for the CMA equalizer filter. The cost function gradient was computed using

$$\nabla J(k) = \frac{1}{L_{pkt}} m(k), \quad -L_1 \leq k \leq L_2 \tag{4.36}$$

where

$$m(n) = \sum_{m=0}^{L_{pkt}-1} z(m)\rho(n-m) \tag{4.37}$$

and

$$\rho(n) = r^*(n). \tag{4.38}$$

One CMA iteration took 88.774 ms to execute computing ∇J using frequency-domain convolution also applying $\mathbf{c}_{\text{CMA}}^{b}$ and computing $\mathbf{c}_{\text{CMA}}^{b+1}$. Note that all other frequency-domain convolution in this thesis 2^{14} or $16{,}384$ points, but the convolution length required to compute $\nabla J(k)$ is $12672 + 12672 - 1$ which is greater than $16{,}384$. The FFTs in the computation of $\nabla J(k)$ are 2^{15} or $32{,}768$ point FFTs.

Figure 4.6 shows a block diagram of how the CMA equalizer runs on the GPU. Note that the detection filter is applied only on the last iteration. Table 4.3 lists the comparison on computing $\nabla J(k)$ using convolution. By reformulating the computation of ∇J, the execution time was reduced by a factor of 4.74. Implementing ∇J directly only provided time for 2 iterations while using convolution to compute $\nabla J(k)$ provided time for 12 iterations.

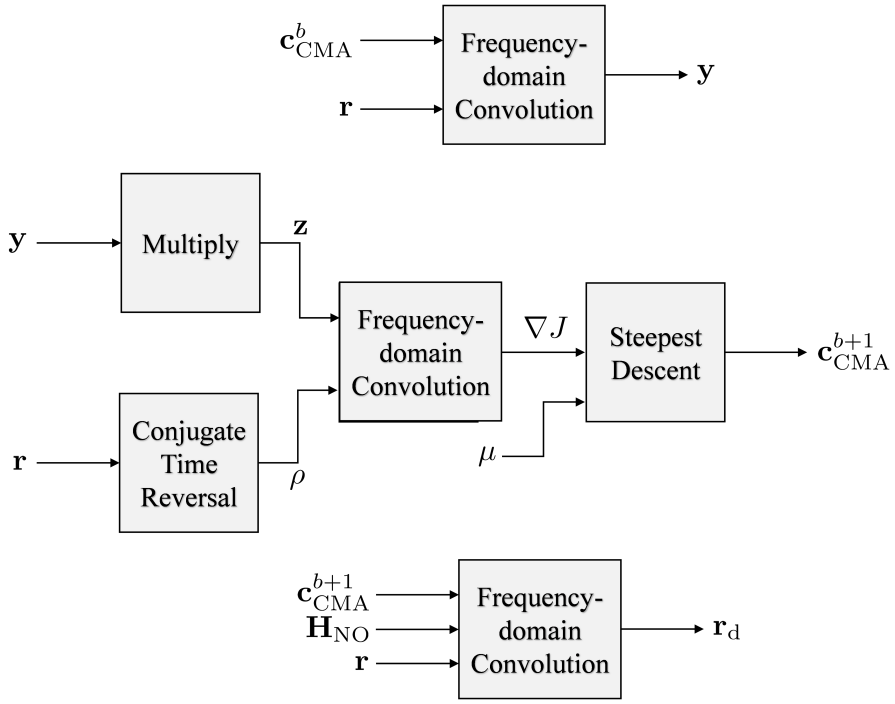

Figure 4.6: Block Diagram showing how the CMA equalizer filter is implemented in the GPU using frequency-domain convolution twice per iteration.

4.3 Frequency Domain Equalizer One and Two GPU Implementation

The Frequency Domain Equalizers (FDEs) were by far the fastest and easiest to implement in GPUs. The FDE1 and FDE2 block diagrams look just like the frequency-domain convolution block diagram in Figure 4.2 except that complex multiplication is now complex multiplication and division.

Frequency Domain Equalizer One (FDE1) and Frequency Domain Equalizer Two (FDE2) are very similar structure. FDE1 and FDE2 are adapted from Williams and Saquib [11, eq. (11) and (12)] [**?**]. The frequency domain equalizers are the frequency-domain equivalent to the MMSE equalizer.

Using circular convolution analysis, frequency-domain equalization performed on a packet structure must have cyclic prefix that is longer than the channel response [6–9]. Half of the iNET preamble is used as the cyclic prefix because it has eight repetitions of $\mathrm{CD98}_{\mathrm{hex}}$. Figure 4.7 shows how the iNET packet is used as a cyclic prefix. The length of the cyclic prefix is half the preamble

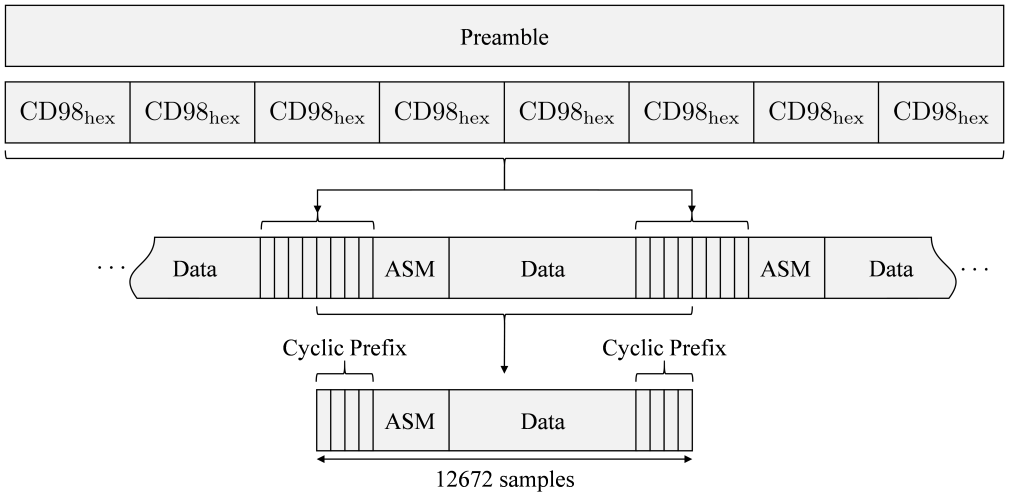

Figure 4.7: A diagram showing how the iNET packet is used as a cyclic prefix.

length $L_{\text{P}}/2 = 128$. The length of the cyclic prefix is much longer than channel impulse response $L_h = 38$.

4.3.1 Frequency Domain Equalizer One

FDE1 is the MMSE equalizer applied in the frequency domain from [11, eq. (11)]:

$$C_{\text{FDE1}}(e^{j\omega_k}) = \frac{\hat{H}^*(e^{j\omega_k})}{|\hat{H}(e^{j\omega_k})|^2 + \frac{1}{\hat{\sigma}_w^2}} \quad \omega_k = \frac{2\pi}{N_{\text{FFT}}} \text{ for } k = 0, 1, \cdots, N_{\text{FFT}} - 1 \tag{4.39}$$

where $N_{\text{FFT}} = 2^u = 16{,}384$ where $u = \lceil \log_2(L_{\text{pkt}}) \rceil = 14$. The term $\lceil \log_2(L_{\text{pkt}}) \rceil$ is the ceiling of $\log_2(L_{\text{pkt}})$. The term $C_{\text{FDE1}}(e^{j\omega_k})$ is the frequency response of FDE1 at ω_k. The term $\hat{H}(e^{j\omega_k})$ is the kth element of the length N_{FFT} of the channel estimate $\hat{\mathbf{h}}$ frequency response at ω_k. The term $\hat{\sigma}^2$ is the noise variance estimate, this term is completely independent of frequency because the noise is assumed to be spectrally flat or white.

Equation (4.39) is straight forward to implement in GPUs. FDE1 is extremely fast and computationally efficient.

FDE1 is the frequency-domain equivalent to the MMSE equalizer from Equation (4.39)

$$C_{\text{FDE1}}(e^{j\omega_k}) = \frac{\hat{H}^*(e^{j\omega_k})}{|\hat{H}(e^{j\omega_k})|^2 + \frac{1}{\hat{\sigma}_w^2}} \quad \omega_k = \frac{2\pi}{N_{\text{FFT}}} \text{ for } k = 0, 1, \cdots, N_{\text{FFT}} - 1 \tag{4.40}$$

where $N_{\text{FFT}} = 16{,}384$ points. Since FDE1 is applied in the frequency domain, the FFT of the received signal $R(e^{j\omega_k})$ is computed and the signal is equalized by performing a N_{FFT} point-to-point complex multiplication and division. The pre-computed FFT of the detection filter $\hat{H}^*(e^{j\omega_k})$ is also applied in the point-to-point complex multiplication and division. The FFT of the equalized and detected signal is

$$R_{\text{d1}}(e^{j\omega_k}) = \frac{R(e^{j\omega_k})\hat{H}^*(e^{j\omega_k})H_{\text{NO}}(e^{j\omega_k})}{|\hat{H}(e^{j\omega_k})|^2 + \frac{1}{\hat{\sigma}_w^2}} \quad \omega_k = \frac{2\pi}{N_{\text{FFT}}} \text{ for } k = 0, 1, \cdots, N_{\text{FFT}} - 1. \tag{4.41}$$

4.3.2 Frequency Domain Equalizer Two

FDE2 is also the MMSE equalizer applied in the frequency domain. Unlike FDE1, FDE2 incorporates knowledge of the SOQPSK-TG power spectral density. The frequency response of FDE2 is [11, eq. (12)]

$$C_{\text{FDE2}}(e^{j\omega_k}) = \frac{\hat{H}^*(e^{j\omega_k})}{|\hat{H}(e^{j\omega_k})|^2 + \frac{\Psi(e^{j\omega_k})}{\hat{\sigma}_w^2}} \quad \omega_k = \frac{2\pi}{L} \text{ for } k = 0, 1, \cdots, L - 1 \tag{4.42}$$

where $\Psi(e^{j\omega_k})$ is the power spectral density of SOQPSK-TG. Figure 4.8 shows $\Psi(e^{j\omega_k})$ derived using welch's method of averaging periodograms based on length $N_{\text{FFT}} = 16{,}384$ FFTs of SOQPSK-TG samples at a sample rate equivalent to 2 samples/bit. The term $\Psi(e^{j\omega_k})$ eliminates out of band multipath that may be challenging to estimate and over come.

FDE2 is the frequency-domain equivalent to the MMSE equalizer from Equation (4.42)

$$C_{\text{FDE2}}(e^{j\omega_k}) = \frac{\hat{H}^*(e^{j\omega_k})}{|\hat{H}(e^{j\omega_k})|^2 + \frac{\Psi(e^{j\omega_k})}{\hat{\sigma}_w^2}} \quad \omega_k = \frac{2\pi}{N_{\text{FFT}}} \text{ for } k = 0, 1, \cdots, N_{\text{FFT}} - 1 \tag{4.43}$$

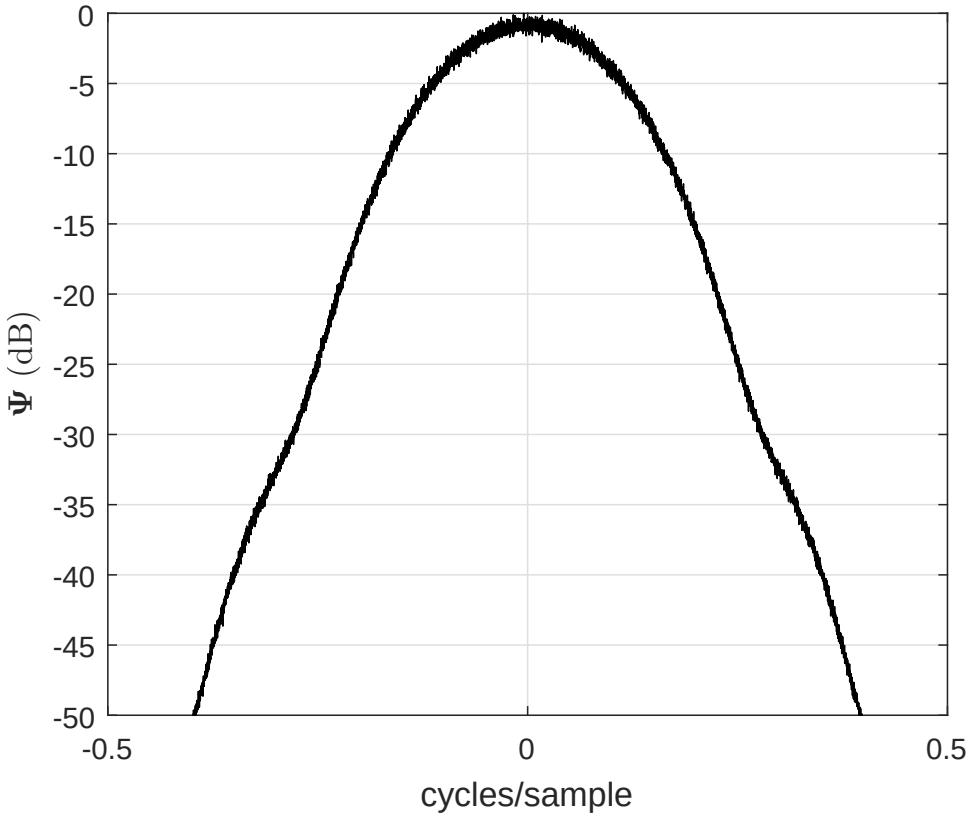

Figure 4.8: SOQPSK-TG power spectral density.

where $N_{\text{FFT}} = 16{,}384$ points. Since FDE2 is applied in the frequency domain, the FFT of the received signal $R(e^{j\omega_k})$ is computed and the signal is equalized by performing a N_{FFT} point-to-point complex multiplication and division. The pre-computed FFT of the detection filter $\hat{H}^*(e^{j\omega_k})$ is also applied in the point-to-point complex multiplication and division. The FFT of the equalized and detected signal is

$$R_{\text{dl}}(e^{j\omega_k}) = \frac{R(e^{j\omega_k})\hat{H}^*(e^{j\omega_k})H_{\text{NO}}(e^{j\omega_k})}{|\hat{H}(e^{j\omega_k})|^2 + \frac{\Psi(e^{j\omega_k})}{\hat{\sigma}_w^2}} \quad \omega_k = \frac{2\pi}{N_{\text{FFT}}} \text{ for } k = 0, 1, \cdots, N_{\text{FFT}} - 1. \tag{4.44}$$

Figures 4.9 and 4.10 show the block diagrams for GPU implementation of FDE1 and FDE2. As expected, these figures look just like the frequency-domain convolution block diagrams shown in Figure 4.2. Table 4.4 shows the execution times for calculating and applying FDE1 and FDE2.

Table 4.4: Execution times for calculating and applying Frequency Domain Equalizer One and Two.

Algorithm	Execution Time (ms)
Frequency Domain Equalizer One	57.156
Frequency Domain Equalizer Two	58.841

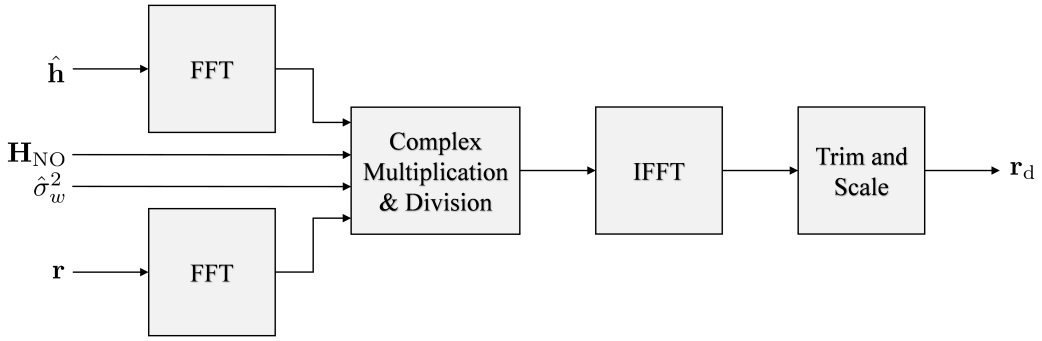

Figure 4.9: Block diagram showing Frequency Domain Equalizer One is implemented in the frequency domain in GPUs.

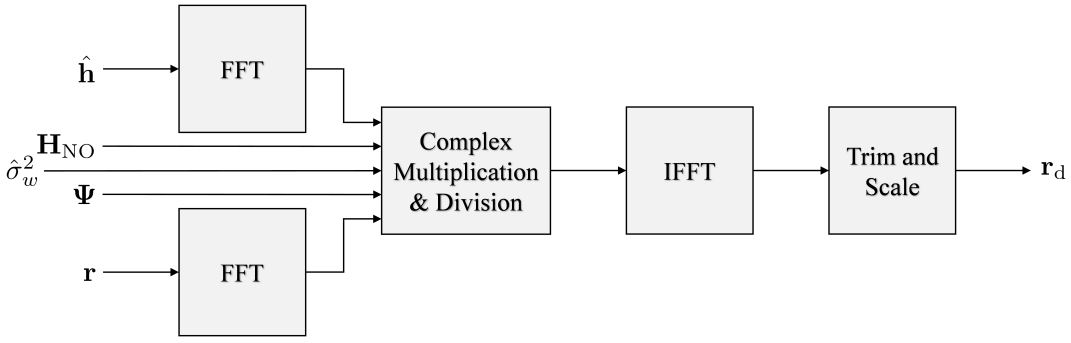

Figure 4.10: Block diagram showing Frequency Domain Equalizer Two is implemented in the frequency domain in GPUs.

Chapter 5

Summary and Conclusions

5.1 GPU Implementation

Based on measured execution times of GPU kernels, multiple data-aided equalization filters where implemented for the purpose of equalizing an aeronautical telemetry channel. Using GPU libraries and batch processing rather than custom designed GPU kernels produced massive speed ups. Also, reformulating algorithms into frequency-domain convolution produced impressive speed ups.

For implementation in one Tesla K40c and two Tesla K20c GPUs the execution times for all equalizers met the real-time constraint. It was shown that the frequency-domain equalizers are the easiest to implement and have the fastest execution time. The CMA equalizer was shown to be the hardest to implement and has the slowest execution time. The execution time did not provide the CMA the opportunity to iterate many times. The ZF and MMSE equalizers were shown to be computationally challenging to implement but had an acceptable execution time.

Because data-aided equalizers are implemented for a real-time telemetry receiver system, the execution time results must be considered along with the bit error rate performance. As of this writing the FDE1 equalizer is recommended, marking the best tradeoff between performance and computational complexity.

5.2 Contributions

Through the years of working on the PAQ project I:

1. Implemented algorithms using batch GPU libraries to reduce execution time on average by 5.

2. Reduced GPU convolution time by using batch GPU librarys and cascading filters in the frequency domain.

3. Implemented linear solver libraries to make ZF and MMSE equalizers feasible and real-time.

4. Reformulated the CMA to leverage the speed of GPU convolution.

5. Implemented new ADC to drive success of the PAQ project.

6. Implemented resampling polyphase filters in GPUs.

7. Participated heavily in flight tests at Edwards AFB.

8. Presented a paper frequency offset compensation for equalized SOQPSK at International Telemetering. Conference (ITC) [20].

5.3 Further Work

The Levinson-Durbin algorithm GPU implementation only leveraged the toeplitz structure of the channel estimate auto-correlation matrix. A hybrid sparse Levinson-Durbin algorithm could leverage the sparseness of the channel estimate auto-correlation matrix and the vector $\hat{\mathbf{h}}_{n_0}$.

Bibliography

[1] M. Rice, M. S. Afran, and M. Saquib, "Equalization in aeronautical telemetry using multiple antennas," in *Proceedings of the IEEE Military Communications Conference*, Baltimore, MD, November 2014. 1

[2] M. Rice, M. S. Afran, M. Saquib, A. Cole-Rhodes, and F. Moazzami, "On the performance of equalization techniques for aeronautical telemetry," in *Proceedings of the IEEE Military Communications Conference*, Baltimore, MD, November 2014. 1, 11, 12, 14

[3] M. Rice *et al.*, "Phase 1 report: Preamble assisted equalization for aeronautical telemetry (PAQ)," Brigham Young University, Tech. Rep., 2014, submitted to the Spectrum Efficient Technologies (SET) Office of the Science & Technology, Test & Evaluation (S&T/T&E) Program, Test Resource Management Center (TRMC). Also available on-line at http://hdl.lib.byu.edu/1877/3242. 3, 13, 14

[4] M. Rice, *Digital Communications: A Discrete-Time Approach*. Upper Saddle River, NJ: Pearson Prentice-Hall, 2009. 4

[5] M. Rice and E. Perrins, "On frequency offset estimation using the inet preamble in frequency selective fading," in *Military Communications Conference (MILCOM), 2014 IEEE*. IEEE, 2014, pp. 706–711. 11

[6] H. Sari, G. Karam, and I. Jeanclaud, "Frequency-domain equalization of mobile radio and terrestrial broadcast channels," in *Global Telecommunications Conference, 1994. GLOBECOM'94. Communications: The Global Bridge., IEEE*. IEEE, 1994, pp. 1–5. 15, 79

[7] B. Ng, C.-T. Lam, and D. Falconer, "Turbo frequency domain equalization for single-carrier broadband wireless systems," *IEEE transactions on wireless communications*, vol. 6, no. 2, 2007. 15, 79

[8] N. Al-Dhahir, M. Uysal, and H. Mheidat, "Single-carrier frequency domain equalization," 2008. 15, 79

[9] J. Proakis and M. Salehi, *Digital Communications*, 5th ed. New York: McGraw-Hill, 2008. 15, 79

[10] J. Coon, M. Sandell, M. Beach, and J. McGeehan, "Channel and noise variance estimation and tracking algorithms for unique-word based single-carrier systems," *IEEE Transactions on Wireless Communications*, vol. 5, no. 6, pp. 1488–1496, June 2006. 15

[11] I. E. Williams and M. Saquib, "Linear frequency domain equalization of SOQPSK-TG for wideband aeronautical telemetry channels," *IEEE Transactions on Aerospace and Electronic Systems*, vol. 49, no. 1, pp. 640–647, 2013. 15, 16, 79, 80, 81

[12] E. Perrins, "FEC systems for aeronautical telemetry," *IEEE Transactions on Aerospace and Electronic Systems*, vol. 49, no. 4, pp. 2340–2352, October 2013. 17

[13] Wikipedia, "Graphics processing unit," 2015. [Online]. Available: http://en.wikipedia.org/wiki/Graphics_processing_unit 21

[14] ——, "Fastest fourier transform in the west," 2017. [Online]. Available: http://www.fftw.org/ 38

[15] J. W. Cooley and J. W. Tukey, "An algorithm for the machine calculation of complex fourier series," *Mathematics of computation*, vol. 19, no. 90, pp. 297–301, 1965. 38

[16] A. Haidar, T. Dong, P. Luszczek, S. Tomov, and J. Dongarra, "Optimization for performance and energy for batched matrix computations on gpus," in *Proceedings of the 8th Workshop on General Purpose Processing using GPUs*. ACM, 2015, pp. 59–69. 45

[17] M. Hayes, *Statistical Digital Signal Processing and Modeling*. New York: John Wiley & Sons, 1996. 71

[18] Wikipedia, "Sparse matrix," 2017. [Online]. Available: https://en.wikipedia.org/wiki/Sparse_matrix 72

[19] NVIDIA, "Cuda toolkit documentation," 2017. [Online]. Available: http://docs.nvidia.com/cuda/ 72

[20] J. Ravert and M. Rice, "On frequency offset compensation for equalized SOQPSK," in *Proceedings of the International Telemetering Conference*, Glendale, AZ, October 2016. 86